الجمهورية الجزائرية الديمقراطية الشعبية

People`s Democratic Republic of Algeria

The Ministry of Higher Education and Scientific Research

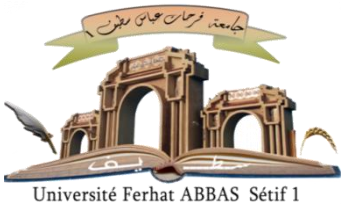

FERHAT ABBAS UNIVERSITY – SETIF 1

FACULTY OF TECHNOLOGY

THESIS

Presented in the Department of Electrotechnics

To obtain the diploma of

DOCTORATE OF SCIENCES

Option: electric networks

by

Khaled BELHOUCHET

TOPIC

Contribution to the study and improvement of the electric performance of high voltage insulators

Presented publically in 22/02/2020 in front of the Jury:

GHERBI Ahmed	Prof.at Ferhat ABBAS university of Setif -1-	President
BAYADI Abdelhafid	Prof.at Ferhat ABBAS university of Setif -1-	Thesis supervisor
HAMOU Nouri	Prof.at Ferhat ABBAS university of Setif -1-	Examiner
MOULAI Hocine	Prof.at Houari Boumediene university Algiers	Examiner
TEGUAR Madjid	Prof.at the National Polytechnic School, Algiers	Examiner
MEKHALDI Abdelouahab	Prof.at the National Polytechnic School, Algiers	Examiner

Declaration

This work has not previously been accepted in substance for any degree and is not concurrently submitted in candidature for any degree.

Signed : ……..... (BELHOUCHET Khaled) Date:.....

STATEMENT 1

This thesis is being submitted in partial fulfilment of the requirements for the degree of PhD

Signed : ……..... (BELHOUCHET Khaled) Date: .....

STATEMENT 2

This thesis is the result of my own work/investigation, except where otherwise stated. Other sources are acknowledged by explicit references.

Signed : ……..... (BELHOUCHET Khaled) Date: .....

STATEMENT 3

I hereby give consent for my thesis, if accepted, to be available for photocopying and for inter-library loan, and for the title and summary to be made available to outside organisations.

Signed : ……..... (BELHOUCHET Khaled) Date: .....

List of publications

K. Belhouchet, A. Bayadi, L. Ouchen, "Optimization and parameter identification of arc constants in insulators flashover voltage using real-coded genetic algorithm approach". The 8th National Conference on Electrical engineering (ICEE). EMP. 2013.

K. Belhouchet, A. Bayadi, ME. Bendib, "Artificial neural networks (ANN) and genetic algorithm modeling and identification of arc parameter in insulators flashover voltage and leakage current , 4th International Conference on Electrical Engineering (ICEE), 1-6. 2015.

https://ieeexplore.ieee.org/document/7416698

K. Belhouchet, A. Bayadi, ME. Bendib, "Artificial neural networks and genetic algorithm modelling and identification of arc parameter in insulators flashover voltage and leakage current". International Journal of Computer Aided Engineering and Technology 11 (1), 1-13. 2019.

https://www.inderscience.com/info/inarticle.php?artid=96708

K Belhouchet, A Bayadi, H Belhouchet, M Romero, " Improvement of mechanical and dielectric properties of porcelain insulators using economic raw materials" Boletín de la Sociedad Española de Cerámica y Vidrio 58 (1), 28-37.2018.

https://www.sciencedirect.com/science/article/pii/S0366317518300475

Dedication

This thesis is dedicated

To...

My dear parents

My supportive wife

My little prince "Barae Imade Eddine"

My brothers and sisters

&

All my friends and work colleagues

Acknowledgements

In the name of God, the Most Gracious, the Most Merciful.
Peace and blessings are upon His final Messenger Muhammad

Firstly, I am grateful to "**ALLAH"** for the good health and wellbeing that were necessary to complete this thesis.

I am so grateful to **Prof. A. BAYADI** for giving me the opportunity to carry out this research. His expert advice and continuous support have been a permanent source of great help.

I am also deeply thankful to **Pr. BELHOUCHET Hocine** for his invaluable guidance encouragement, support and advice.

My sincere thanks also go to **Pr. GHERBI Ahmed**, for honoring my jury by presiding it.
I would like to extend my gratitude also to;

Pr. HAMOU Nouri, Pr. MOULAI Hocine, Pr. TEGUAR Madjid and Pr. MEKHALDI Abdelouahab who kindly accepted to participate in the defense of this thesis as examiners.

I thank all who in one way or another contributed in the completion of this thesis

Finally, I must express my very profound gratitude to my parents, my supportive wife and to my little prince "Barae" for providing me with unfailing support and continuous encouragement throughout my years of study and through the process of researching and writing this thesis. This accomplishment would not have been possible without them.

Thank you.

Khaled Belhouchet

ملخص الرسالة

تعتبر العوازل من بين الأجزاء الأكثر أهمية في نظام الطاقة. لهذا الصدد تمت دراسة العوازل السيراميكية وغير السيراميكية المستخدمة في خطوط نقل الطاقة الكهربائية في هذا البحث بهدف الحد من تدهور أسطحها وبالتالي تقديم ها أفضل أداء. تم تنفيذ هذه الأطروحة من أجل تحليل أداء العوازل عن طريق دراسة توزيع الحقل الكهربائي. سيساعد تحسين توزيع المجال الكهربائي على تحسين أداء العوازل على المدى الطويل.

الجزء الأول من هذا البحث يهدف إلى دراسة استخدام الحلقة الاكليلية في نهايات أطراف العوازل المركبة (غير السيراميكية) و تأثيرها على توزيع الحقل الكهربائي وتخفيض قيمه القصوى. للقيام بذلك ، تم تطوير خوارزمية الخفافيش (BAT Algorithm) المستندة إلى تقنية التحسين للحصول على معايير التصميم الأمثل للحلقة الاكليلية. لقد تم تصميم نموذج للعازل المركب للمح اكاة وتم استخدام طريقة *الحدود المتناهية* (FEM) لدراسة توزيع الحقل الكهربائي على طول سطح هذا العازل.

الجزء الثاني من الأطروحة يتعلق بالبورسلان. حيث يدرس هذا الجزء إمكانية تطوير البورسلان من مواد خام محلية وباستعمال الزجاج المعاد تدويره. كما أجريت محاكاة لسطح هذا العازل في الحالتين: مغلف و غيرمغلف. وقد أظهرت النتائج أن الغلاف المستخدم يحسن من مقاومة العازل وأن توزيع الحقل الكهربائي على طول هذا سطح يظهر تحسنا ملحوظا.

إن النتائج التي تم الحصول عليها تعطي معلومات أكثر دقة للعثور على أفضل الحلول لمشاكل عوازل الجهدالعالي.

الكلمات المفتاحية: عازل مركب ، حلقة كورونا ، الحقل الكهربائي ، خوارزمية الخفافيش ، طريقة الحدود المتناهية (FEM)، بورسلان ، إنشا ء.

Résumé

Les isolateurs sont parmi les parties les plus importantes du système d'alimentation électrique. Les isolateurs céramiques et non céramiques utilisés dans les lignes de transport d'énergie ont été étudiés dans le but de réduire la dégradation de la surface et d'offrir les meilleures performances. Cette thèse a été réalisée dans le but d'analyser les performances des isolateurs via leur distribution de champ électrique. En améliorant la distribution du champ électrique, cela contribuera à améliorer les performances à long terme des isolateurs.

La première partie de ce travail vise à étudier l'utilisation de l'anneau corona au niveau du raccord d'extrémité HT pour améliorer le champ électrique et les distributions de potentiel, puis pour minimiser les décharges par effet corona sur un isolateur polymérique. Pour ce faire, un algorithme BAT basé sur une technique d'optimisation est développé pour obtenir les paramètres optimisés de l'anneau corona. L'isolateur polymérique est modélisé pour la simulation et une méthode FEM a été utilisée pour étudier la contrainte de champ électrique le long de la surface de cet isolateur.

La deuxième partie de la thèse concerne l'isolateur en porcelaine. Cette partie étudie la possibilité de développer une porcelaine à partir de matières premières locales et de verre recyclé. Des simulations de surfaces isolantes revêtues et non revêtues de porcelaine ont également été effectuées. Les résultats obtenus montrent que le revêtement améliore la résistance à la rupture de la porcelaine et que la distribution de la tension le long de la surface montre une amélioration significative.

Les résultats obtenus présentent une conclusion plus précise dans la recherche des meilleures solutions aux problèmes des isolateurs haute tension.

***Mots-clés** : isolateur composite, anneau corona, champ eléctrique, algorithme chauve-souris, MEF, porcelaine, élaboration.*

Abstract

Insulators are the important part of the power system. Ceramic and non ceramic insulators used in power transmission lines were studied with the aim of reducing degradation over its surface and presenting the best performance. This thesis has been made to analyze insulator performance via their electric field distribution. By improving the electric field distribution, it will help in enhancing their long term performance of insulator. The first part of this work is aimed to investigate the use of corona ring at the HV end fitting for improving the electric field and potential distributions and then for minimizing the corona discharges on composite insulator. To achieve this, optimization technique based Bat algorithm is developed for obtaining the optimized corona ring parameters. Composite insulator is modeled for simulation and FEM method has been employed to investigate the electric field stress along the insulator surface.

The second part of the thesis concerns the porcelain insulator. In this part the possibility of development porcelain from locally raw materials using recycled waste glass is studied. Simulations for coated and uncoated insulator surfaces of porcelain were also performed. The obtained results showed that Coating enhances the breakdown strength of the porcelain and the voltage distribution along the leakage surface of coated ceramic insulators show a significantly improvement.

The obtained results present more accurate result in finding best solutions for high voltage insulators problems.

***Keywords** : composite insulator, corona ring, electric field, bat algorithm, FEM, porcelain, elaboration.*

Table of contents

Chapter 03

Optimization of Corona Ring Design for Improved Electric Field Performance

Chapter 04

Performance Analysis of non Ceramic Insulator

Chapter 05

Characterization and Improvement of porcelain insulator

Chapter 06

General Conclusions

Bibliographic References

List of figures

List of tables

List of abbreviations

HV	**H**igh **V**oltage
CR	**C**orona **R**ing
GRTE	**S**ociété **A**lgérienne de **G**estion du **R**éseau de **T**ransport de l'**E**lectricité
FEM	**F**inite **E**lement **M**ethod
2D/3D	Two/three **D**imensional
BA	**B**at **A**gorithm
PSO	**P**article **S**warm **O**ptimization
GA	**G**enetic **A**lgorithm
NO	**N**euro **O**ptimizer
BSO	**B**ee **S**warm **O**ptimization
ANOVA	Analysis of variance
OA	**O**rtoganal **A**rray
EPRI	**E**lectric **P**ower **R**esearch **I**nstitute
AC	**A**lternating **C**urrent
DC	**D**irect **C**urrent
XRD	**X**-**R**ays **D**iffraction
FT-IR	**F**ourier-**T**ransform infrared spectroscopy
DTA	**D**ifferential **T**hermal **A**nalysis
SEM	**S**canning **E**lectron **M**icroscope
AFM	**A**tomic **F**orce **M**icroscopy
UV	**U**ltra **V**iolet
Hv	**H**ardness **v**ickers

List of symbols

mm	Millimeter
cm	Centimeter
m	Meter
H	Corona ring height
D_r	Corona ring tube diameter
R	Corona ring radius
E	Electric Field
F^2	Coefficient of determination
s	second
kV	Kilovolt
mg	Milligram
G	Glass
N	No glass
MHz	Megahertz
kHz	Kilohertz
ε'	Dielectric Constant
ε"	Dielectric loss factor
tng δ	Loss tangent
θ	Angle phase
TiO_2	Titanium dioxide

Chapter 01

General Introduction

Chapter 01

General Introduction

1.1. Background

In recent years, electricity has become one of the most important necessities in human life and extra high voltage power lines have been widely used to transmit the electric energy from the power stations to the end users. Insulators are among the key devices of the electric power transmission systems. They play a significant role in maintaining the reliability of the network. They are used to support, separate and contain conductors at high voltage. The insulators need to withstand not only regular voltages and over voltages, such as lightning, but also various environmental stresses such as rain, snow and pollution.

Insulators are made from dielectric materials such as glass, ceramic and composite materials. An insulator ideally is a substance which does not allow electric charge to flow through it and has no effect on the electric fields [1.1]. Therefore, dielectric materials which have high electric resistance and dielectric constants are used as an insulator. Starting with simple glass and porcelain insulators, it has rapidly developed since early of the century. These types of insulators can be considered as classic insulators and may put into the same category called as ceramic insulators. From research and service experience [1.2], they are reliable and cost effective for major outdoor installations. Although porcelain and glass insulators have good performance over the years, their main disadvantages are due to their bulky size which make them difficult to install in remote area, vulnerable to vandalism and most importantly is their poor performance in polluted environment. The modern style of polymeric outdoor insulators was introduced to replace ceramic insulators. The reason of this replacement was not a failure of ceramic insulators but

the benefits offered by polymeric insulators over ceramic ones.

During recent decades, polymer insulators have been introduced and widely used due to their better pollution performance. Insulators made of polymer materials are often called composite or non-ceramic insulators. They are mostly preferred because of their superior insulation performance. The most important factor that determines the physical dimensions of outdoor insulators is their performance under pollution conditions. Depending on the pollution severity and the wetting conditions of the site, outdoor insulators need to have sufficient surface leakage length to ensure that dry band formation and surface arcing is minimized.

Pollution flashover is one of the main problems that endanger the reliability of an electric power system. The presence of contamination on the insulator surface, combined with highly humid and wet conditions such as fog, dew or rain, is particularly responsible for many insulator pollution flashovers [1.3]. With higher and higher voltages, the problem of insulator pollution flashover increases and the penalties increase sharply due to the damage to the equipment. Therefore, more and more attention must be paid to improve the pollution performance of insulators.

Reliability of the insulator is the most important property that must be taken into consideration whether it is a polymeric (composite) insulator or ceramic insulator. The good insulator should offer optimum electrical and mechanical strengths [1.4].

1.2. Problem statement

Most of the insulators being used nowadays are of the porcelain and glass insulators considering their well known field performance. However, there is favorable improvement in the use of non-ceramic insulators which have shown advantages compared to ceramic and glass insulators such as low weight construction, good performance in contaminated environments and easy handling. At higher voltages, electric fields can be high enough to cause surface flashover on porcelain/glass insulator, in case of polymeric type insulator damage to the insulator sheath due to the corona discharge.

The performance of polymeric insulators is important for both dry and wet condition. These insulators are exposed to various environmental stresses, which include many forms of precipitation, UV radiation and pollution. The voltage and electric field near conductors is much higher than other area of the insulator, which may lead to corona discharge and even flashover. The study of electric field on polymeric insulator when subjected to high voltage provides an important insight to improve the performance of the insulator. The design of a post insulator plays an important role in the insulator's performance. The performance and reliability of insulators may improve with the continuous improvement in the design. Several researchers have focused on the electric field optimal distribution along non-ceramic insulators string in order to reduce corona degradation. In addition, different techniques and insulators materials are developed. Among them, the installation of conventional corona rings. There are no specific standards for the design and placement of corona rings. Each manufacturer makes their own recommendations for the use of corona rings.

On the other hand, porcelain and glass insulators have outstanding insulating properties and weather resistance. However, they are lack in terms of their bulky size which becomes more difficult to install in remote area, vulnerable to vandalism. Moreover, their performances in polluted area are poor. This is due to its hydrophilic properties which enable water to easily form a continuous conductive film along the creepage path. This formation has encouraged the flashover and could cause the failure in power transmission lines.

In order to improve porcelain insulator performance, coatings were used to mitigate surface leakage current, surface discharges and reduce flashover occurrence on existing and installed porcelain insulators.

Optimized design of corona ring of the insulator and coatings are needed to ensure that the insulator can perform better and can provide longer service.

1.3. Objectives

The reliability of the insulator is the most important property that must take into consideration whether it is a ceramic insulator or polymeric insulator. The performance and reliability of insulators may improve with the continuous improvement in the design. The study of electric field on insulators when subject to high voltage provides an important insight to improve the performance of the insulator. The overall works of the project will stress on the optimization of the electric fields around the composite insulator and assess the performance of coating used to minimize leakage current on a new prepared porcelain insulator.

The principal aims of this research work are as follows:

1. To identify the optimum corona ring location installation to improve the electric field around the composite insulator.
2. To examine the effectiveness of a new developed nature-inspired optimization approache that links the electric field strength to the corona ring structure parameters.
3. To simulate and analyse electric field distribution around composite insulators.
4. To develop porcelain from locally available raw materials.
5. To improve the mechanical and dielectric properties of the porcelain insulator.
6. To evaluate the effect of coating on the performance of the prepared porcelain by comparing its leakage current suppression and its flashover voltage performance in comparison with non coated porcelain.

In order to achieve these aims, it was required to use computer techniques to evaluate the electric field and leakage current:

- COMSOL MULTIPHYSICS
- MINITAB
- The simulations are done by using Finite Element Methods (FEM).

1.4. Contributions of this thesis

The results of this project show that:

- The design parameters (corona ring height, corona ring radius and corona ring tube diameter) can be successfully optimized using Bat Algorithm;
- Maximum electric field on the live end side is importantly reduced around the composite insulator below the corona threshold;
- by glass addition, mechanical and dielectric properties of porcelain prepared at low temperature are improved;
- When applied to the porcelain insulator, coating minimized the leakage current over its surface.

1.5. Thesis Organization

The thesis contains six chapters.

Chapter 1 mainly focuses on the background of the project which is the problems faced by polymer insulators and the objectives that driven this project.

Chapter 2 provides a general overview of different outdoor insulators along with their role in the power system networks. Further, the factors accelerating insulation degradation for insulators either ceramic or non ceramic insulators are reviewed. The objectives of the research are presented.

This chapter providing also a review of the literature related to the work concept and the previous works by other researchers**.**

Chapter 3 reviews the influence of electric field on insulator performance and the techniques to optimize the electric field. The experimental methods, bat algorithm and Finite element method which are employed for insulator modeling to determine electric potential and field distribution along the non-ceramic insulator. Also, a model of polymer insulators is used to study the effect of optimization techniques employed.

Chapter 4 discusses the results of and analysis. One of the factors governing the electrical performance of polymeric insulator is characterized by its field distribution along their length. By improving the electric field distribution, it will help in enhancing their long term performance of insulator.

Chapter 5 discusses the possibility of developing porcelain using locally economic raw materials and studies the effect of coating on its electrical properties.

Chapter 6: presents the conclusions based on the findings from this study and outlines some recommendations for future investigations.

Chapter 02

High voltage insulators: A literature review

Chapter 02

High voltage insulators: A literature review

2.1. Introduction

The transport of electrical energy requires the use of high voltage lines. Overhead transmission lines are responsible for delivering electric power from generators to industrial and residential customers. The outdoor insulation is an important component of an electric power system. High voltage insulator plays an important role by serving two important functions [2.1]:

- They isolate the conductor electrically from the grounded tower structure and
- They serve as mechanical support for the conductor.

Nowadays insulators adopted for transmission/distribution are made of ceramic, glass or polymeric type. Porcelain and glass insulators have been used for a long time and there is considerable experience in manufacturing, installation and their field performance is well known. Composite insulator represents the last acquisition in the field of outdoor insulation; their use begun recently and knows an explosive development in the last years. Figure 2.1 shows the classification of the main types of insulators. Insulators are able to handle electrical and mechanical stresses when the line is energized. Most of the insulators have outdoor applications where they are subjected to environmental conditions such as moisture, high temperature, contamination, and icing. To choose the right type of insulator before the installation, the environmental conditions of the site have to be studied**.**

The aim of this chapter is to present both the advantages and disadvantages of each of porcelain and composite insulator and also focuses on the problems faced by these outdoor insulators. A review of the literature related to the work concept and the previous works by other researchers is presented.

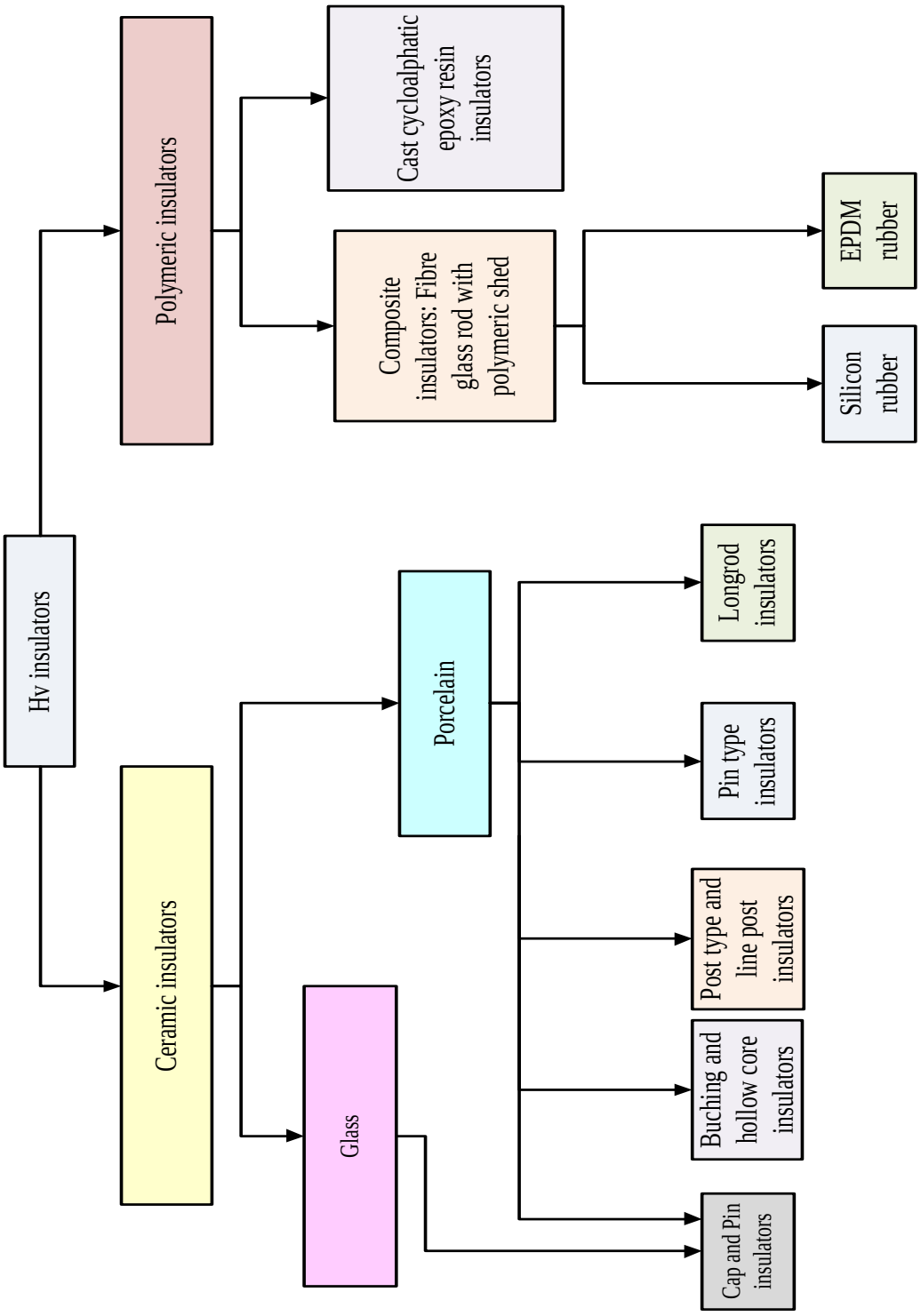

Figure 2. 1 Classification of power line insulators

2.2. Ceramic insulators

Ceramic insulators have been in use for more than 100 years [2.2]. They have proven to give excellent service history backed by years of manufacturing experience from reputable firms. The basic components used to make the ceramic insulator are clay, fine sand quartz and feldspar. The design and manufacturing of the ceramic insulators are being researched and improved in order to carter the needs of today's power distribution and transmission system. However, limitations are given on their sheds design to meet the surface electrical leakage distance needed for higher voltage transmission. Ceramic insulators present a high mechanical strength; they provide excellent resistance to material degradation cause by electrical stress and discharge activities. They demonstrated also a proven track record in various aspects of the insulation performance, particularly ageing and lifespan. Ceramic insulators can be divided into two types namely porcelain and glass which give a little difference regarding to their cost and performance. The design and manufacturing of the ceramic insulators are being researched and improved in order to carter the needs of today's power distribution and transmission system. However, limitations are given on their sheds design to meet the surface electrical leakage distance needed for higher voltage transmission. To smooth the surface of the insulator, glazing is used apart from increasing the mechanical strength and improving the surface's hydrophobicity [2.3].

2.2.1. Porcelain insulator

Earlier insulators are made from high quality glazed porcelain and pre-stressed or toughened glass. They are reliable and cost effective for major outdoor insulations. Porcelain insulators have a long journey of history. Initially, it has been used in the telegraph line. It has been in the market since 1910. A considerate number of these insulators are now in service in Algeria. They are by far the most commonly used outdoor insulator in service. The market of glass and porcelain insulators is still dynamic at the moment, with all the disadvantages related to their mass, the assembly and installation costs, and the fragility to mechanical stresses or vandalism. Figure 2.2 shows the structure of porcelain insulator.

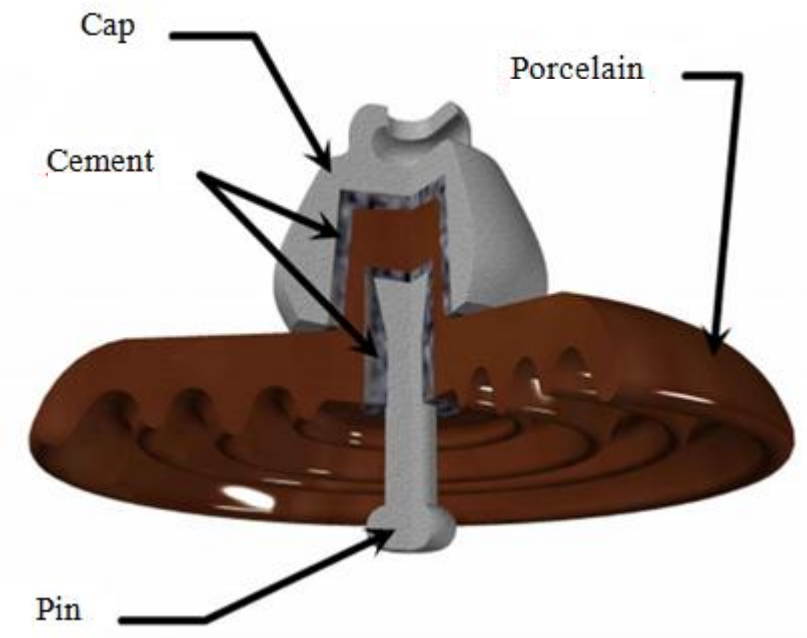

Figure 2. 2 Porcelain insulator structure

The different insulator configurations are:

- Cap and pin insulator
- Station post insulators
- Transformer and circuit breaker bushings

The large lifetime was the main reason for maintaining these types of insulators in operation, and, in certain cases, they represents the reliable solution. The weight of porcelain insulators used to be a problem, but the newer generations do not suffer from the weight issue anymore [2.4].

2.2.1.1. Mechanical and electrical performance of porcelain

Electrical properties of insulators come from the dielectric that they are made of. to study the electrical properties of porcelain insulators, dielectric properties of porcelain should be studied. There are two dielectric property measures; volume dielectric property and surface dielectric property [2.5]. The mechanical performance of insulators on the overhead transmission lines is as important as the electrical performance. These properties such as internal attachment of the metal pins to the dielectric are mainly concerned during the manufacturing process.

2.2.1.2. Failure of traditional porcelain

Porcelain insulators can fail due to a variety of reasons. Prior to the installation, some insulators might get physically damaged during shipping and transportation. Vandalism is another reason of porcelain insulators failure. It suffers from having hydrophilic surface properties, which means that water can easily form a continuous conductive film along the creepage path, thus allowing high surface leakage currents to flow on their wetted surfaces. Such currents cause dry bands at areas of high current density and lower wetting rates, which eventually cause surface arcing and frequently complete flashover of the insulator. Poor manufacturing and low quality control are two other reasons of porcelain insulators failures.

2.2.2.2.1. Radial Cracking

This type of failure has been attributed to cement growth phenomenon as depicted in figure2.3. Cement can absorb moisture during wet conditions, thus escalating the expansion process. Such radial cracking of porcelain disks can eventually result in internal puncture. There are no reliable statistics regarding the incidence of this type of failure but it is widely published that failure rates of porcelain insulators due to cement growth problems are generally associated with specific production batches [2.6].

Figure 2. 3 Radial cracking due to cement growth on porcelain insulators [2.6].

2.2.2.2.2. Hardware corrosion

Figure 2. 4 Corroded pin in porcelain insulator

Corona discharge can occur as a result of inappropriate electric stress grading at the cap of the insulator near the line end of a string of insulators. The metallic cap subsequently becomes exposed to corrosion as the discharge slowly degrades the protective galvanizing layer. Leakage current may also flow on the surface of the insulator during contamination and wet atmospheric conditions, which create a salt solution on the surface. Pin corrosion produced by electrolytic action can weaken the mechanical and cross-sectional strength of the pin. Damage of this sort can lead to an event as serious as conductor dropping. Figure 2.4 is an example of hardware exhibiting a very high degree of corrosion.

2.2.2.2.3. Insulator contamination

Under humid and moist conditions, surface contamination can cause flashover, which leads to system outages. Dust, rubber particles, sand, industrial pollution, and salt from the sea are some of the primary sources of insulator surface contamination. The deposition of contaminating particles is dependent on a number of factors, such as the speed and direction of the wind, the insulator type, and the orientation of the transmission line. Although, rain and heavy winds can wash away dust accumulated on insulators' surface; the dust can still be accumulated on the bottom ribs. The

orientation of the insulator string also influences the amount of contamination. Vertically oriented insulators, also known as an information, are prone to greater contamination than are V-shaped and horizontally oriented insulators. During moist conditions, the surface becomes highly conductive and the magnitude of the leakage current increases [2.7]. Dry band arcing that leads to flashover is the main problem under heavy contamination conditions [2.8]. Equivalent salt deposit density (ESSD) and non-soluble deposit density (NSSD) are the factors used for quantifying the level of contamination. ESSD is the amount of sodium chloride that, when dissolved, provides the same conductance as that of the natural deposit removed from the surface of the insulator divided by the area of that surface. NSSD is the amount of non-soluble residue removed from a given surface of the insulator divided by the area of that surface

2.3. Composite insulators

During recent decades, polymer insulators have been introduced and widely used at distribution voltage levels due to their better pollution performance. Composite insulators or known as non-ceramic insulators are widely used to replace porcelain and glass insulators in transmission lines. They were introduced in 1960's and start to be installed in United States in 1970's and since then, they become major option for utility companies around the world. Non ceramic insulators are usually made up of silic one rubber, Poly-Tetra -Fluoro-Ethane (PTFE) or Ethyl Propylene Diene Monomer (EPDM) rubber.

Figure 2.5 shows the structure of polymeric insulators with all three components flanges crimped to a fibre reinforce rod (FRP) encapsulated within weather shed polymeric housing.

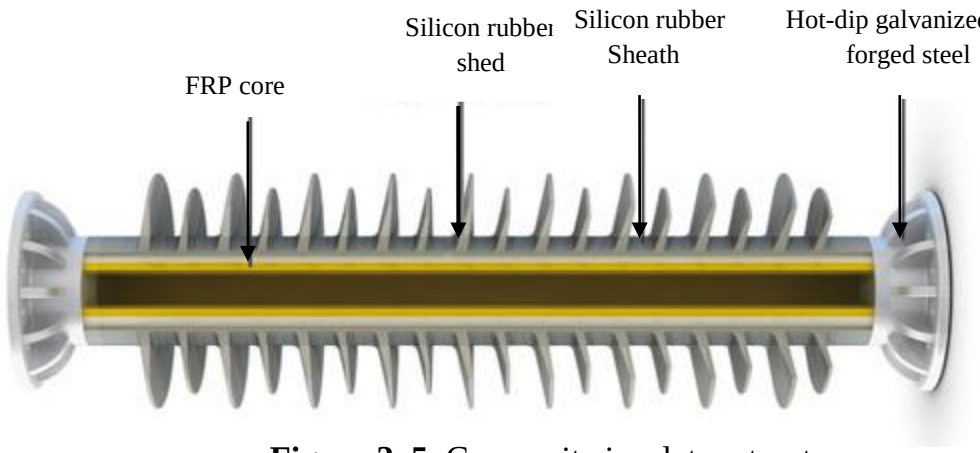

Figure 2. 5. Composite insulator structure

Composite Insulators consist of three parts :

- Steel/aluminium end fitting terminals to support mechanical loads on conductors,
- Fiber reinforced rod (FRP) core to carry mechanical load and insulation between two terminals,
- Polymeric weather shed housing to protect the FRP rod against environmental influences, external pollution and humidity..

With the improvements in design and manufacturing, polymeric insulator becomes more attractive to the utility companies around the world to use it. The developments of new materials continue to grow with a number of new insulating materials that have been developed.

2.3.1. Advantages of composite insulator

Composite insulators become popular due to various advantages offered. Polymeric outdoor insulators made of polymeric material, especially silicone rubber, exhibit excellent electrical performances under moderate to heavily polluted environments [2.9]. In a wet atmosphere, water tends to bead up on the polymeric surface, thus reducing the leakage current and the probability of dry band formation, which

consequently results in reduced flashover voltages. Interestingly, this property can also be transferred to an overlying pollution layer [2.10] enabling improved pollution performance for insulation systems in highly contaminated regions such as coastal and industrial areas. Even though silicone housing can temporarily lose its hydrophobicity under severe conditions, the materials have been reported [2.11, 2.12] to be able to regain hydrophobicity after a sufficient resting period with the absence of discharge activity. Polymeric insulators offer significant weight reduction compared to the corresponding ceramic insulation systems [2.13]. There is less need for strong heavy support and cranes for installation, which results in easier handling and substantial savings in overall installation, operation and maintenance costs. In addition, voltage up rating and compact transmission tower design for Ultra-High Voltage (UHV) distribution networks can be practically realized with polymeric insulators. Polymeric insulators have a high mechanical strength to weight ratio that allows for longer spans and less expensive tower structures. They provide improved mechanical strength under bending, deflection and compression stress. It has been reported [2.14-2.16] that polymeric insulators passed mechanical tests under extreme conditions without any permanent damage. Insulation housing with elastic properties also helps to prevent the risk of breakage during transportation or vandalism from gunshots that could lead to cascading failure as was experienced with ceramic insulators. In addition, complex weather shed designs are feasible and easily moulded using polymeric composite material.

2.3.2. Degradation of composite insulator

Despite the abovementioned advantages, polymeric outdoor insulators however suffer from a problem of material deterioration as shown in figure 2.6, known as ageing. This is primarily due to concurrent stresses; environmental, electrical and mechanical stresses encountered in diverse range of service conditions [2.12].

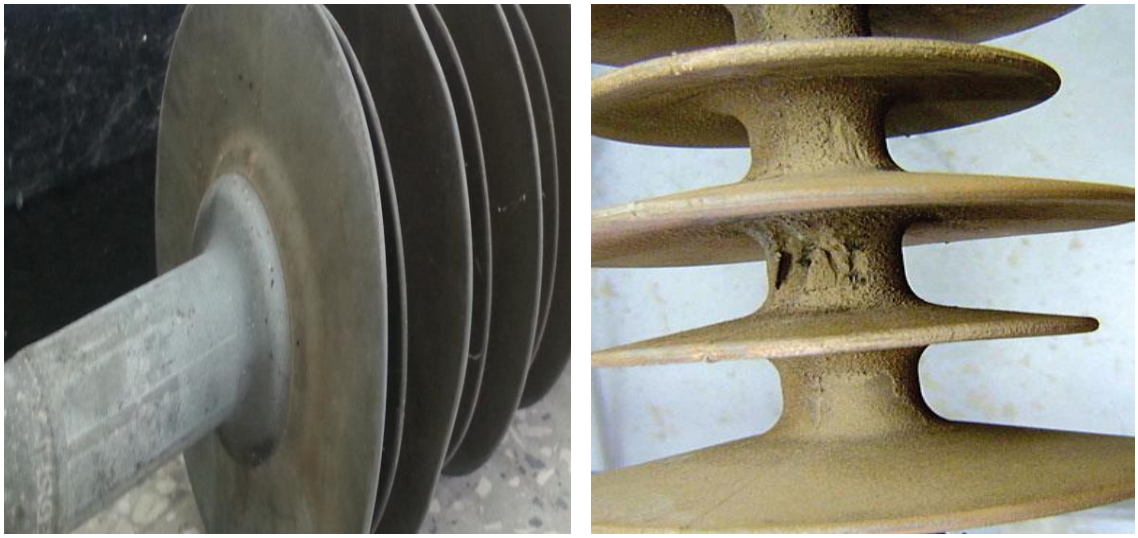

Figure 2. 6 Degradation of composite insulator

2.3.2.1 Electrical stress

The electric field distribution is not uniform along high voltage insulator where the highest field regions are at the high voltage end terminals and core areas. Electric discharges in the form of corona, dry band arcing and flashover will occur due non-uniform and high fields on the insulator [2.17, 2.18].

2.3.2.1.1. Corona discharges

Corona is phenomenon that has the capability for degrading insulators, and can cause systems to fail. It is also known as partial discharge where type of localized emission resulting from transient gaseous ionization in an insulation system when the voltage stresses or voltage gradient exceeds its critical value. There are three types of corona which are plume, brush and glow. Plume is the most spectacular corona and it is called as so because of its general resemblance to a plume. It also has audible manifestations which are rather intense snapping and hissing sound. Brush corona is a streamer projecting radially from the conductor. The audible manifestation that is associated with brush corona is generally a continuous background type of hissing or frying sound. The glow corona is a very faint, weak light which appears to hug the conductor‟s surface and there is generally no sound that is associated with it.

Corona discharges occur at the insulator surface when the electric field gradients on the surface exceed the air breakdown strength. Corona formation is dependent upon atmospheric conditions such as air breakdown, humidity and insulator geometry. Corona cause radio and TV interference, noise, ozone, and energy loss. Corona accelerates the polymer aging by producing ozone and ultra-violet light [2.19, 2.20].

The effects of corona in transmission lines can be summarized as below:

- a violet glow is observed around the conductor.
- produces a hissing noise,
- produces ozone which can be readily detected by its odor,
- the glow is maximum over rough and dirty surfaces of the conductor,
- accompanied by a power loss
- charging current under corona condition increases because the corona induces harmonic currents.

Figure 2.7 shows corona discharge activity.

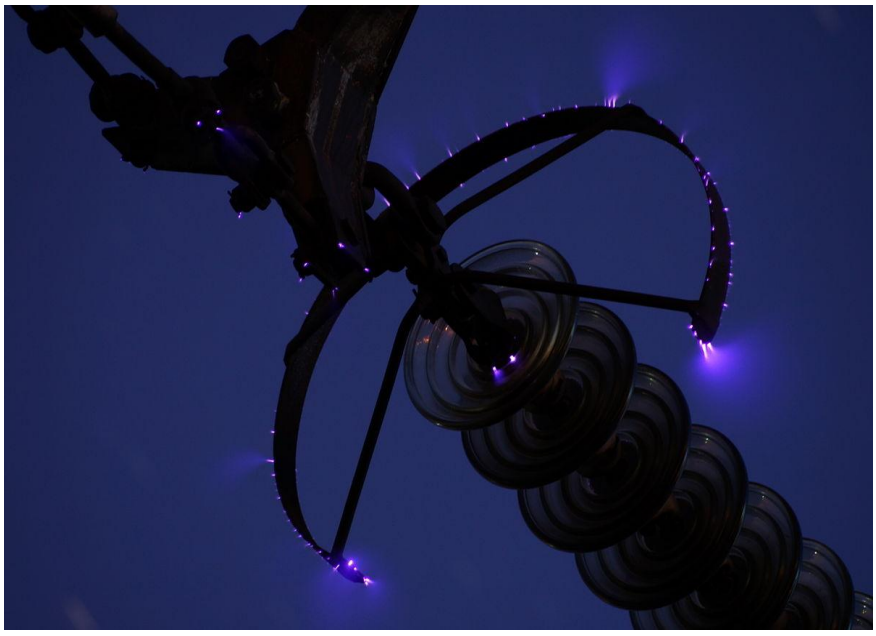

Figure 2. 7 Corona discharge

2.6.2.1.2. Insulator Flashover

Active discharge activities from corona, water droplets and dry band arcing generate considerable thermal heating that cause further drying on the insulator surface. Electric discharges that are short at the beginning gradually elongate as the dry regions widen. Under favourable conditions, successive discharges may extend over multiple dry bands and join with other electric discharges that can eventually lead to a complete flashover [2.21]. In the event of prolonged wetting and heavy rain, polymeric weather sheds can be bridged by the water stream. The role of the creepage path along the insulator surface in limiting leakage current in this case is not effective. Water cascading promotes inter-shed arcing, and can easily lead to insulator flashover even at lower pollution severity. In addition, the flashover can occur at much lower voltage levels than the rated value. Polymeric insulators with an alternating shed design can be a good practice to minimise the probability of water bridging the weather sheds [2.22].

2.3.2.2. Environmental Stress

2.3.2.2.1. Pollution

Environmental pollution is one of the major threats to polymeric outdoor insulation systems. Depending on the location and the surrounding area, insulators encounter different types of pollutants: sand and soil elements in desert and mining areas, metallic and chemical substances in industrial and agricultural lands, and salt particles in coastal regions. Deposits of these airborne particles gradually form a solid pollution layer on the insulator surface, which has a significant effect on both short and long-term performance of the insulation system. Electric field distribution is highly distorted by a non-uniform pollution layer on the insulator surface [2.23]. This contributes to localised field enhancement which could trigger corona and random partial discharges over the polymeric surface. In the presence of moisture, soluble contaminants dissolve in water establishing a conductive pollution film that allows the flow of leakage current along the creepage distance, increasing the risk of damaging dry band discharges. In some cases, the insulator may also be subjected to conductive

moisture sources such as salt water, industrial acid fog, chemical mist and fertilizers, crop spraying and acid rain. These electrolyte-type pollutants can cause instantaneous leakage current and trigger flashover voltage even without the accumulation of pollution on the insulator surface [2.24, 2.25].

2.3.2.2.2. Ultra-violet radiation

Polymeric insulators installed for outdoor applications are open to ultra violet (UV) radiation from sunlight. The surfaces are attacked by UV photons that release substantial energy to break crosslink chains or individual molecules within the base matrix [2.26]. Polymeric compounds for high voltage insulation housing contain impurities such as vulcanizing agents, catalysts and fillers that are vulnerable to UV radiation due to their weak molecular bond. The presence of these additives weakens the strong carbon-based polymer i.e. C-C, C-H and Si-O bonds, thereby reducing the resistance of polymeric weather sheds housing to UV exposure. Thermal and photooxidation cause chain scissions that destroy hydrophobicity and lead to surface cracking and degradation of the polymeric material [2.27]. The condition is exacerbated in high temperature regions such as deserts. From service experience reported in [2.28], polymeric surfaces that faced the sun appeared to be less hydrophobic and showed chalking and discoloration compared to those on the shaded side.

2.3.2.3.Mechanical Stress

An important function of the line insulator is to transfer mechanical support from the transmission tower to hold the heavy overhead conductor well in the air. Line insulators experience vertical load (tensile and compression stress) or cantilever/transverse load (bending stress) depending on system configuration and tower structure. Suspension insulators, when first installed on transmission towers, for example, encounter constant axial stress by the loading of bundle cables in which the weight could reach up to several tonnes for UHV transmission systems. Over time, continuous strain could gradually deteriorate and weaken the joint between the core

and the terminal, which will eventually result in the mechanical failure of the polymeric insulators. Extra mechanical stress may also develop when strong winds move the line, causing oscillation. The consequent vibrations can cause the formation of fissures at the joint interface between the core and the metal flanges. In some cold-climate countries, ice accretion on both the conductor and weather sheds housing could generate additional loading stress on the polymeric insulator. In hot desert regions, the average temperature can easily reach 40°C during the day, and drop below 10°C at night. This considerable change in ambient temperature results in a cyclic process of thermal expansion and shrinkage that can loosen the connection at the core-end fitting interface, affecting the mechanical strength of the polymeric insulators.

In the face of these problems, insulation materials must have some specific properties. Such as,

1. It must be mechanically strong, so that to carry tension and weight of the conductors.
2. The dielectric strength must be very high, so that to withstand the high voltage stress.
3. The insulation resistance must be high, so that to prevent the leakage current to the earth.
4. It must be free from unwanted impurities and should not be porous.
5. It should be non-hydroscopic.
6. Its physical and electrical properties must be less affected due to change in temperature.

Table 2.1 shows the advantages of composite materials (SIR) over ceramics.

Table 2.1 Advantages of composite materials (SIR) over ceramics

Advantages of composite materials (SIR) over ceramics		
Criteria	Ceramic	Composite (SIR)
weight	Heavy	Leger (90% Lighter)
transport	Expensive and risky of breakage	Resistance to shocks
installation	Risky, expensive, need for more labor	Easy and economic
vandalism	Susceptible	Very resistant
breaking behavior	Fragile shock and vibration / brittle fracture	Insensitive to shock
resistance to electric arcs	low	High
erosion resistance	Very low	High
dielectric strength	lower	Exellente
Pollution behavior	Facilitated affected	Not affected
hydrophobicity	Hydrophilic-formation of water film on the surface that increases the risk of electric arc	Hydrophobic-formation of water droplet
contamination	Presence of salute, sand, salt and snow	Absente
maintenance	Cleaning	No maintenance
conception	Limited flexibility design - wider and heavier structure	Gain weight, size and cost

2.4. The evolution of the use composite insulators according to GRTE

In Algeria, Composite insulators introduced since 2000. They are used in 60 and 220 kV transmission line. Figures 2.8 and 2.9 represent the evolution of the use composite insulators and evolution of the installation of polymeric insulator chains with respect to the total length of the network in Algeria, respectively. It is noted that the percentage of the installation of polymeric chains is very low as shown in figure 2.9 .it begin by installing 330 insulating chains. This number is increased 4400 in 2002. Due to vandalism acts, the installation of composite insulator is decreased in 2006 and 2007 before it started to rise again in 2008 by installing 3801 insulator chains.

A high voltage level is introduced by SONELGAZ (the Algerian society of electricity and gaz) due to the increasing demand for a continuous electric power supply and high quality service. For this, M. Bouhaouche et al. [2.29] proposed integring composite insulators in the 400 kV transmission lines which are recently begin in service with the objective of improving Electric field distribution. Reported results confirm that to use

of this type of insulators instead the glass insulation will be useful on the 400 Kv in transmission in Algeria. Experimental test under dry, clean and uniformity polluted surface conditions show also that the maximum electric field gets its minimum value when composite is used compared the glass one.

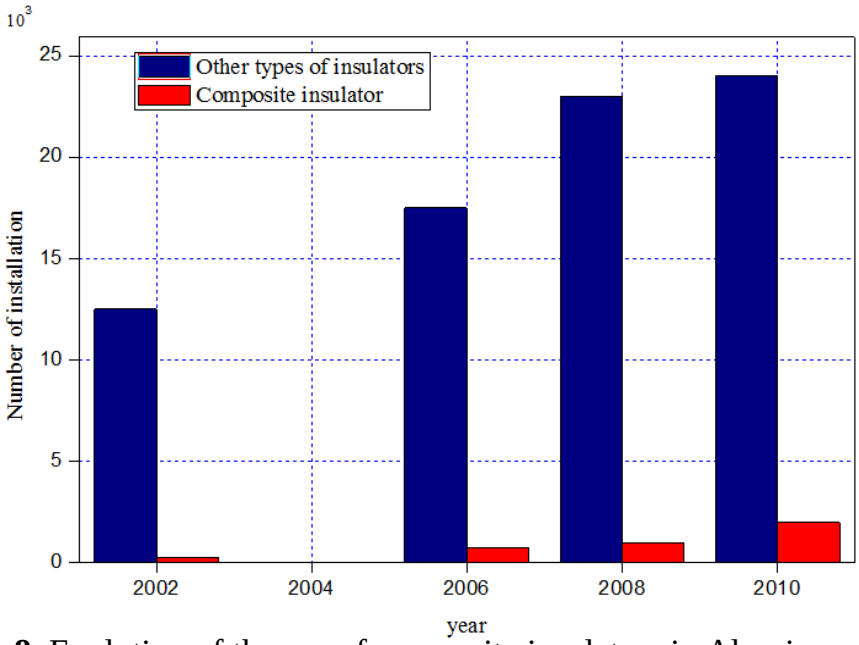

Figure 2. 8 Evolution of the use of composite insulators in Algeria according to GRTE

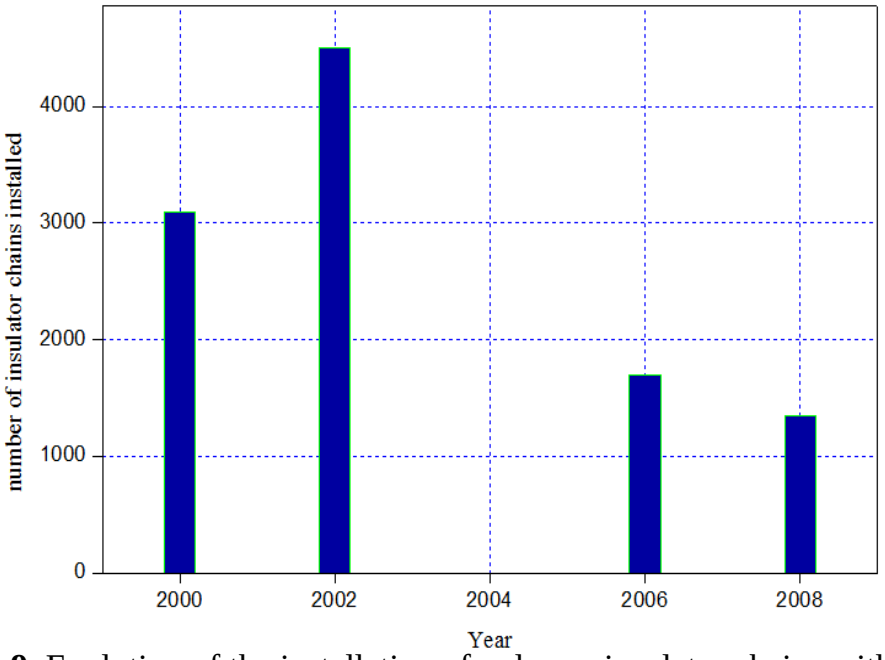

Figure 2. 9 Evolution of the installation of polymer insulator chains with respect to the total length of the network

2.5. Literature survey

The following paragraphs show some of the project referred in completing this thesis.

Yang Qing et al. proposed a new optimization Method on Electric Field Distribution of Composite Insulator [2.30]. The results show that by his proposed method, the electric field distribution near the ends of composite insulators is significantly reduced, which can prevent the partial discharge and the aging of the composite material.

W. Sima et al. studied the optimization of corona ring design for long-rod insulators using FEM based computational analysis [2.31]. This research presents a method to optimize the location and the dimensions of the corona ring for transmission line composite. The procedure used to optimize the corona ring design, which handles more than one parameter, has been verified with examples that have an analytical solution or known optimal values.

D. Cruz Dominguez used two electrical stress grading techniques for non-ceramic insulators. In both techniques some parameters were optimized for a 115 kV non ceramic insulator with the objective of optimizing the electric field grading systems in non-ceramic insulators [2.32].

Edward Niedospial et al proposed a study about the application of corona and grading rings for composite insulators [2.33]. The addition of a corona ring to a polymer insulator will improve the insulators performance, but it must be the right ring used for the right reasons to realize the benefits.

E. Akbari et al. analyzed the effects of disc insulator type and corona ring on electric field and voltage distribution over 230-kv insulator string by numerical method [2.34]. According to the results, distribution of voltage and electric field over insulator strings without corona ring and the degree of improvement of voltage distribution using corona ring depends on insulator material and profile, as well as the corona ring configuration parameters.

Suat İlhan [2.35] studied the effect of corona ring application to the electric field stress and potential distribution along insulator. He found that the usage of corona ring will significantly decrease the voltage percentage. That is, potential distribution will be more uniform with the help of corona ring. Furthermore, the maximum electric field strengths on the live end side will importantly decrease with the usage of corona ring. Moreover, the electric field on the corona ring surface can also change with the design parameters.

Zhao [2.36] studied the electric field and potential distribution along non-ceramic insulators. Results showed that the maximum electric field strength decreases when the length of the conductor increases; and the tower structure in the vicinity of the insulator and the diameter and the location of the grading ring are important in determining the maximum E-field.

S. M Braini investigate and assess on his thesis titled “coatings for outdoor high voltage insulators” the performance of different coating materials used to minimize leakage current, reduce the heat and eliminate flashover in high voltage insulators that run in polluted environments. He found that with a nano-coating applied to the porcelain insulator, the surface becomes highly hydrophobic. It suppressed leakage current and reduced the energy dissipated over, the surface but the nano-coated insulator had a lower flashover voltage than an uncoated porcelain insulator having similar geometry. The nano-coated insulator lost its hydrophobicity showing a water film on its surface when exposed to fog application as seen through polluted wet tests [2.37].

2.6. Conclusion

This chapter allowed us to present the notions useful to the good conduct of this research project. We have discussed about the overview of benefits and limitations of polymeric and ceramic insulators also, a literature survey related to the work concept and the previous works by other researchers is presented**.**

Chapter 03

Optimization of Corona Ring Design for Improved Electric Field Performance

Chapter 03

Optimization of Corona Ring Design for Improved Electric Field Performance

3.1. Introduction

The performance of composite insulators depends on E-field distribution along the surface of insulators. It is essential to understand the E-field distribution along the length of insulator. The electric field distribution of non-ceramic insulator is different compared to porcelain insulators. Generally the electric field distribution of a non-ceramic long insulator is more nonlinear than that of a porcelain insulator. The reason is that there are no intermediate metal parts for a non-ceramic insulator.

The electric field strength on non-ceramic insulators needs to be controlled for the following reasons [3.1]:

• To prevent significant discharge activity on the surface material of non-ceramic insulators under both dry and wet conditions which may result in the degradation of the pollution performance of non-ceramic insulators.

• To avoid the internal discharge activity inside the fiberglass rod and the sheath rubber material that could result in mechanical or electrical failure of non-ceramic insulators.

• To prevent corona activity from the metal hardware or the non-ceramic insulator, which may cause radio interference and acoustic emissions.

3.2. Field Optimization techniques

Surface discharge process and continuous corona on the insulator contribute to generate degradation. It causes the reduction of the long term performance of composite insulators [3.2].To minimize this phenomenon, many methods of optimizing electric field distribution on composite insulator are discussed, such as modifying insulator weather sheds profile, applying non-linear field grading material as insulator fillet, or by installing corona rings. The last one is discussed in many previous studies [2.33-2.36]. Each of these studies confirmed that the usage of corona ring in a composite insulator will significantly decrease the electric field distribution. Several studies have been carried out to optimize the design of the corona ring because there is no available standard for its design and placement.

3.2.1. Corona Ring Installation

The electric field (E-field) distribution along the insulator is an important factor which impacts the life expectancy as high E-field can result in a discharge activity which in-turn can damage the insulating material resulting in failure [3.3]. In order to prevent or reduce the discharge activity, it is important that the utilities ensure that the electric field distribution is managed to keep maximum recorded values below threshold levels. To this end, corona rings are applied. The function of the corona ring is to grade or disperse the electric field gradient, thus reducing the voltage stress on the rubber housing near the line end fitting. The corona ring can be attached to the composite insulator directly or as part of the hardware. When applied as part of the hardware, the grading device is commonly referred to as a Corona Shield [3.4]. Insulator strings (Figure3.1) are equipped with auxiliary apparatus to provide connections and to improve insulator string performance. Both the geometry and the design of these apparatus are dependent on the transmission voltage level and the insulator type.

Figure 3. 1 Insulator string equipped with corona rings

Corona rings are the auxiliary fittings used with the insulator strings and can be used with any type of insulator. They improve the performance of insulator string in several ways:

- They reduce corona discharges on the terminals of the insulator string,

- They reduce the audible noise, radio interference (RI) and television interference (TVI) voltages,

- They can adjust the voltage distribution along the insulator string; reducing the maximum electric field strength [3.5].

The corona rings are also used for arc protection. For insulator flashovers, it is necessary to keep the power arc away from the insulator and to fix the root of the arc on the ring to avoid heating of the end fittings. Moreover, some testing experience has demonstrated that certain design of corona rings have a favorable effect of preventing dry band arcing near the end fittings of the composite insulators in polluted conditions [3.6].

In addition, corona rings can affect the AC, lightning impulse, switching impulse withstands/flashover levels of the insulator strings.

Many research works have been carried out to optimize the design of the corona ring because there is no available standard for its design and placement [3.7-3.9].

In [3. 7, 3.8], particle swarm optimization (PSO) algorithm was used and a relationship between the maximum E-field and the geometrical parameters of the corona ring was established. A similar study was done in [3.9], in which the above relationship was modeled and optimized using the response surface methodology and reported results show the influence of the ring tube diameter on the E-field distribution. In [3.10], the authors evaluated the use of corona rings on 115 kV non-ceramic insulators to reduce the maximum electric field on its surface based on the geometry modifications. It is found that the tangential electric field can be reduced with the adequate geometry and relative permittivity value of the housing material. Diako et al. [3.11] have applied Neuro optimizer (NO) and genetic algorithm (GA) methods to study and compare the impact of distance and the size of the corona ring, on the magnitude and distribution of electrical potential across the polymer insulators.

In fact, there is many optimization problems related to design high voltage insulation used the meta-heuristic approaches to minimize different proposal mathematical models of the objective functions, in presence of various constraints. Based on a previous literature survey, and to the author's knowledge, no work has been conducted to optimize corona ring design using Bat algorithm.

3.3. Insulator model

This chapter presents the proposed corona ring optimization for a composite insulator which consists of fiberglass rod and metal end fitting. The insulator profile is shown in Figure. 3.2. The numerical values of the basic parameters are listed in table 3.1, were P is the dry arcing distance, L is the creepage distance, d_1/d_2 is the sheds spacing, N_1/N_2 is the number of sheds, D_1/D_2 is the shed diameter and d is the rod diameter, respectively. The insulator unit contains 25 large and 25 small sheds.

Table 3. 1 Design parameters of studied composite insulator in mm.

N_0	P	L	d_1/d_2	N_1/N_2	D_1/D_2	D
A	2037	6510	36/75	25/25	140/110	25

Relative permittivities of the silicone rubber and the fiber glass rod are assumed to be 4.3and 7.2 respectively [3.9]. The composite insulator model as shown in Figure. 3.2 was created using COMSOL Multiphysics. In order to make the simulation faster without affecting results accuracy, insulator model is simplified into a two-dimensional (2D) problem.

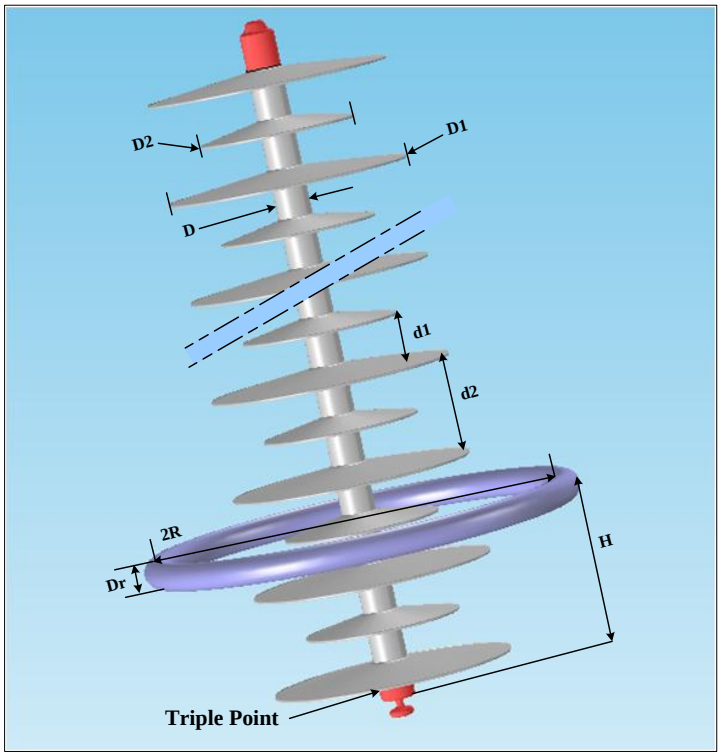

Figure 3. 2 Model of composite insulator and corona ring.

3.4. Bat Algorithm

This section is discussing on how the work is carried out in order to obtain the aims of this project. We presented a general review on Bat algorithm. It is proposed to determine the optimal design of corona ring. A composite insulator is modeled using FEM to study the E-field distribution on its surface. The main and interaction effects of the corona ring parameters have been evaluated using the variance analysis technique using the MINITAB software in combination with COMSOL.

Nowadays, many optimization issues in engineering have been solved based on animals swarm behaviors, such as bees, particles, fishes and more others. These animals, in nature, basically cooperate to solve a big problem for the swarm which is found in foods; from this idea researchers inspired their optimization algorithms such as PSO, BSO, etc.

Bat algorithm (BA) is a new nature-inspired algorithm developed by Xin-She Yang [3.12] in 2010, considered as a new metaheuristic algorithm based on Bat behavior. In this chapter, a short review of the natural and biological behavior of bats is described. Then, the original Bat algorithm and its several variants are described. Finally, a review of BA applications is presented.

3.4.1. Natural Bat behavior

The BA is formulated based on the studies made on the biological behaviors of bats, from which the fascinating concept of echolocation in the form of a sonar system is identified. The bats use this technique to move around, find preys, detect objects, and locate their crevices in the dark [3.13, 3.14]. In the process of echolocation, bats create pulses that vary depending on their hunting strategies and the species. These pulses are generated within a high-frequency range of 25–100 kHz, and the pulses can be differentiated from the other sounds in the ambient environment. Where, each pulse last's up to 10 ms and each ultrasonic burst may last for 5–20 ms, and bats emit approximately 10–20 of such sound bursts every second [3.13, 3.14]. The pulse emission rate increases depending on how close the bats are to the prey. These emitted pulses are in the ultrasonic spectrum and can vary from the loudest range (up to 110 dB and occurs when they are seeking for a prey) to the quietest range (occurs when they are homing toward the prey). This procedure shows the great communication and signal processing of the bats in their prey searching behavior [3.13, 3.15]. Figure 3.2

illustrates the principle of the Echolocation behavior in bats, where the blue pulses represent the sonar waves that are sent by the bat and where the red lines indicate the reflected signal that is sent back from the prey or the obstacle. This significant

behavior used by the bats is mathematically modeled as an optimizing algorithm called the bat algorithm. It has been developed to behave as a band of bats tracking prey/foods using their capability of echolocation.

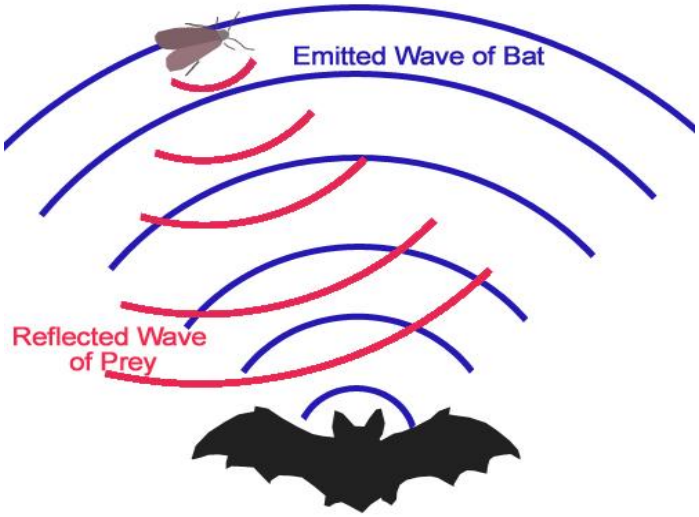

Figure 3. 3 A bat use echolocation to determine prey.

For this aim, Yang has proposed three main rules to simulate micro-bats [3.16] behavior, as follows:

1) All bats use echolocation to sense distance, and they also guess the difference between food/prey and background barriers in some magical way.

2) Bats fly randomly with velocity V_i at position X_i with a fixed frequency f_{min}, varying wavelength λ and loudness A_0 to search for prey. They can automatically adjust the wavelength (or frequency) of their emitted pulses and adjust the rate of pulse emission $r \in [0, 1]$, depending on the proximity of their target.
3) Although the loudness can vary in many ways, we assume that the loudness varies from a large (positive) A_0 to a minimum constant value A_{min}. Each step of basic bat algorithm is explained below:

a) Initialization of Bat Algorithm

Initial population is generated randomly for number of bats. Each individual of the population consists of real valued vectors with dimensions. The following equation is used to generate the initial population.

$$x_{ij} = x_{\min j} + rand\,(0.1)(x_{maxj} - x_{minj}) \quad (3.1)$$

Where *i=1,2……., n; j= 1,2…..,d;*The x_{maxj} and $x_{\min j}$ are the upper and lower boundaries for dimension *j*.

b) Solution, Frequency & Velocity

Step size to generate new solution in Bat algorithm is defined by the frequency. The pulse frequency is an arbitrary value for each solution, ranges between upper and lower boundaries f_{min} and f_{max}. The frequency controls the pace and range of the movement and updates the bat position and velocity. The velocity and position of bat is updated using the following equations [3.17].

$$f_i = f_{min} + (f_{max} - f_{min}) * \beta \quad (3.2)$$

$$v_i^t = v_i^{t-1} + [v_i^{t-1} - x^{best}]f_i \quad (3.3)$$

$$x_i^t = x_i^{t-1} + v_i^t \quad (3.4)$$

Where β indicates randomly generated number, f_i is the frequency generated for solution i, v_i represents the new velocity for solution *i*, x^{best} represents the global best solutions in the population. In *r* (pulse rate) probability, a solution is selected amongthe best solution and random walk is applied in order to increase exploration. Thus a new candidate solution is generated.

$$x_{new} = x_{old} + \varepsilon A^t \quad (3.5)$$

Where $\varepsilon \in [-1,1]$is a random number and A^t is the average loudness of all the bats at time t. The new solution replaces the old one when the loudness criterion is satisfied and the new solution is better than the old one [3.17].

c) Loudness and Pulse Emission Rate

Basically, as bats approach to their preys, they need to update the loudness *A* and rate *r,* where the pulse emission rate increases while loudness usually decreases, as follows [3.18]:

$$A_i^t = \alpha \tag{3.6}$$

$$r_i^t = r_i^0(1 - r^{\gamma t - 1}) \tag{3.7}$$

$$x_i^t = [x_1^t, x_1^t, \ldots . x_i^t, \ldots . x_{Bn-1}^t, x_{Bn}^t \quad] \tag{3.8}$$

Where α, γ are constants, r_i^0 and Ai are factors which consist of random values and A_i^t can typically be [0, 2], while r_i^0 can typically be [0, 1]. Bat algorithm balance between global and local search by adjusting the loudness and pulse rate. However, there are so much loudness and pulse rate combinations, that it is hard to choose the most proper one for different problems.The following figures show the characteristics of equation (3.6) and (3.7) as the iteration proceeds.

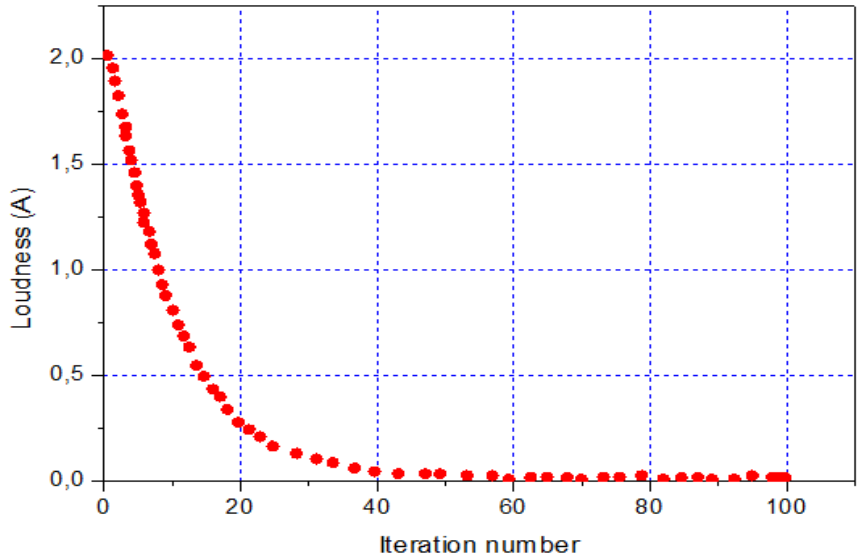

Figure 3. 4. Loudness (A)

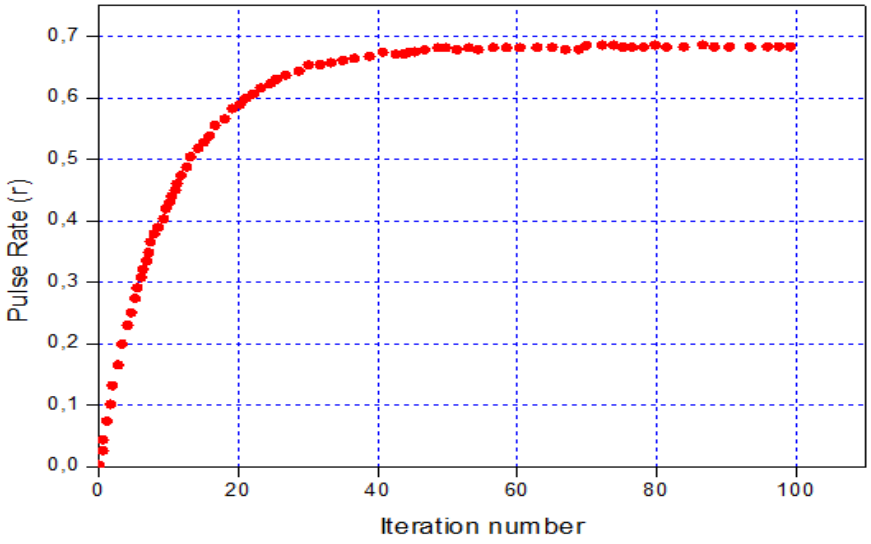

Figure 3. 5 Pulse Emission Rate (*r*)

The pseudo-code of the Bat algorithm is given as follows:

Algorithm 01: Bat algorithm

1: **Input:** empirical parameters: MaxIter, P.

2: **Output:** the best solution x_{best} and its corresponding value f_{min} = min ($f(x)$).

3: Objective function $f(x_i)$; $x_i = (x_{i1}; x_{i2}; \ldots; x_{ip})^T$;

4: Initialize the bat population x_i and v_i for (i = 1, 2,.., p) ;

5: Define pulse frequency f_i at x_i ;

6: Initialize pulse rates r_i and the loudness A_i ;

7: **while** (t < Max number of iterations) **do**

7.1: Generate new solutions by adjusting frequency and updating velocities and locations/solutions using equations (2) to (4).

7.2: **if** ($rand > r_i$) **then**

7.2.1: select a solution among the best ones ;

7.2.2: Generate a local solution around the selected best solution ;

end if

7.3: Generate a new solution by flying randomly

7.4: **if** ($rand < A_i$ and $f(x_i) < f(x^*)$) **then**

7.4.1: Accept the new solutions

7.4.2: Increase r_i and reduce A_i

end if

7.5: Rank the bats and find the current best x^*;

end while

8. Post-process results and visualization.

3.4.2. Variants of Bat Algorithm

The standard bat algorithm has many advantages, and one of the key advantages is that it can provide very quick convergence at a very initial stage by switching from exploration to exploitation. This makes it an efficient algorithm for applications such as classifications and others when a quick solution is needed. However, if we allow the algorithm to switch to exploitation stage too quickly by varying A and r too quickly, it may lead to stagnation after some initial stage. In order to improve the performance, many methods and strategies have been attempted to increase the diversity of the solution and thus to enhance the performance, which produced a few good and efficient variants of bat algorithm. From the literature survey, we found the following bat algorithm variants:

- Fuzzy Logic Bat Algorithm (FLBA) : Khan et al. (2011) presented a variant by introducing fuzzy logic into the bat algorithm, they called their variant fuzzy bat algorithm.

- Multiobjective bat algorithm (MOBA): Yang (2011a) extended BA to deal with multiobjective optimization, which has demonstrated its effectiveness for solving a few design benchmarks in engineering.

- K-Means Bat Algorithm (KMBA) : Komarasamy and Wahi (2012) presented a combination of K- means which is one of the mainly popular clustering methods and bat algorithm. The proposed combination have been utilizes the concepts of Bat optimization techniques and K-Means Algorithms for efficient clustering. Clustering is one of the popular data mining methods aiming at representing large dataset by a collection of cluster.

- Chaotic Bat Algorithm (CBA) : Lin et al. (2012) presented a chaotic bat algorithm using L´evy flights and chaotic maps to carry out parameter estimation in dynamic biological systems.

- Binary bat algorithm (BBA): Nakamura et al. (2012) developed a discrete version of bat algorithm to solve classifications and feature selection problems.
- Differential Operator and L´evy flights Bat Algorithm (DLBA) : Xie et al. (2013) presented a variant of bat algorithm using differential operator and L´evy flights to solve function optimization problems.
- Improved bat algorithm (IBA) : Jamil et al. (2013) extended the bat algorithm with a good combination of L´evy flights and subtle variations of loudness and pulse emission rates. They tested the IBA versus over 70 different test functions and proved to be very efficient.

3.4.3. Bat flowchart

The following describes the execution steps of the standard bat algorithm;

Step 1: initialize the bat population *t*, the pulse frequency, after that we define the pulse rates.

Step 2: Update the velocities to update the location of the bats, and decide whether detonate the random walk process.

Step 3: Rank the bats according to their fitness value, find the current near best solution found so far, and then update the loudness and the emission rate.

Step 4: check the termination condition to decide whether go back to step **2** or end the process and output the result. Detailed steps about the standard bat algorithm are presented in figure 3.6.

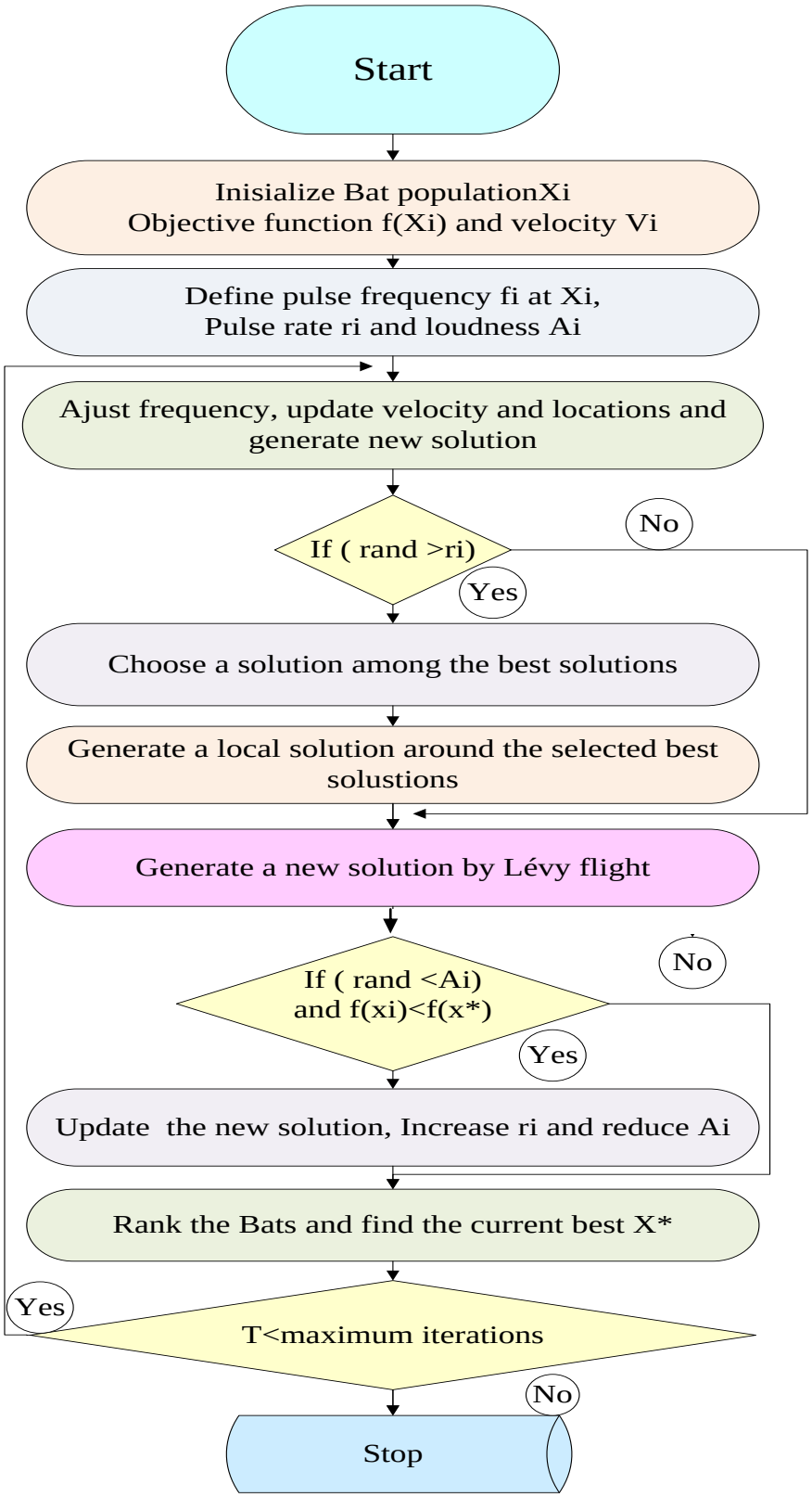

Figure 3. 6 Flowchart of Bat Algorithm

3.4.4. Bat algorithm applications

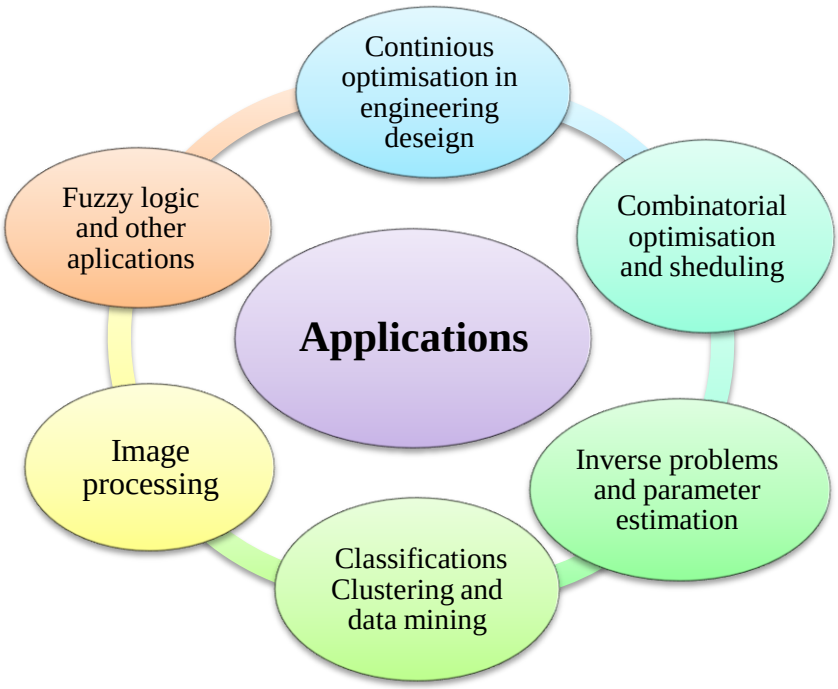

Figure 3. 7 Bat algorithm applications

Bat algorithm has already proven its efficiency since its first application in continuing optimization [3.16]. This makes researchers use bat algorithm to solve several problems in many fields and disciplines, such as: optimization, image processing, scheduling, data mining and others, as illustrated in Figure 3.6. In the following, we detailed the most works that use bat algorithm.

3.4.4.1. Optimization

Optimization is the biggest discipline that uses nature inspired algorithms to find the optimal solution for each problem. It has four main types: Continues, Con- strained, Unconstrained and Multi-objective optimization, where bat algorithm has been applied with success. In [3.13], Yang has put the original BA in application for continues optimization with several benchmark functions. This work proves the improvement of convergence rate against GA and PSO. This rate has been more improved in another work. In which BA was hybridized with differential evolution strategies [3.13]. Moreover, in [3.19] a hybridization with harmony search is made which speed up the global convergence rate without losing the strong robustness of the basic BA. Xie et al.

[3.20] proposed a new BA with a differential operator and Levyights to cope with the slow convergence rate and low accuracy of BA. The experiments showed that the proposed algorithm was feasible and effective, and also had superior approximation capabilities within high-dimensional spaces. Gandomi et al.[3.21] have used BA for a constrained optimization, The authors declare, after testing with classical benchmarks and real world constrained problems, that BA is very efficient and overcome, in many cases, the existing algorithms.

Also, BA has a better dynamic control of exploration and exploitation. On the other hand, Goel et al. [3.22] tested the performance of BA for unconstrained optimization using five standard test functions. The results prove that for bat algorithm to work efficiently for unconstrained optimization problems the dimension of the algorithm should be kept small whereas the population size should be large. In addition, BA has been successfully applied within multi objective optimization problems. As mentioned above, Yang [3.23] has proposed a version of BA to deal with multi-objective optimization problems which proved its efficiency against other methods. Other work [3.24] proposed a multi-objective version that deals optimization problems in binary search space.

3.4.4.2. Data mining

Data mining is one of the fastest growing domains in computer science due to the large data stored last years. Many efficient algorithms are developed for data mining where nature inspired algorithms is some of them. In the last five years bat algorithm has been applied to many times for many problems in data mining, such as: classification, clustering, feature selection and association rule mining, etc. In [3.25] a model has been developed for classification using a bat algorithm to update the weights of a Functional Link Artificial Neural Network (FLANN) classifier. The results show the superiority of bat algorithm against FLANN and PSO-FLANN. In [3.26], the authors proposed a comparison of BA, GA, PSO, BP

and LM for training feed forward neural networks in e-Learning context. Moreover, Bat algorithm has been applied for clustering. Khan et al. [3.27] presented a method

called fuzzy bat clustering for ergonomic screening of office workplaces. The results of the experiments showed that the method is fast, efficient and provides better performance in-face-of fuzzy c-means clustering algorithm. The same authors presented a study of clustering problems using bat

algorithm and its extension as a bi-sonar optimization variant with good results [3.28]. Komarasamy [3.29] studied K-means clustering using bat algorithm and they concluded that the combination of both K-means and BA can achieve higher efficiency and thus performs better than other algorithms. Recently, Aboubi et al [3.30] have applied BA for Clustering large data sets called BAT-CLARA. That is based on BA and k-medoids partitioning. The computational results revealed that BAT-CLARA outperforms all compared algorithms to solve the clustering problems. Also, a new version of BA called the Binary bat algorithm (BBA) was developed for feature selection which is a technique aims to find important information from a set of features. As well, the experiments performed on fivve standard datasets prove the superiority of BBA in face of PSO, FFA and GSA. In [3.31] a combination of Bat Algorithm with a support vector machine (SVM) classifier for simultaneous feature and optimal SVM parameters selection, to reduce data dimensionality and to improve IDS detection.

3.4.4.3. Engineering

Engineering is a crucial field for nature inspired algorithm applications. Thus, BA becomes important technology applied for solving issues in engineering practice. In image processing, Senthilnath et al. [3.32] proposed to use BA to classify Multi-spectral Satellite Image. In this proposal, a partitional clustering used to extract information in the form of cluster centers, and then the extracted clusters are validated. The performance of the Bat Algorithm is compared with the traditional K-means, GA and PSO, which prove BA can be successfully applied to solve crop type classification problems. Other work can be found within the field of image processing in [3.33]. This later presented a new bat algorithm with mutation, known as BAM, between bats during the generation of new solutions for image matching issues. The results

illustrated that this method was more efficient than differential evolution and studied genetic algorithm models. Within the same field, Abdel-Rahman et al. [3.34] proposed to use bat algorithm for articulated human motion tracking from multi-view video data. Results showed that BA performs better than Particle Filter, Annealed Particle Filter and Particle Swarm Optimization algorithms. Scheduling problem is one of the biggest issues in engineering where BA has been applied successfully. Musikapun and Pongcharoen [3.35] solved multi-stage, multi- machine, multi-product scheduling problems using bat algorithm, and they solved

a class of non-deterministic polynomial time (NP) hard problems with a detailed parametric study. In addition, BA was used to solve multistage hybrid or shop scheduling problems which are known as strongly NP-hard problem. The computational results show that the proposed BA is an efficient approach for solving the HFS scheduling problems [3.36]. In [3.37] optimal design of Power System Stabilizers (PSSs) in a multi-machine environment parameter tuning problem is converted to an optimization problem which is solved by BAT algorithm. Another work uses BA to obtain the optimal solution of economic load dispatch [3.38]. Experimentation showed that BA has good convergence property and better in quality of solution than PSO.

3.5. Finite Element Method

In this work, the potentials and electric fields distribution along developed polymeric insulator has been evaluated using Finite Element Method (FEM) computational simulation. Finite element method (FEM) is a numerical method to solve various partial differential equations (PDE) that represents a physical system. The basic idea of FEM is to discretize the domain of interest, where the PDE is defined, in order to obtain an approximate solution of the PDE by a linear combination of basic functions defined within each subdomain. Then, the assembly of subdomains, which is based on the process of putting the finite elements back into their original positions, results in a discrete set of equations which are analogous to the original mathematical problem.

3.6. COMSOL Multiphysics Software

In this project, COMSOL Multiphysics is used to simulate the finite elements for the insulator. The simulation is performed in three consecutive stages namely pre-processing, solving, and post processing stages. Geometrical, material and boundary properties, and meshing criteria of the elements are the inputs in the pre-processing stage. The mathematical model express as differential equations that describe the physical problem is executed in solving stage. Finally, the plot processing stage is that of the plot generated by simulation in terms of variables or parameters.

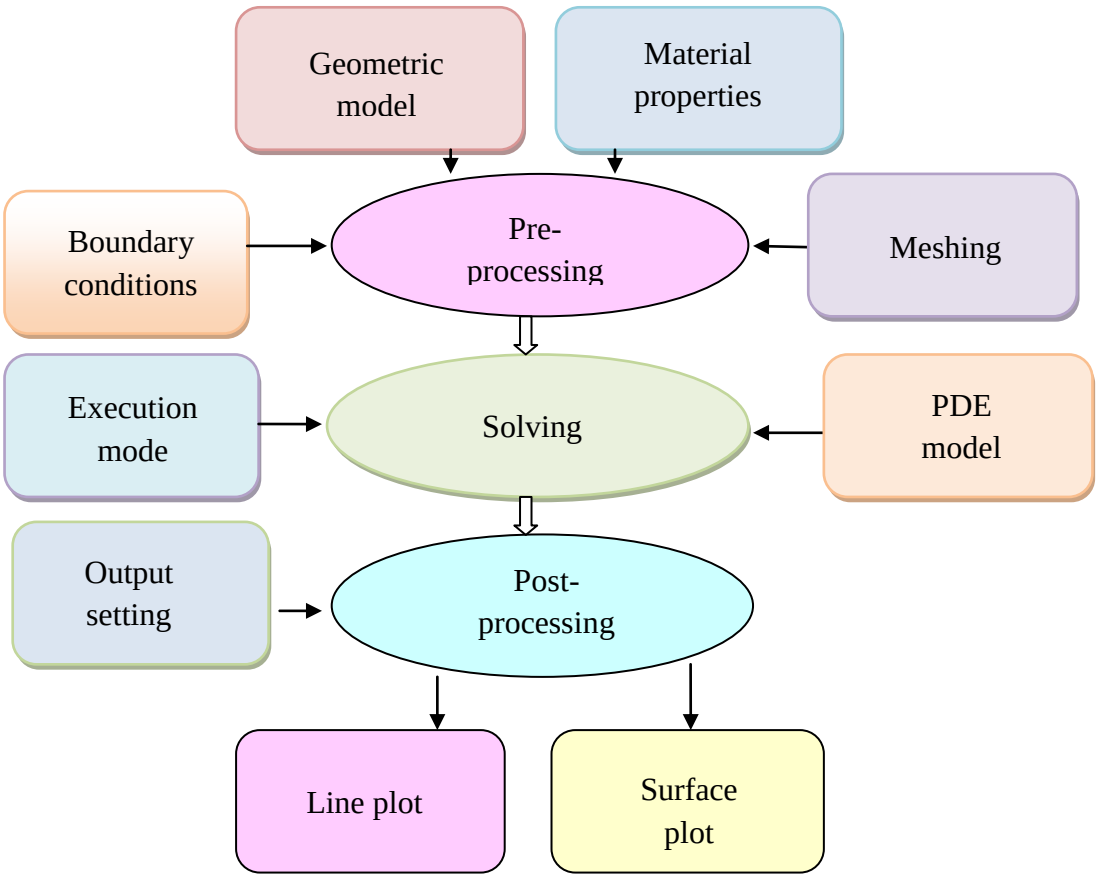

Figure 3. 7 General procedures of FEM simulations

3.7. Minitab software

Minitab is a statistical software package that provides a wide range of data analysis capabilities. In this thesis, the obtained test data were analyzed by L27 Taguchi standard orthogonal array and an analysis of variance (ANOVA) using Minitab. Design of Experiments using Taguchi approach is a powerful technique to study the effect of multiple variables simultaneously and then the tests number to obtain the solution is reduced. Moreover, in this method the number of factors studied can be very large, the detection of interactions between factors is possible, it gives better details on the results and mathematical modeling of the results is also possible. Finally, when combined with BAT algorithms, the approach can economically satisfy the needs of problem solving to estimate the ring parameters to control the E-field lower than the maximum recommended threshold. With the proposed methodology the time required for tests investigations is significantly reduced and then it can be considered as an efficient fast working tool.

The simulation based on the finite element method combined with the experimental design methodology and the BAT optimization method found to be very efficient tool to evaluate their effects on the E-field distribution increasing the insulator long term performance.

3.8. Project Process Flow

In obtaining and analyzing electric fields distribution along composite insulator, the process flow of the project can be simplified in Figure 3.8. The flow diagram shows all of the processes involved starting from the initial stage until the desired results is obtained.

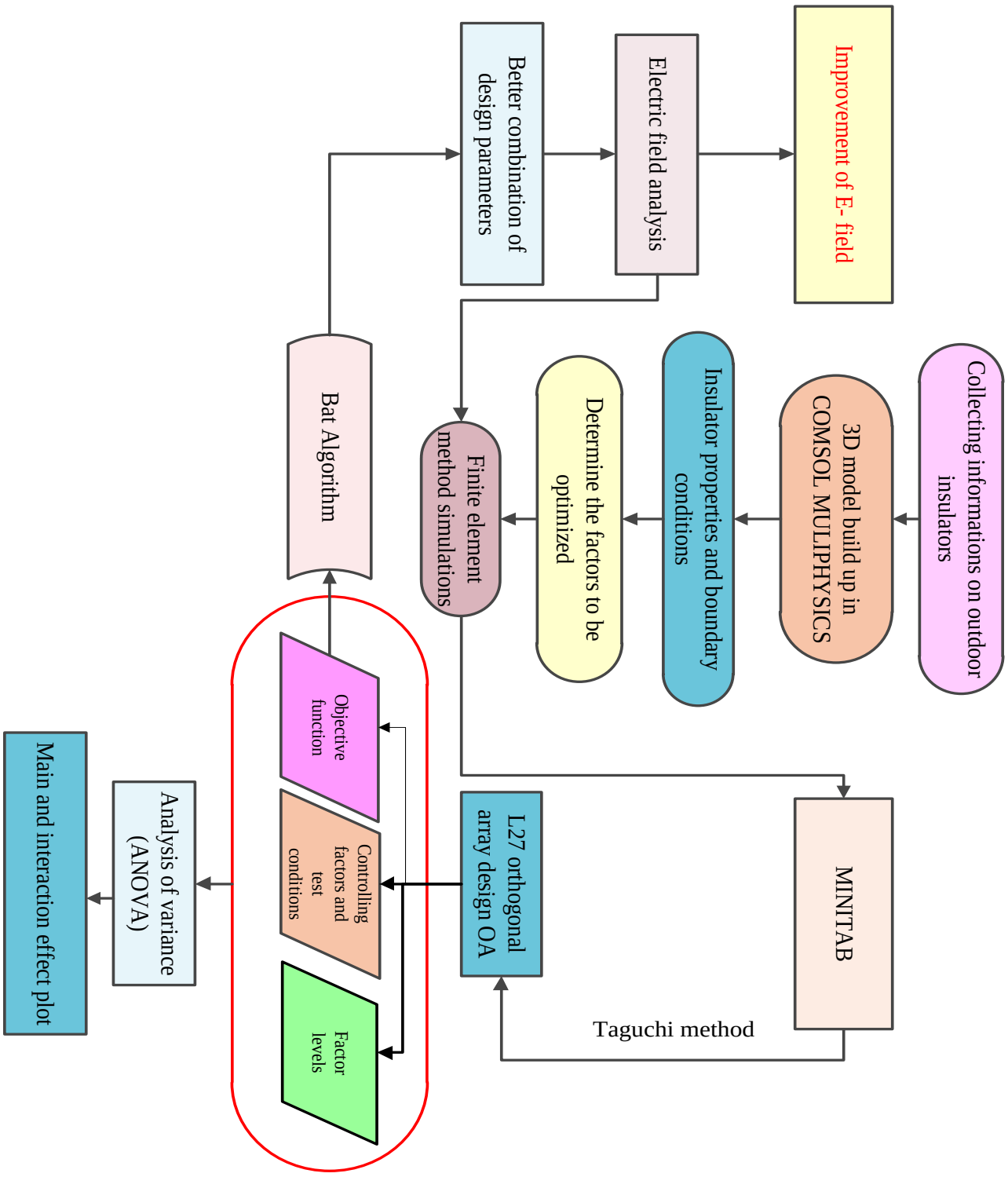

Figure 3. 8 Flow diagram of electric field optimization for polymeric insulator

3.9. Conclusion

This part of the thesis discussed on how the work is carried out in order to obtain the aims of this project. It discussed the installation of corona ring as a useful technique for optimizing electric field on outdoor polymeric insulators. To define the optimum location of the corona ring, experimental methods are used. The main and interaction effects of the corona ring parameters have been evaluated using the variance analysis technique using the MINITAB software in combination with COMSOL.

Finite element method is employed for insulator modeling to determine electric potential and field distribution along the non-ceramic insulators. For this, a model of polymer insulators is developed to evaluate the optimization techniques employed. This chapter discussed a new nature inspired bat algorithm as a new and efficient tool of optimization.

The definition of this algorithm, its variants, and applications are reviewed.

Chapter 04

Performance Analysis of non Ceramic Insulator

Chapter 04

Performance Analysis of non Ceramic Insulator

4.1. Introduction

To advance the previous studies on Corona ring optimization, this chapter presents a new approach to minimize the electric field under the threshold value and by consequence, improving the performance of composite insulator. Bat algorithm (BA) is proposed to determine the optimal design of corona ring. This algorithm leads to the optimization of the Corona ring parameters which are then verified by FEM.

4.2. Optimization structure of the Corona rings based on BAT algorithm

4.2.1. Problem formulation

The MINITAB® software in combination with COMSOL® was used to obtain an optimum design. ANOVA statistical analysis has been performed to obtain an optimum response using a 2nd degree polynomial model. The analysis of the obtained response takes into account the effects of the factors and their interactions. A quadratic model by regression was established and given by the following form:

$$Y = a_0 + \sum_{i=1}^{3} a_i X_i + \sum_{i=1}^{3} a_{ii} X_i^2 + \sum_{i<j}^{3} a_{ij} X_i X_j \quad (4.1)$$

Where, Y is the desired response, a_0 is constant. A_i, a_{ii} and a_{ij} are the coefficients of linear, quadratic and cross-product terms, respectively. X_i is the coded factors related to the considered parameters. The maximum applied voltage at the ends of the insulator was $220 * \frac{\sqrt{2}}{\sqrt{3}} = 179.629$ kV as shown in Figure 4.1.

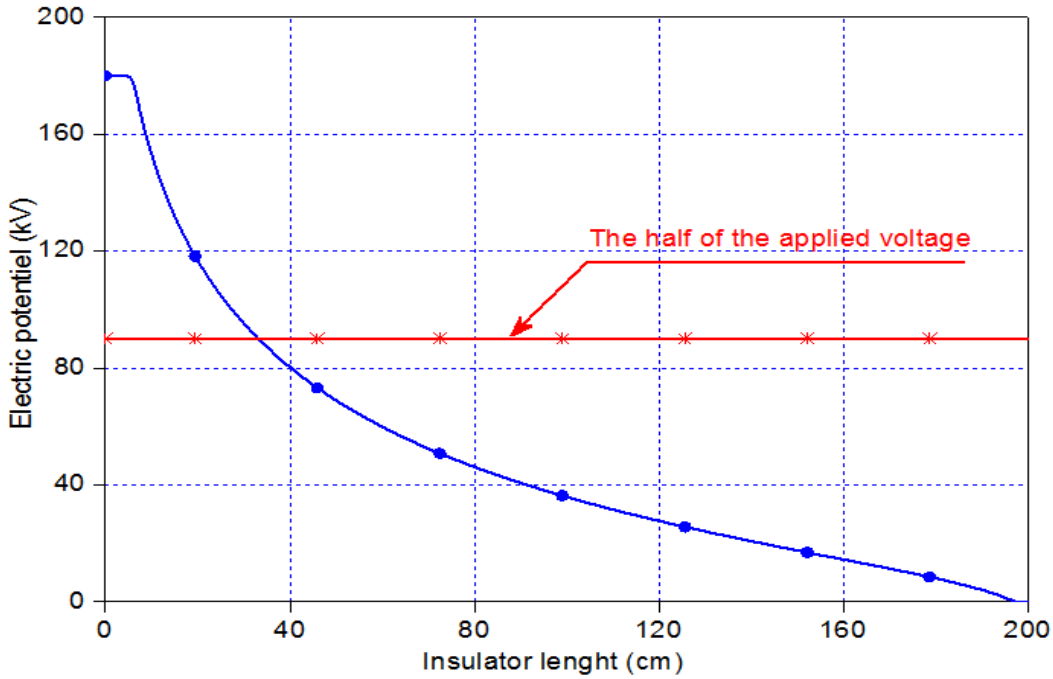

Figure 4.1 Electric potential distribution without corona ring.

Solve design problems by means of optimization techniques have an objective function. The optimal design is achieved by reducing the electric field via this function. The objective function consisting of a mathematical relation between the electric field magnitudes and corona ring parameters. It is represented as follows:

$$E = 4.296 + 10^{-6}(13H^2 + R^2 + 113Dr^2 - 4HR + 13HDr + 19RDr - 4383H + 213R - 37910Dr) \quad (4.2)$$

Using statistical analysis, the coefficient of determination (F^2) was found to be nearly 0.98 (F^2, approaches the unity) which can be considered a good estimate. In this work; we studied the influence of important design parameters on the maximum electrical field stresses. Variation ranges of all important design parameters are shown in Table. 4.1. Corona ring position (H), corona ring radius (R) and corona ring tube diameter (D_r), are the important design parameters. They affect the electric field and the potential distributions along the insulator. To improve the electric field distribution of composite insulator and identify the effect of the ring, variation range of each parameter is chosen and will in turn be evaluated by the simulations. They are 0,200, and 400 mm for the ring position, 150, 250, and 350 mm are for the ring radius and finally, 20, 50 and 80 mm for the ring tube diameter. Previous research results indicated that the choice of design parameters of corona ring was necessary to limit the

surface E-field on insulators for compact transmission lines. The E-field values were obtained for all configurations indicated in table 4.2. In this work, we studied the influence of important design parameters on the maximum electrical field stresses.

Table 4. 1 Corona ring parameters and their levels

Parameters	**significations**	**variation ranges**		
Corona ring position	H	0	200	400
Corona ring radius	R	150	250	350
Corona ring tube diameter	D_r	20	50	80

Table 4. 2 Computational results.

CR Parameters			**Results**
H	**R**	**D_r**	**E**
0	150	20	4.100
0	150	50	3.235
0	150	80	2.610
0	250	20	4.260
0	250	50	3.545
0	250	80	3.035
0	350	20	4.480
0	350	50	3.860
0	350	80	3.410
200	150	20	3.460
200	150	50	2.650
200	150	80	2.093
200	250	20	3.850
200	250	50	3.120
200	250	80	2.615
200	350	20	4.200
200	350	50	3.550
200	350	80	3.100
400	150	20	4.140
400	150	50	3.580
400	150	80	3.205
400	250	20	4.240
400	250	50	3.665
400	250	80	3.280
400	350	20	4.420
400	350	50	3.870
400	350	80	3.490

Physically, to avoid an impractical or even impossible corona ring size in applications, the variation range of ring parameters must be carefully chosen depending upon the geometric feasibility, since the installations of corona rings minimize the dry arcing length and change the air gap. Corona rings with big diameters and higher installation (over 400mm) further reduce the dry arcing distance, which is not desirable. The research space (0-400mm), for the ring height, is enough to characterize the best position of the ring. It should be also noted that large tube diameters more (more than 80mm) are not economical. Radius value R varies between 150mm and 350mm. R lower than 150mm causes undesirable contact with the large shed of the insulator. On the other hand, installing corona ring with radius beyond 350 mm did not reduce the electric field significantly.

4.3. Main effect plots and interactions effect of corona ring parameters

The main effect plots and interactions effect of corona ring parameters can be represented graphically as shown bellow.

Figure 4.2 presents the effect of plots of corona ring parameters on the maximum value of E-field is represented in. It is seen that, corona rig position has a decreasing effect on the maximum E- field. After 200 mm, the position has an increasing effect on the maximum E- field. On the other hand, Corona ring radius has an increasing influence on the maximum E- field and corona ring tube radius has a decreasing effect.

The interaction effect plots of corona ring parameters on the maximum E-field is shown in figure 4.3 This plot shows the influence of the interactions on the relationship between factors and responses. When lines are parallel, there are no interactions. Interactions appear when the lines become not parallel. The interaction between position (H) and corona ring radius (R) is the most observed. However, the interaction between corona ring position and corona ring tube diameter is slight. A high decreasing impact of corona ring radius on the maximum E- field when the corona ring tube diameter is higher; if the interaction between these two parameters is analyzed.

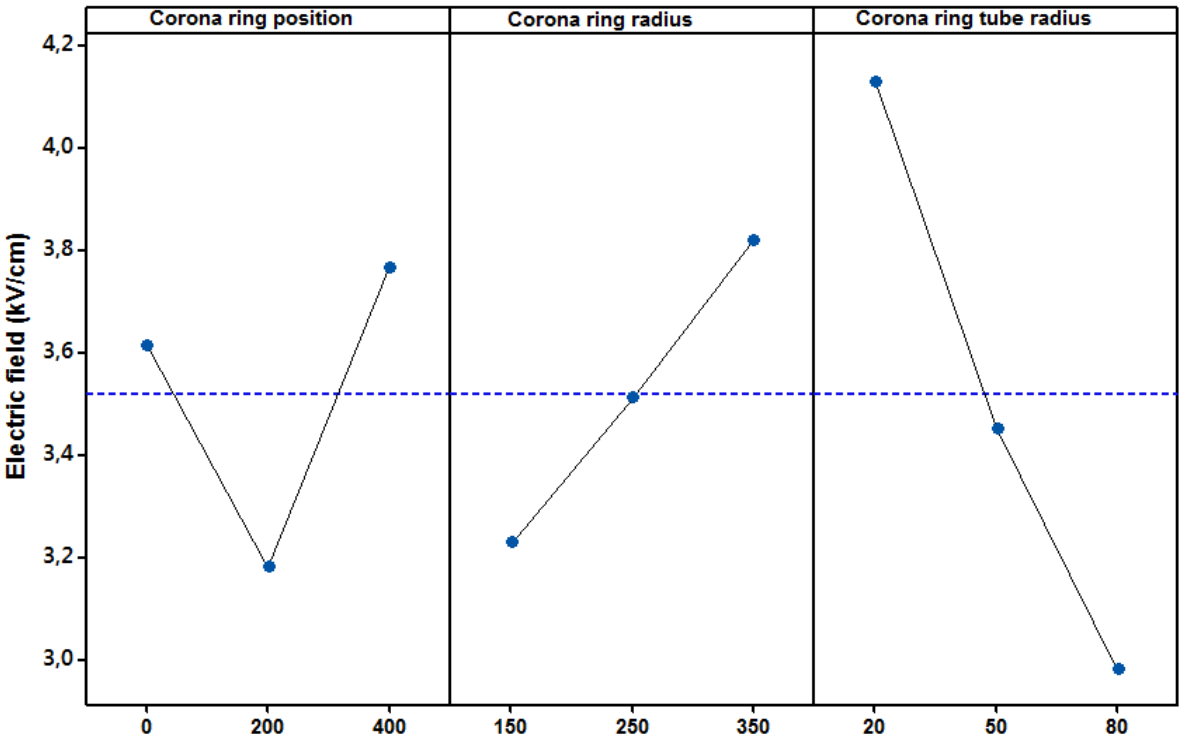

Figure 4. 2 Main effect plots of corona ring parameters H, R and D*r* on the maximum value of E-field.

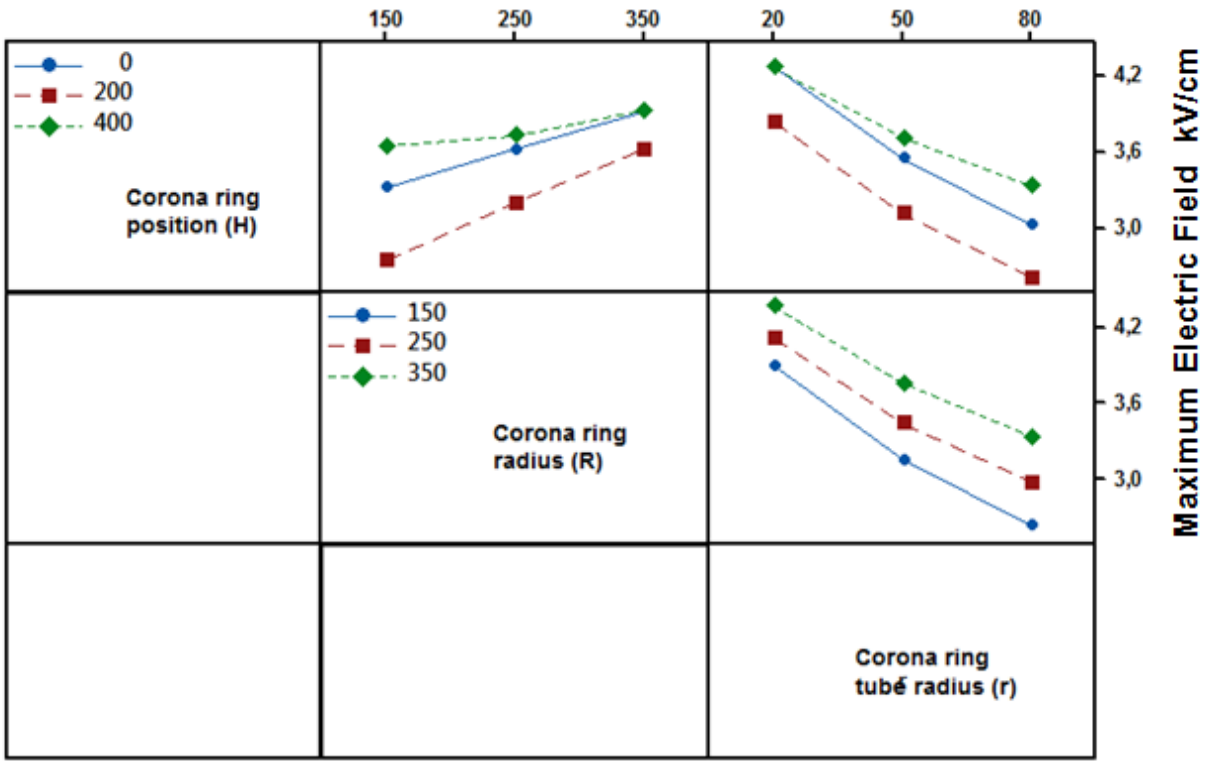

Figure 4. 3 Interaction effect plots of corona ring parameters H, R and D_r on the maximum E-field

4.4. Implementation of the bat algorithm in designed corona ring

As the corona ring parameters affect the electric field on the end fittings and the surface of the composite insulator, the optimization with Bat algorithm, are performed. In this section, the optimization process of the technique used to reduce electric field on the surface of the insulator is described. The objective is to maintain the electrical field intensity lower than the threshold value of 420 kV/m [4.1- 4.2].The bats in the BA refer to a duty cycle in Equation (3.8), which can be a solution for the CR optimization. B_n in this equation refers to the number of bats that participate in the optimization, and the objective function is the electric field (E). An appropriate stopping condition is required for the algorithm to end the tracking process and finalize an appropriate duty cycle for a steady-state operation [4.3].

Predefined algorithm iteration is considered in many studies for the stopping conditions of optimization. In this work, the number of iterations taken for generating optimal solution in BA is 200. Stopping condition occurs when the fitness difference of all participating bats is less than a small predefined error or when the iteration count crosses the predefined iteration count which could be configured when running the simulation results. This is the place where the optimization algorithm converges [4.1, 4.4].

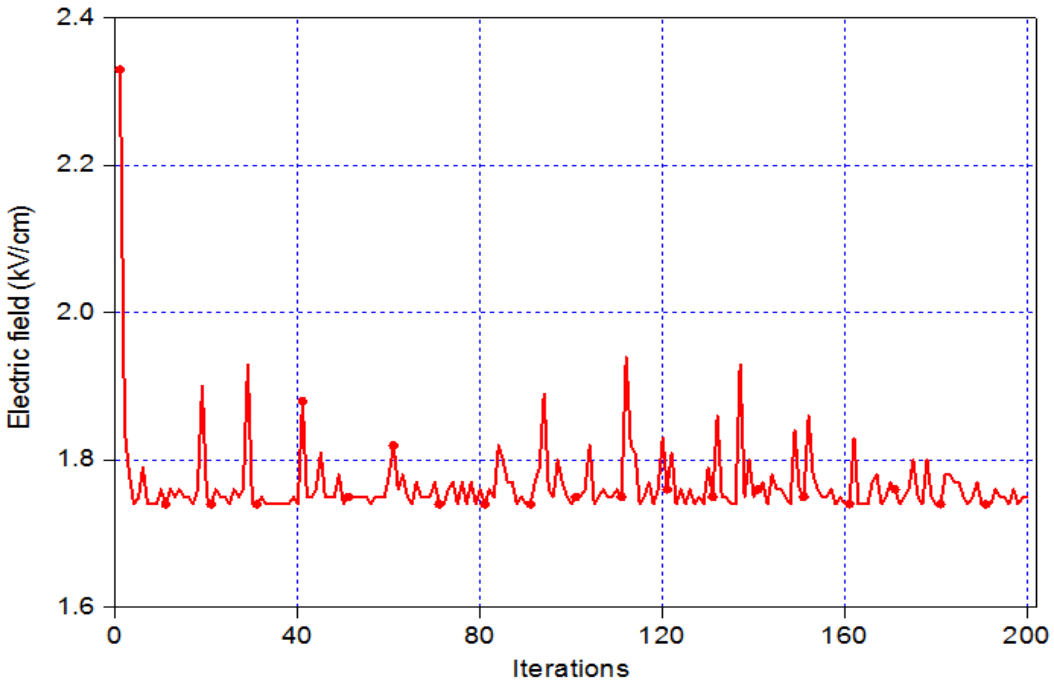

Figure 4. 4 Convergence of objective function during the optimization model.

The convergence characteristics are shown in Figure. 4.4 From this figure, it can be seen that the objective function reaches its lowest value after the few number of iterations and after there is no change. The simplicity of the BA reduces the computation time. It is clearly seen that the optimization using bat algorithm reduces the computational time in average, if it compared with the case without optimization. Bat method is used to get the minimum value for E-field and select the optimum location of the Ring. A good agreement was achieved between the results of Bat method and COMSOL. The optimized parameters of the corona ring are presented in table 4.3.

Table 4. 3 Optimized CR Parameters Values

Parameters (mm)	Optimized value	Electric Field [kV/cm]
Corona ring position (H)	128.2	
Corona ring radius (R)	150	1.75
Corona ring tube diameter (D_r)	80	

4.5. Simulation Analysis

The investigations are carried out in order to analyze the influences of corona ring along the studied insulator. Simulations of potential and E-field distributions are conducted in this section. Fig.4.5 represents the maximum E-field variation along the insulator length with, without corona ring and with recommended corona ring versus the applied voltage. For the same applied voltage (180 kV), the maximum E- field is found to be 6.93 kV/cm and 2.68 kV/cm for the cases without CR and with the recommended CR, respectively. However, the field is only 1.74 kV/cmfor the case of the optimized CR which is much lower than the two previous cases. The maximum E-field is then significantly reduced close to the fitting end. Numerically, the percentage of E- field has decreased by about 75 % compared to the E-field in the case without corona ring and by about 35% compared to the case of the recommended CR. This is due to the best placement of the optimized ring. The EPRI recommended threshold value (4.2 kV/cm) is shown by the horizontal line. Note that for all analysis, the maximum E-field is computed based on the line voltage. On the other hand, it is clearly seen that the optimized corona ring, decreases the field gradient below the corona threshold and becomes lower by about 58.6%.

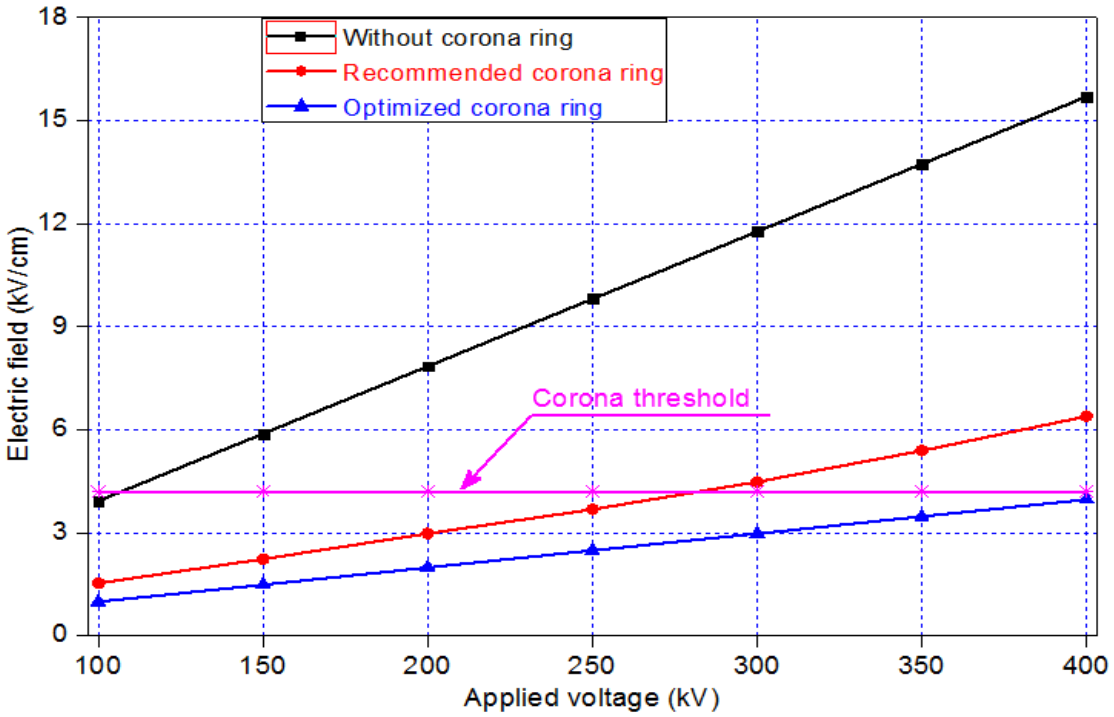

Figure 4. 5 Maximum electric field as a function of applied voltage.

Figure.4.6 illustrates a comparison of the electric field distribution along the composite insulator between the three studied cases. It shows a decrease in the electric field for the two cases, with optimized CR and recommended CR. In presence of optimized corona ring, the magnitude of field is decreased and takes place away from energized end. It can make the field more uniform by decreasing it at HV side and increasing it slightly at earth side. The reduction in the energized end is attributed to the presence of the phase wire and the clamp that helps to reduce the non-uniformity of the electric field at such end of the insulator. Figure.4.7 presents the effects on electric potential distribution along the studied length of composite insulator, in the case of insulator with and without CR. The results show that the electric potential significantly decreases from the HV end fitting. The potential near the energized end is similar to the line voltage, due to the material permittivity and the insulator form, the voltage rapidly falls off from the energized ends of the insulator, such a voltage repartition creates high E-field in the vicinity of energized end [4.5], as shown in figure.4.7 because the half of the applied voltage is supported only by 33.20 cm of the insulator length in absence of corona ring. However, by using the optimized corona ring, this distance reaches 65.40 cm. The corona ring height has a significant influence on the electric field and potential. The optimization discussed previously, is responsible for

the obtained minimum E-field. For this case, new mathematical relationship (objective function) between the electric field and the corona ring parameters is established. Using Bat algorithm technique, the optimized corona parameters retained are those giving the minimal value of the maximum E-field at the considered central axis point.

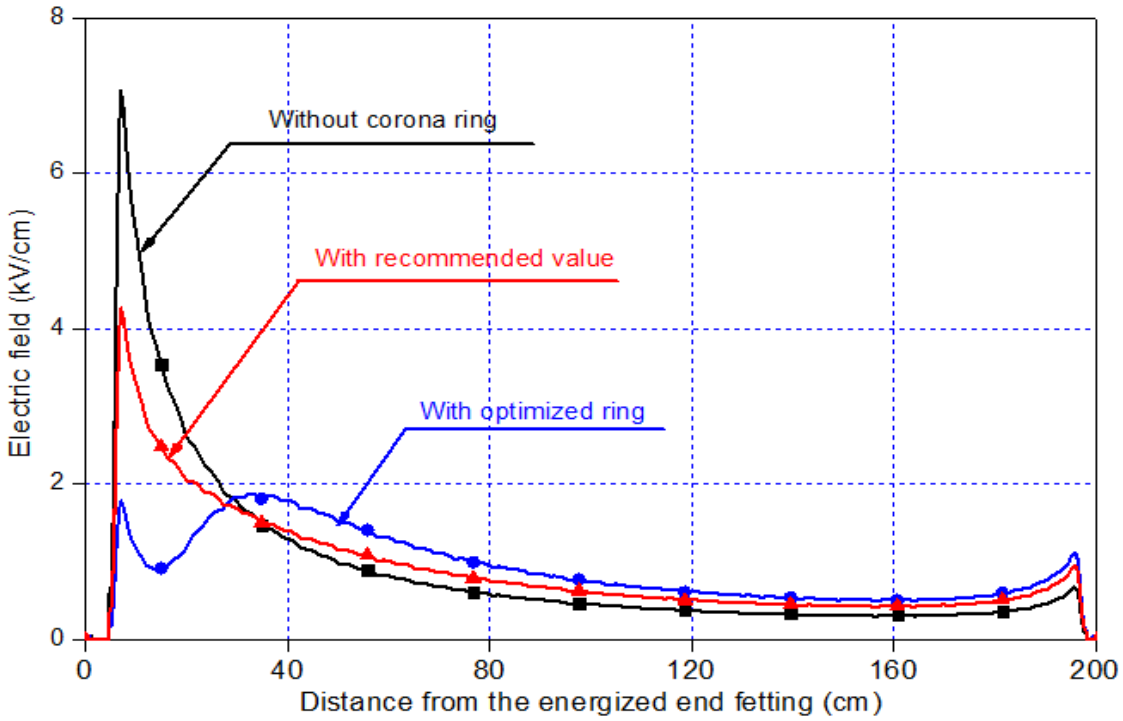

Figure 4. 6 E-field variation along the insulator length with and without corona ring.

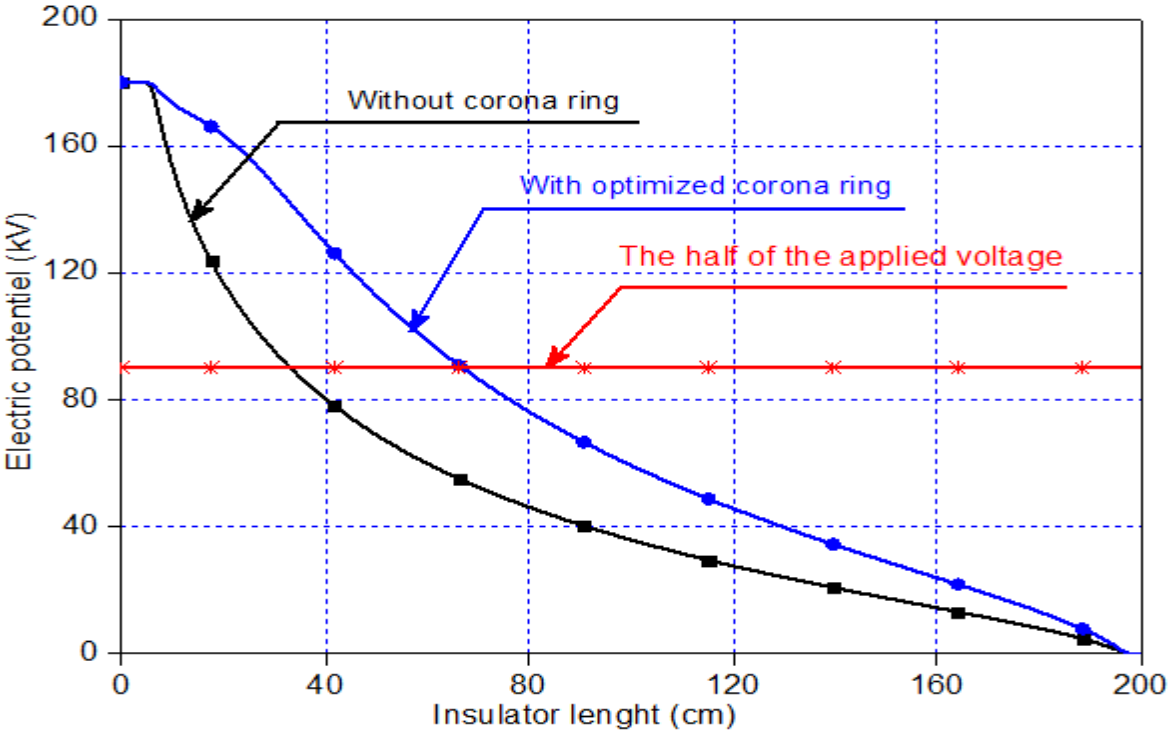

Figure 4. 7 Electric potential along the studied composite insulator.

A comparison of results to similar work ‑ that uses different approaches - in terms efficiency was made using the same insulator profile as in [4.3] where particle swarm optimization (PSO) algorithm with dynamic population size is employed to deal with the optimization of corona ring. Table 4.4 gives the obtained results. As can be seen, the results show that the computational time taken by BA is lower than PSO. In addition, the optimized corona ring parameters proposed by Bat algorithm seems to be optimum value minimizing significantly the E- field. This evaluation clearly indicates that bat algorithm is fast and better in terms of identifying the best solution.

Table 4. 4 Comparison between PSO and BA

Method	PSO	Bat Algorithm (BA)
Electric Field [kV/cm]	1.55	1.29
time(s)	178	4
Convergence	convergence	Fast and better
Accuracy	Accurate	more accurate
complexity	complex	Less complex

4.6. Potential and Electric field distribution analysis

Electric potential and field distributions along the insulator surfaces are the basic standards to evaluate the corona and flashover phenomena. Computing these two parameters becomes easy using computer technologies. There are several commercial software packages, based on Finite Element for 2D and 3D electric field problems

This section presents and discusses the results of finite element analysis of the studied composite insulator using COMSOL MULTIPHYSICS software.

Electric field distribution and equipotential distribution in case without ring are given in Figure. (4.8a) and Fig. (4.8b), respectively.

As can be seen, in the case of absence of CR, the electric field magnitude is higher at the HV side, this magnitude decreases exponentially along the composite insulator length. This situation reduces the long term performance of composite insulators.

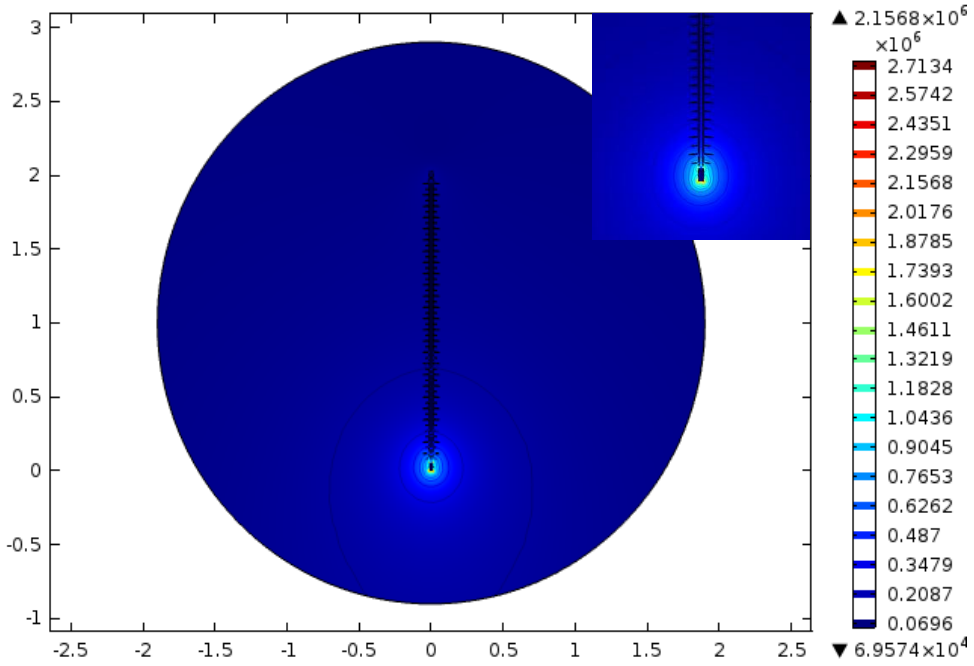

(a)

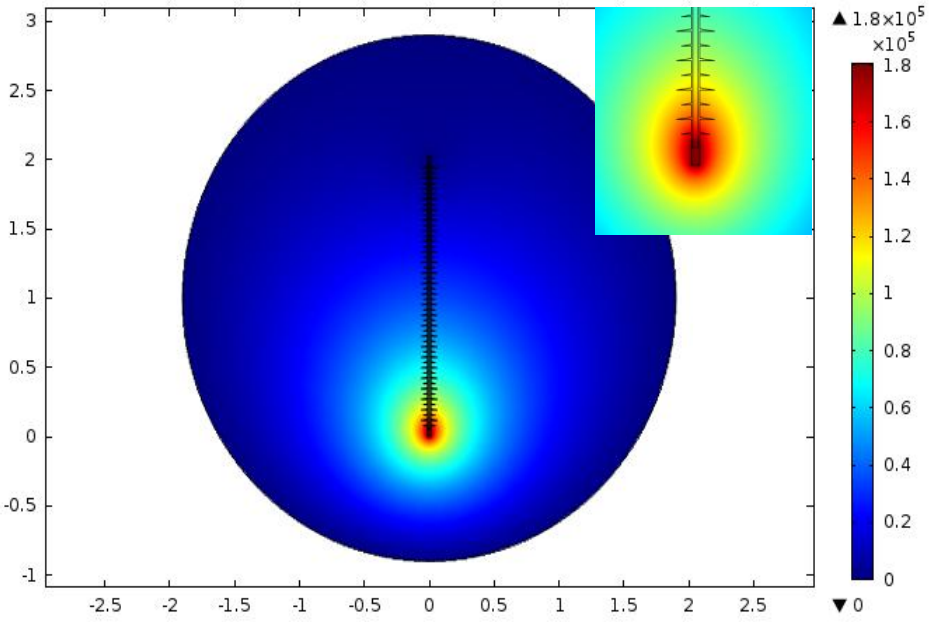

(b)

Figure 4. 8 (a): Electrical field distribution , (b): Equipotential contours around composite insulator in the case without Corona ring**.**

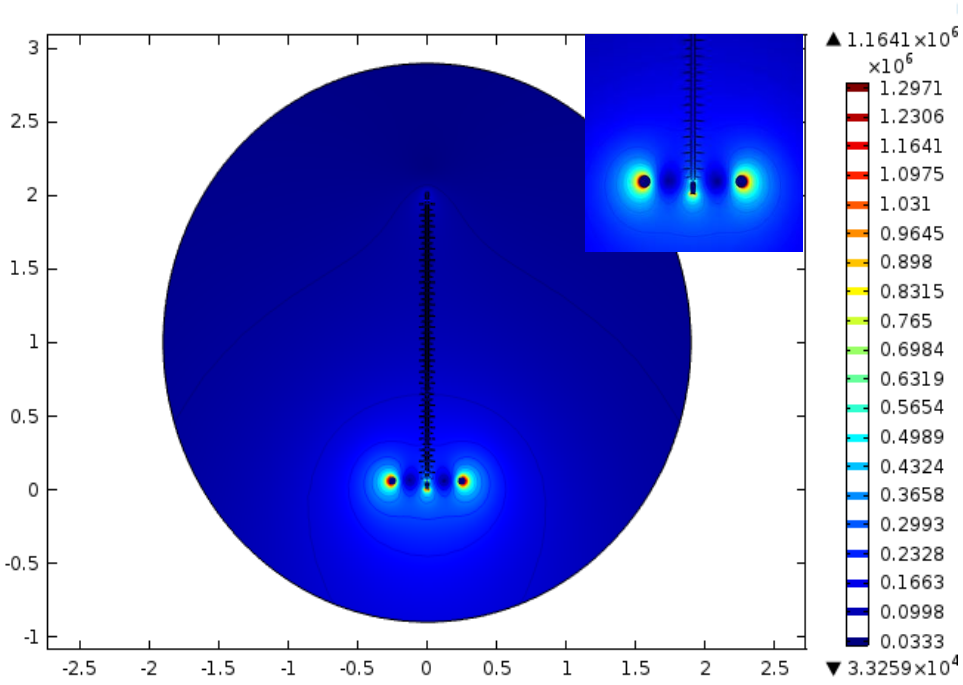

(a)

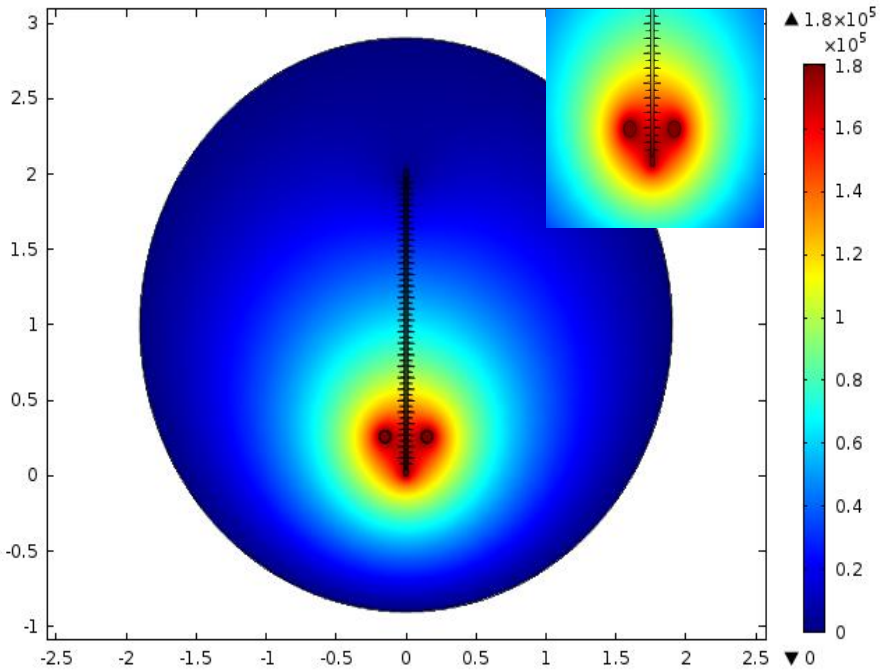

(b)

Figure 4. 9 (a): Electrical field distribution, (b): Equipotential contours around composite insulator in case with Corona ring

Electric field distribution and equipotential distribution for R = 150 mm, H= 128.2 mm and D_r =80 are given in Fig. (4.9a) and Fig. (4.9b), respectively. One can see that, using the optimized ring, the electric field gradient near the high voltage end and ground end of the composite insulator decreases significantly. Thus the E-field distribution along the whole composite insulators is improved and the installation of optimized CR leads to uniform voltage distribution. Moreover, the maximum electric field strengths on the live end side will importantly decrease. The obtained results lead to long term performance of the insulator.

4.7. Conclusion

The aim of this chapter was the study of the electric field distribution along the composite insulator. The use of corona ring at the HV end fitting for improving the electric field distribution is archived by using an optimization technique based on the Bat algorithm which is developed for obtaining the optimized corona ring parameters. Reported results show that the maximum electric field strengths on the live end side was importantly decreased when the optimized corona ring parameters is used. Compared to the case without corona ring, the potential distribution has become more uniform in the case with optimized corona ring parameters.

The proposed technique gives an efficient fast working tool to examine and optimize the performance of the composite insulator.

Chapter 05

Characterization and Improvement of Porcelain Insulator

Chapter 05

Characterization and Improvement of porcelain insulator

5.1. Introduction

Today, the majority of porcelain manufactured is still obtained from silico-aluminous mineral raw materials that are available in nature in large quantities forming the bulk of the earth's crust. The development and manufacture of porcelain have been the object and interest of researchers and industrialists. Among the materials used once can cite: kaolin (45-50%), quartz (20-25%) and feldspar (20-25%). Our country has several deposits of kaolin (Jebel Debbagh, Tamazert, ...) and quartz (Tamanrasset). The characterization of the raw material used and their behavior during the different stages of preparation are indispensable in porcelain industry. Porcelain is often obtained by sintering, generally between 1000 and 1400 ° C depending on the composition of the mixture used and the physicochemical properties of its compounds. This step, which is essential for the porcelain manufacturing process, is accompanied by a transformation of minerals. These phenomena, controlled by the kinetics of material transfer, are of course dependent on the conditions of the heat treatment carried out. The phases created in the silico-aluminate binary systems have an important role on the porcelain properties.

In this part of the thesis, we have prepared and studied several blends from local raw materials: DD2 kaolin, quartz, feldspar and glass. Feldspar is replaced with a windshield glass to recycle it. In this work, the improvement of mechanical and dielectric properties of the porcelain insulator sintered at different temperatures has been investigated. To reduce the fabrication cost of these materials, the effects of recycled waste glass in partial replacement of K-feldspar on the crystallization behavior of porcelain prepared from Algerian kaolin (DD2), quartz and feldspar were also studied. The second part of this chapter discusses the influence of coating with TiO_2 on the electric performance of the prepared porcelain.

5.2. Development of new porcelain insulator based on economic raw materials

In this section, we will talk about the development of porcelain from locally available raw materials. This porcelain is prepared from the mixture of kaolin, quartz, feldspar, and recycled waste glass. We have prepared and studied several blends from local raw materials: DD2 kaolin, quartz, feldspar and glass. Feldspar is replaced with a windshield glass to recycle it. For this, the work of this thesis concerns the study of four mixtures: (50% kaolin + 20% quartz + 30% feldspar + 00% Glass); (50% kaolin + 20% quartz + 20% feldspar + 10% glass); (50% kaolin + 20% quartz + 10% feldspar + 20% glass) and (50% kaolin + 20% quartz + 00% feldspar + 30% glass).

5.3. Experimental analysis

5.3.1. Materials and methods

White porcelains were prepared from mixtures of four raw materials: kaolin (DD2) [5.1] from the mine of Djebbel Debbagh (Guelma- Algeria), which is white in color and enriched in alumina; quartz from Tamazert (Algeria), which is white in color and highly pure; feldspar from Spain (beige in colour and with more than 10% of potassium oxide, its formula is $KAlSi_3O_8$) and waste glass derived from broken car glass. The chemical composition of the starting raw materials as determined by X-ray fluorescence (XRF) is shown in Table 5.1.

Table 5. 1 Chemical compositions of the starting raw materials, mass (%)

Oxides	K (DD2)	Quartz	Feldspar	Recycled waste glass
SiO_2	45.52	99.90	69	70.22
Al_2O_3	38.73	00.03	17.15	01.08
Fe_2O_3	0.04	00.01	00.17	00.08
CaO	00.18	-	02.32	12.01
Na_2O	00.05	-	00.37	13.10
K_2O	00.03	-	10.22	00.03
MgO	-	-	-	01.55
SO_3	-	-	00.16	00.38
L.O.I	15.44	00.01	00.42	-
Total	99.99	99.95	99.81	98.45

Four compositions were prepared by milling the ready mixed powder according to the batch compositions shown in Table 5.2.

Table 5. 2 Percentage of additive material of samples, mass (%)

Samples	K (DD2)	Quartz	Feldspar	Recycled waste glass
N00	50	20	30	**00**
G10	50	20	20	**10**
G20	50	20	10	**20**
G30	50	20	00	**30**

The prepared powder mixtures are named as N00, G10, G20 and G30, where N stands for 0% glass while G stands for glass and 10, 20 and 30 denotes the weight percentage of glass in the composition Figure 5.1. This figure shows the forms of all samples heated at different temperatures. The samples G30 start to melt at 1150°C since they contain a large amount of the solvent (Na_2O, CaO), but the samples G20 begin to melt in 1250 °C. The samples G00 and G10 have not absolutely dissolved even when the temperature reached 1300°C. This photo shows the impossibility of measuring the shrinkage of the samples dissolved and this confirms that the temperature of sintering was reduced to 200°C.

Figure 5. 1 samples sintered at different temperatures for 2 h

Recycled waste glass was added to kaolin and quartz to partially replace potash feldspar. Chemical analysis of feldspar (Table 5.2) shows that it is a potash feldspar composed mainly of SiO_2. Its K_2O and CaO content is 10.22 wt. % and 2.32 wt. % respectively. The chemical composition of the recycled waste glass reveals that it is composed of high SiO_2 content (70.22%), (12.01%) CaO and (13.10%) of Na_2O. Raw materials mixtures were charged into zirconia vials (250 ml in volume) together with zirconia balls (15 units). Milling was performed through a planetary ball mill (Fritsch P6) for 5 hours with a rotation speed of 250 rpm. The slurry was dried at 110°C, powdered and sieved through a 100 µm mesh and then compacted at a pressure of 100 MPa using a cold uniaxial press. Disc specimens of 13 mm diameter and about 5 mm thickness were shaped. In order to determine an optimum preliminary sintering temperature, the compacts were thermal treated under atmospheric conditions at different temperatures within the range of 1000-1300°C for 2 h of soaking with heating rate of 10°C/min and cooled down inside the furnace.

- **X-Ray Diffraction (XRD)**

X-ray diffraction (XRD) is a method universally used to identify the nature and structure of crystallized products. This method does not apply until recently, only in crystalline environments (rocks, crystals, minerals, pigments, clays ...) characteristics of the crystalline state, the method clearly distinguish amorphous products (glasses ...) from crystallized products. It also allows studying the conditions of formation of the phases, their evolution as a function of the temperature or atmosphere, so to know the behavior of a material under the conditions use. The diffractometer is one of the most commonly used devices in the industrial world and research, because of its simplicity and ease of use.

XRD analyses were carried out using a Bruker D8 diffractometer (figure 5.2) and The tests conditions were Ni-filtered Cuk α X radiation (35kV-30mA) with a scanning speed of 37° (2θ) per minute and at an increment of 0.05°.

Figure 5. 2 Bruker diffractometer

- **Fourier Transform Infrared Spectroscopy (FTIR)**

Fourier transform infrared spectroscopy (FTIR) is a technique that is used to obtain an infrared spectrum of absorption, emission, photoconductivity or Raman scattering of a solid, liquid or gas. An FTIR spectrometer simultaneously collects spectral data in a wide spectral range. This confers a significant advantage over a dispersive spectrometer that measures intensity over a narrow range of wavelengths at a time.

The chemical functional groups were investigated by FTIR Perkin Elmer (Figure 5.3) within the wave number range of 400-4000 cm^{-1}. The method described in this study is generally adopted with satisfactory results. The substance is finely and smoothly ground under Nujol directly on the KB_r pellet and the mull gently pressed between two KBr pellets in order to reduce it to a thin and uniform layer. After recording the spectrum, the pellets are carefully separated, and Nujol is repeatedly washed with very light petroleum ether leaving the fine powder on the surface of the pellets which are then joined again as a sandwich. A second spectrum on the dry powder is then recorded, normally only in the spectral regions masked by the Nujol bands.

Figure 5. 3 spectroscopy (FTIR) Perkin Elmer 700 type

- **Differential Thermal Analysis (DTA)**

Thermal analysis is a series of techniques that measure the behavior of the sample to be tested during an imposed rise in temperature. Differential Thermal analysis (DTA) is a thermal analysis technique that consists of following the evolution of the difference of the sample temperature and the reference material temperature. All mixtures were subjected to differential thermal analysis (DTA) using Setaram DTA 92 thermal analysis system with 10°C/min heating rate in air. The bulk density and open porosity of samples sintered at different temperature were measured using a densimeter model KERN ARS 220-4 and quantified according to Archimedes principle [5.2]. Water absorption was estimated by immersion in boiling water, according to recent standards [5.3]. Linear shrinkage on firing (L.S%) was evaluated through the equation [5.3]:

$$\mathrm{L.S\%} = \frac{D_1 - D_2}{D_1} \times 100\% \qquad (5.1)$$

where D_1 and D_2 are the outer diameters of the samples before and after sintering, respectively.

The morphology of fracture surface was observed by JEOL JSM-7001F Scanning Electron Microscope on samples etched with 10% HF (High Frequency) for 30s.

Figure 5. 4 Setaram DTA 92 thermal analysis system

- **Morphological observations**
- **- Scanning Electron Microscope (SEM)**

SEM is widely used to investigate the microstructure and chemistry of a range of materials. The main components of the SEM include a source of electrons, electromagnetic lenses to focus electrons, electron detectors, sample chambers, computers, and displays to view the images (Figure 5.5). Electrons, produced at the top of the column, are accelerated downwards where they passed through a combination of lenses and apertures to produce a fine beam of electrons. The electron beam hits the surface of the sample mounted on a movable stage under vacuum. The sample surface is scanned by moving the electron-beam coils. This beam scanning enables information about a defined area of the sample. The interaction of the electron beam with the sample generates a number of signals, which can then be detected by appropriate detectors.

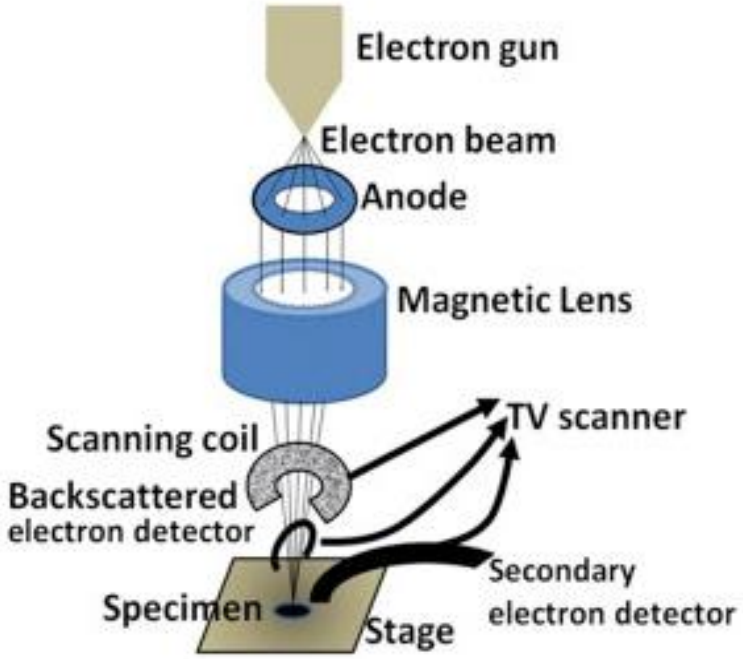

Figure 5. 5 Components of scanning electron microscopy (SEM).

5.3.2. Characterization

5.3.2.1. Microstructural characterization

X-rays diffraction patterns obtained from the samples heated at different temperatures are shown in Figure.5.6.

The XRD (X- Ray Diffraction) diffractogram for N00 sample heat treated at 1000°C shows the peaks corresponding quartz and anorthite (Fig. 5.6a). At 1050°C, the dissolution of anorthite and the formation of mullite as new phase is observed and X-ray patterns of samples fired in [1150° - 1300°C] indicate the dissolution of quartz and the development of a glassy phase.

The XRD spectra for the samples G10 (Fig. 5.6b) shows peaks corresponding to quartz and small peaks corresponding to mullite. From 1050°C, the presence of a new phase of anorthite is revealed. At 1100°C the dissolution of anorthite and quartz is observed. A completely dissolution of quartz is noted at 1200°C. At higher temperature (1250° and 1300°C) the presence of only mullite and glassy phase is observed.

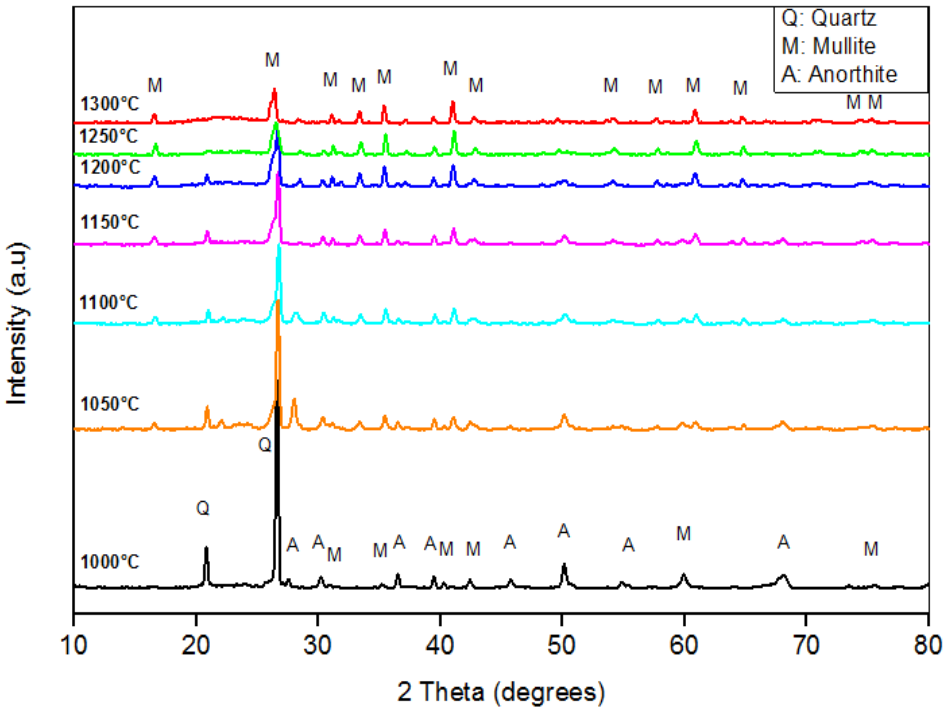
Q: Quartz
M: Mullite
A: Anorthite
1300°C
1250°C
1200°C
1150°C
1100°C
1050°C
1000°C
Intensity (a.u)
2 Theta (degrees)

(a)

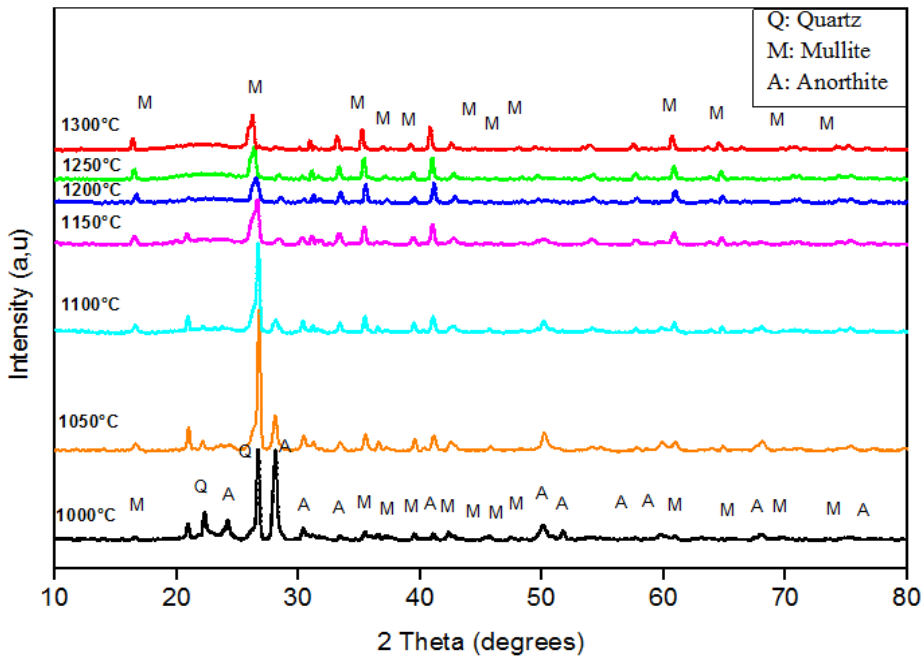
Q: Quartz
M: Mullite
A: Anorthite
1300°C
1250°C
1200°C
1150°C
1100°C
1050°C
1000°C
Intensity (a.u)
2 Theta (degrees)

(b)

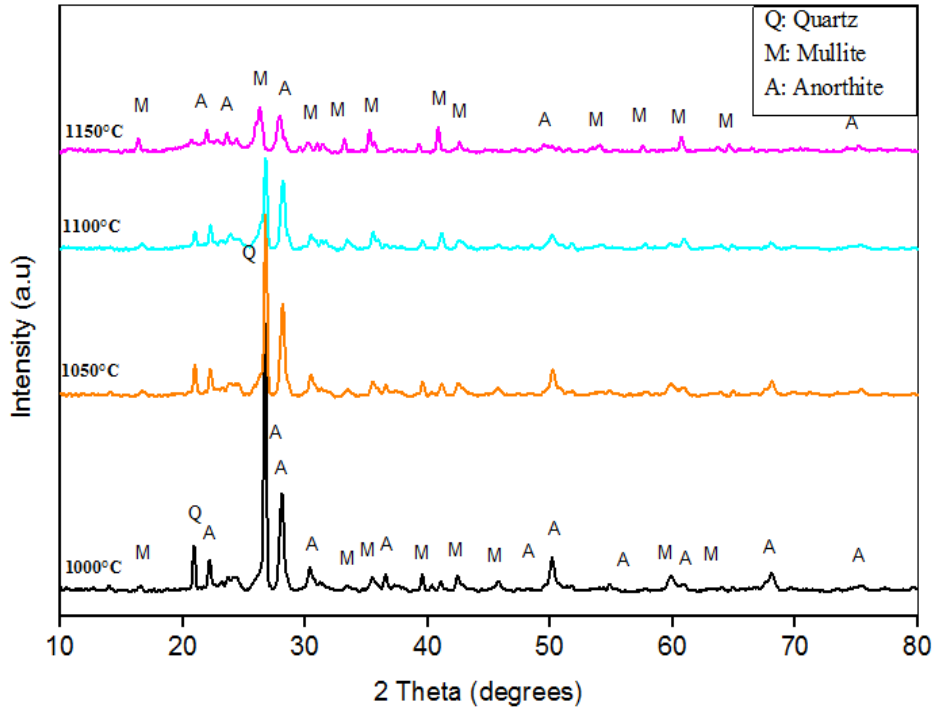

(c)

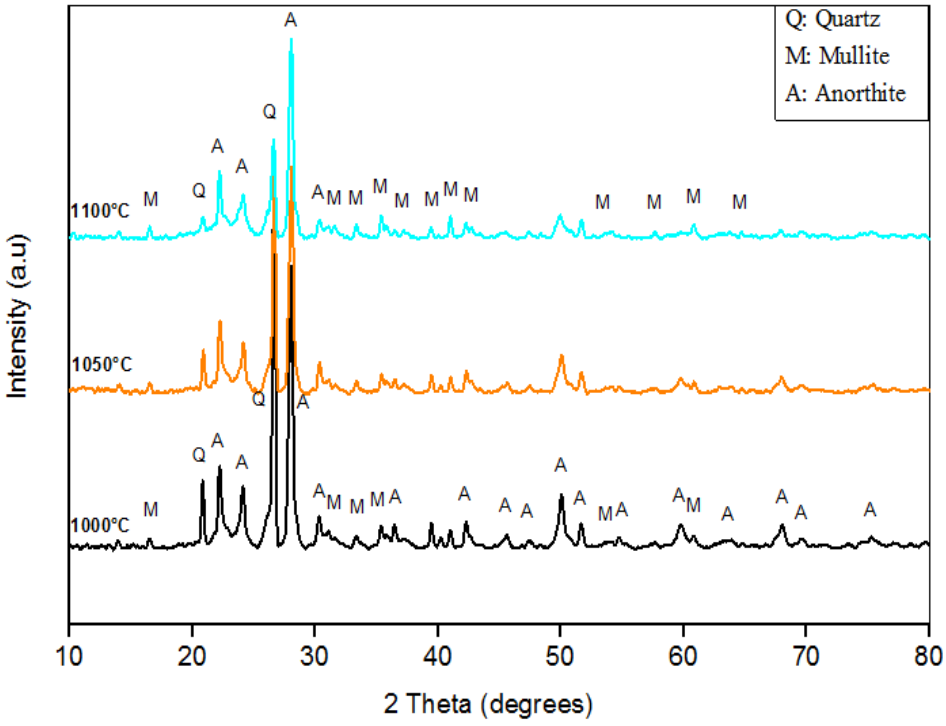

(d)

Figure 5. 6 XRD patterns of samples sintered at different temperatures for 2 h (a) N00, (b) G10, (c) G20 and (d) G30

Fig. 5.6c shows the X–rays diffraction patterns recorded from the samples G20 where a notable decrease in intensity with temperature between 1000° and 1300°C is

observed. At 1000°C, XRD peaks corresponding to quartz, anorthite and mullite are observed. Anorthite and quartz begins to dissolve from 1100°C. At 1150°C, the presence of a glassy phase and mullite were noted.

In the G30 samples (Fig. 5.6d), three phases of mullite, quartz and anorthite were presented at 1000°C [5.4]. The intensity of the peaks corresponding to quartz decreases notably with temperature (1000°–1100°C). At 1100°C, a glassy phase appears.

The functional groups in porcelain samples synthesized at different temperatures were evaluated by FTIR as shown in Figure. 5.7. The spectrum as a whole is divided into two sections; the first one comprises the main sharp distinctive and characteristic absorption bands extending in the mid IR region. From 500 to about 2000 cm^{-1}, and the second part reveals only two small peaks, at about 2851 and 2918 cm^{-1} followed by a broad band in the far IR region centred at about 3616 cm^{-1}. Moreover, an additional small band around 2239 cm^{-1} is also observed [5.5-5.6]. The spectra corresponding to N00 sample heated at 1100°C reveals the presence of two bands at 515 and 542 cm^{-1} relating to the vibrations of bond Si–O [5.7-5.8].

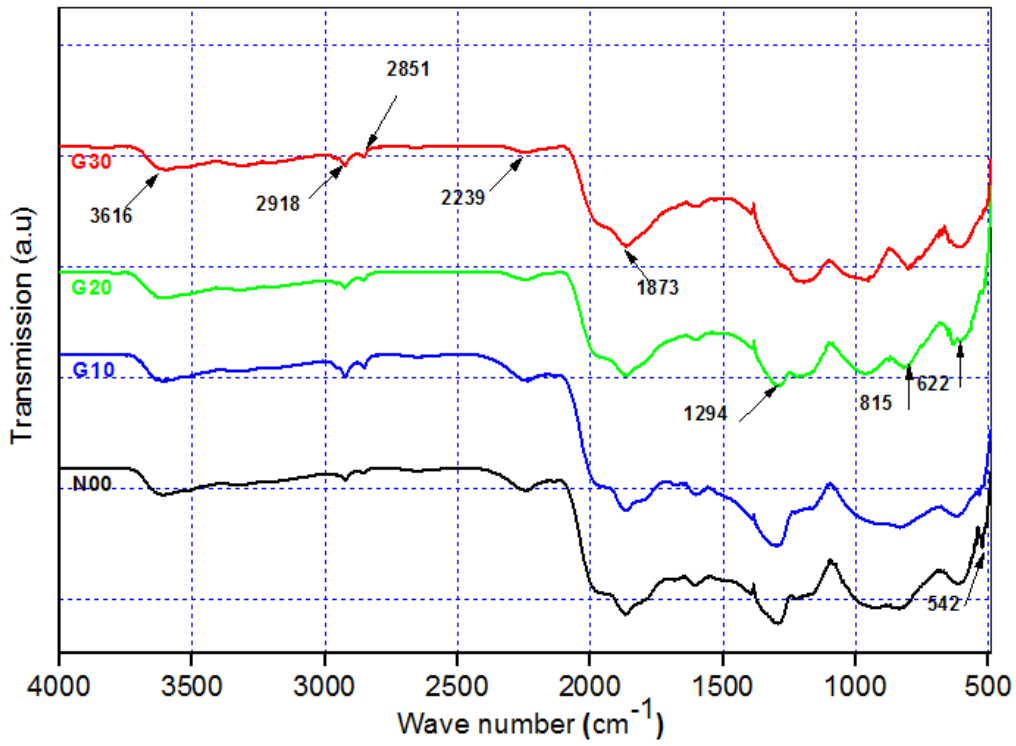

Figure 5. 7 FT-IR spectra of the samples sintered at 1100°C for 2 h

In Figure 5.7, the spectra corresponding to N00 and G10 are almost identical. Other bands around 622 and 815 cm^{-1} are attributed to Si–O–Si symmetric stretching of bridging oxygen between tetrahedral. In G20 samples there is a clear modification of the functional groups [5.9]. A new band at 1294 cm^{-1} corresponding to Si–O in the sample heated at 1100°C appears [5.10-5.11]. Moreover, the band observed at 1873 cm^{-1} can be related to the asymmetric stretching vibration of CO_3^{2-} anions [5.4].

The crystallization kinetics of mullite formation in the porcelain may be determined by the DTA technique, which allows to follow the evolution during a continuous heating (isothermal treatment) from ambient temperature to high temperature (1300°C). DTA curves of studied porcelain samples recorded during heating with a rate of 10°C/min are shown in Figure. 5.8.

On the curves of all samples, two peaks at about 500° and 950°C are observed. The first one (endothermic) is due to the dehydration of kaolinite, while the second peak (exothermic) is due to spinel formation [5.5-5.11].

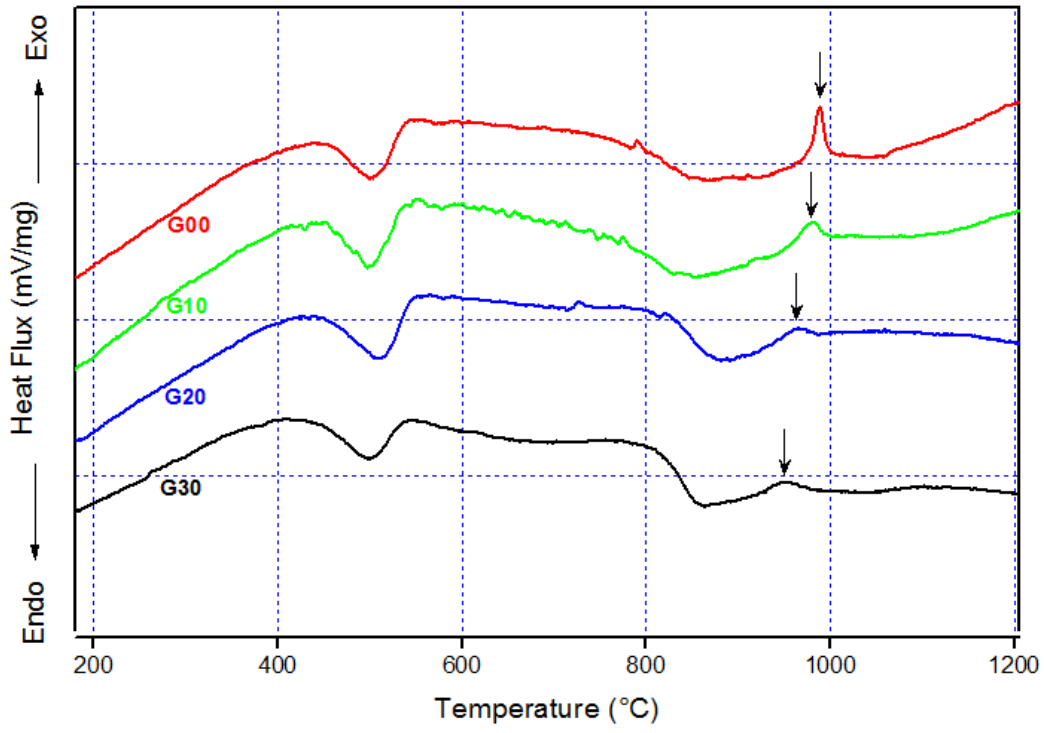

Figure 5. 8 DTA curves for samples mixtures during heating.

The first endothermic peak does not experiment any change with addition of feldspar or recycled waste glass, because this peak is related to kaolinite transformation [5.12]. However both intensity and temperature of the second exothermic peak decrease with recycled waste glass addition from 950° to 990°C for samples N00 and G30, respectively. The proportion of the solvent (CaO, Na_2O, (Table 3) increases with increasing percentage of glass addition, and thus facilitating the formation of spinel phase [5.13-5.14].

Table 5. 3 Chemical compositions of all samples, mass (%)

Elements	N00	G10	G20	G30
SiO_2	63.44	63.56	63.68	63.81
Al_2O_3	24.49	22.92	21.31	19.70
Fe_2O_3	00.08	00.06	00.05	00.04
CaO	00.79	01.75	02.72	03.69
Na_2O	00.14	01.41	02.68	03.95
K_2O	03.08	02.06	01.04	00.02
MgO	-	00.15	00.31	00.46
SO_3	00.05	00.07	00.16	00.11
L.O.I	07.85	07.81	07.76	07.72
Total	99.92	99.79	99.71	99.51

The bulk density and open porosity are shown in figure 5.9.

Figure. 5.9a represents the bulk density of the pellet disks sintered at various temperatures. It is observed that the bulk density represents a maximum value (2.5 g/cm^3) in all the samples after thermal treatment for two hours at 1050°C [5.15]. For N00 samples, it is seen that the bulk density is practically constant between 1050 and 1150°C. Then, it decreases up to 1200°C and becomes constant from 1250°C. This reduction is possibly due to the transformation of residual open porosity into closed porosity and/or the appearance of a new phase (liquid phase) resulting from the presence of K_2O.

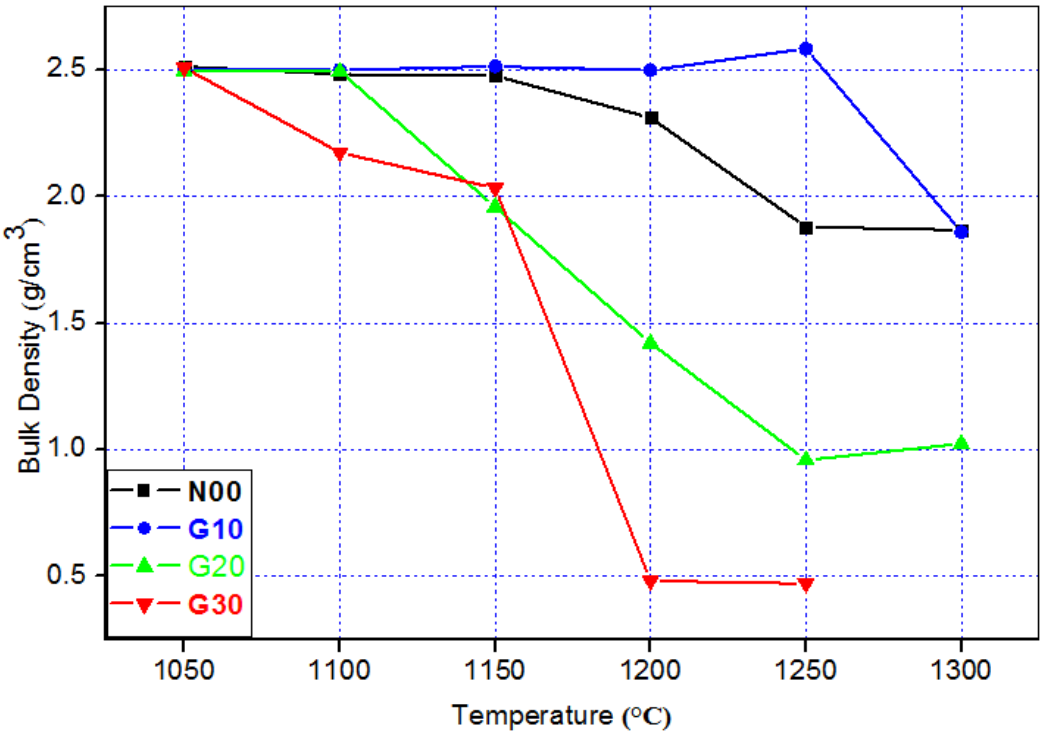

(a)

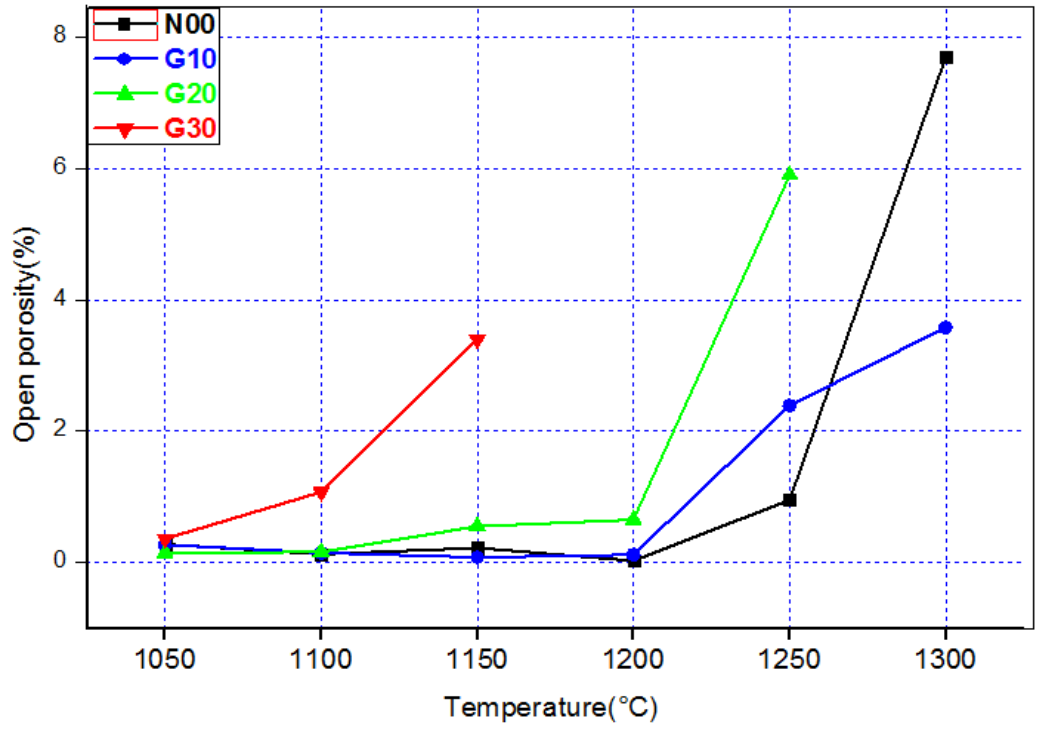

(b)

Figure 5. 9 Bulk density and Open porosity of the samples sintered at different temperatures

In G10 samples, the bulk density is practically constant between 1015° and 1150°C, which is due to the stability of the constituent phases. From 1200°C, a small decrease in bulk density which is due to the appearance of the liquid phases is observed.

In the case of G20 samples, the bulk density is constant between 1050° and 1100°C and is equal to 2.5 g/cm^3. Then, a linear decrease in the bulk density from 1100° to 1250°C is due to the formation of a liquid phase from the presence of a large amount of different fluxes (K_2O, Na_2O and CaO) (See table 5.3). In the case of samples G30, a marked decrease in density can be observed from 1100 °C. This reduction is probably due to the appearance of a large amount of glassy phase. The samples sintered at 1200° and 1250°C show relatively low density values (lower than 1 g/cm^3) due to boiling of the constituent phases [5.15]. Fig. 5.9b shows the evolution of the open porosity in porcelain samples according to the sintering temperature. For N00 and G10 samples, almost zero values have been detected between 1050° and 1200°C, which indicates the final stage of the sintering process. The appearance of the liquid phase at higher temperature (1250° and 1300°C) permits an easy release of gas trapped in the closed pores, which leads to the formation of new open porosity. The role of the liquid phase in microstructure formation and porosity reduction is not as predominant as in vitrified porcelain [5.16]. In the case of G20 and G30 samples, an increase of open porosity at 1100° and 1150°C is observed. The decreasing of temperature where open porosity occurs confirms that porosity is due to the presence of liquid phases.

Fig. 5.10a **s**hows the shrinkage of porcelain samples on firing. All samples show almost constant shrinkage (11-13%) between 1000° and 1150°C. These values are lower than those reported by Kim et al [5.1-5.17]. At 1200 °C, the sample N00 achieves the maximum shrinkage value (18%), which indicates the best sintering temperature. From 1250°C the decrease in shrinkage is due to the appearance of liquid phases.

Generally, the presence of the liquid phases facilitates the sintering process, but in this case, the existence of a great amount of liquid phase with low density leads to a swelling of the samples. The same remarks were noted for G10 sample.

Regarding G20 samples, a significant reduction in the shrinkage from 1150°C is due to the presence of the high quantity of the glassy phase. In samples G30, the melting of the materials after 1150°C (exaggerated swelling) is observed. A high correlation between the shrinkage and bulk density is noted.

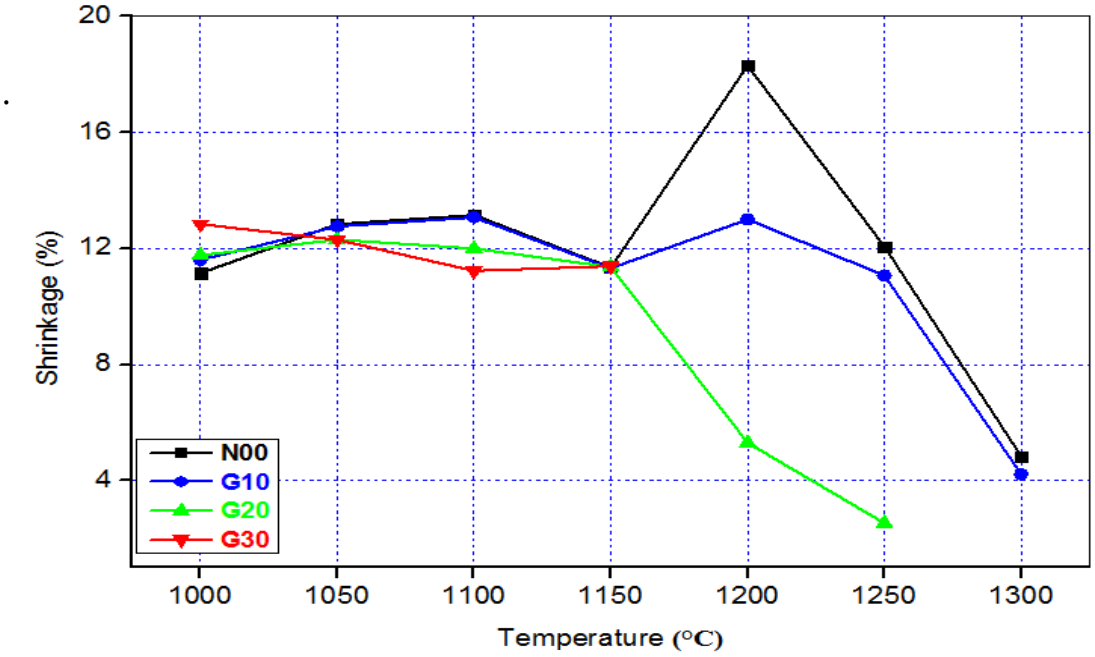

(a)

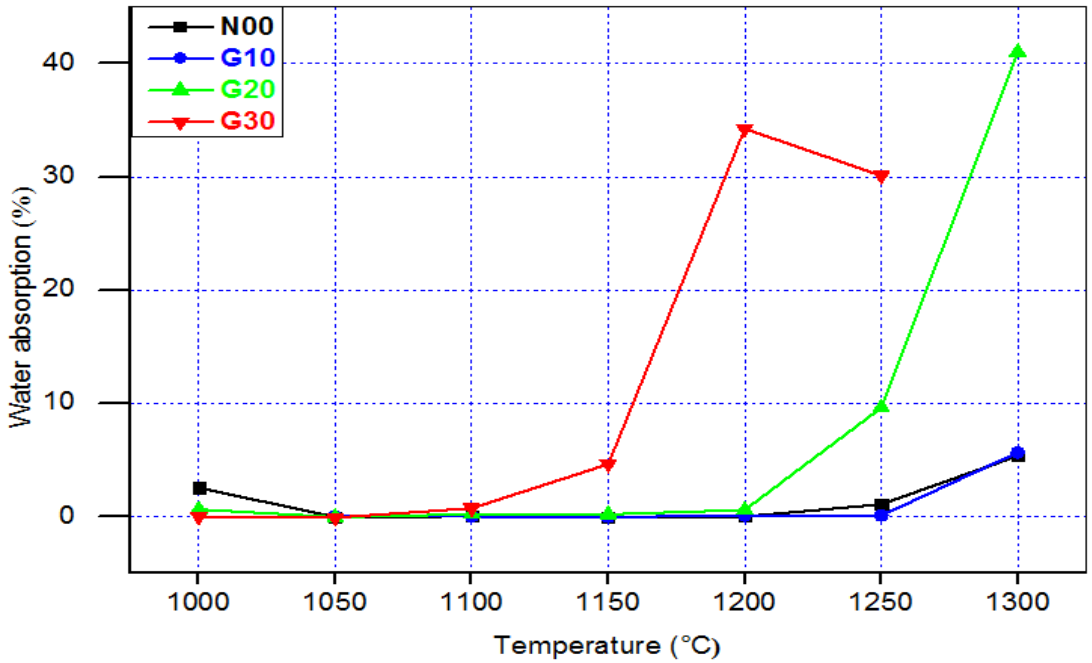

(b)

Figure 5. 10 (a): Shrinkage and (b): Water absorption of the samples sintered at different temperatures

Fig. 5.10b shows the evolution of water absorption of the porcelain samples as a function of temperature. The absorption of water near to zero or very low between 1050° and 1250°C for N00 and G10 samples. This means that the open porosity is completely converted to closed porosity. The appearance of the liquid phase between 1250° and 1300°C causes a swelling of the samples. The release of gases trapped in the closed pores produces a small amount of open porosity. However the absorption of a small amount of water means that the porosity is small.

In the G20 samples, there is a sharp increase in water absorption from 1250°C. This increase is due to the creation of open porosity. For G30 samples, there is a slight increase in water absorption from 1150°C. It also means a strong increase at 1200° and 1250°C, which is explained by the creation of a large degree of open porosity. In general, the water absorption is in agreement with the results obtained in open porosity.

Figure. 5.11 shows the microstructure of all samples sintered at 1100°C for 2 h. Based on phase chemical analysis and phase morphology, it was possible to identify the phases named in Figure 5.11. All fired samples contain quartz. This residual quartz is retained from the original quartz contained the starting raw materials. In N00 and G10 samples, a well-nigh of quartz grains (randomly form with the vitreous phase) and small grains of mullite are observed as shown in Fig (5.11a and 5.11b) respectively [5.18]. In G20 samples, quartz grains are showing different grain sizes, which confirms the relatively good densification of samples sintered at 1100° In this case multiple phases such as mullite and anorthite were revealed (Fig 5.11c). The presence of anorthite was a consequence of the calcium oxide within the waste glass composition. Moreover, the presence of pores is clearly visible in this sample. For the G30 samples (Fig 5.11d), a notably change of the microstructure is observed. There are substantial amounts of both crystalline (quartz) and glassy phases. The sample containing glass 20 wt % and sintered at 1100 °C, shows an improvement on the physical behaviour of the insulator.

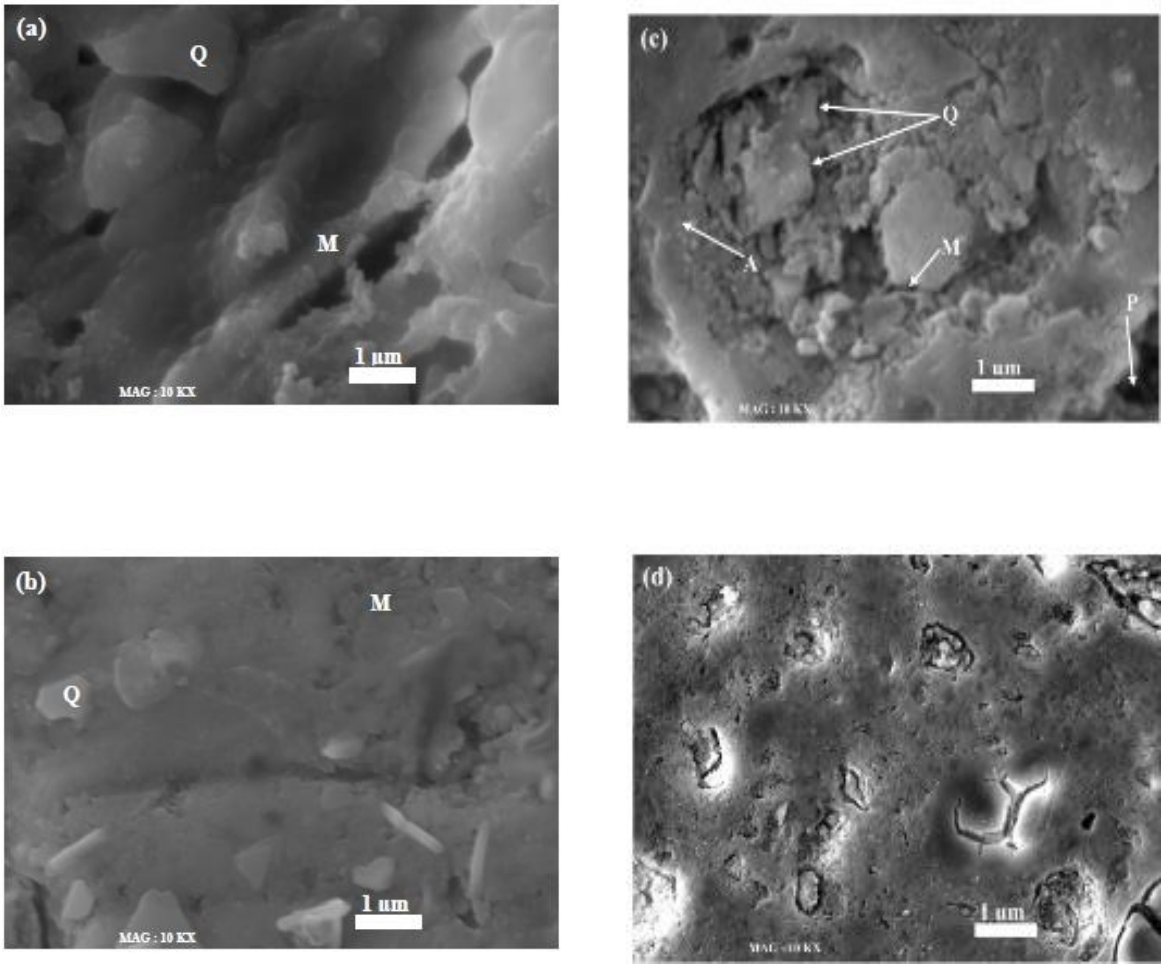

Figure 5. 11 SEM micrographs of the samples sintered at1100°C for 2h :(a) G00, (b) G10,(c) G20,and (d) G30

5.3.2.2. Hardness measurement

The micro-hardness test is an excellent way to evaluate the effect of variables on hardness or resistance to penetration of porcelain samples, mainly after surface etching. This procedure allows the selection of areas free of porosities and allows indentations on heterogeneous areas. The procedure allows determining the Vickers hardness (Hv). It is known from the literature [5.19] that the produced impression dimension is related to the applied load according to the hardness of the material.

Vickers micro-hardness (Hv) of sintered samples were determined using a Zwick microhardness tester model 3210.Hv is measured by pressing a rod tip into the material surface and finding the amount of deformation from the dimensions of the

formed indenter. A load (P) of 500 g was used; this load was optimized through changing the load from 100 g to 500 g [24]. The time period of the indentation was 12 s immediately after the indentation, the diameters (d) of the formed indents were measured. Hv is quantified using the equation

$$Hv = 1.8544 \frac{P}{d^2} \quad (5.2)$$

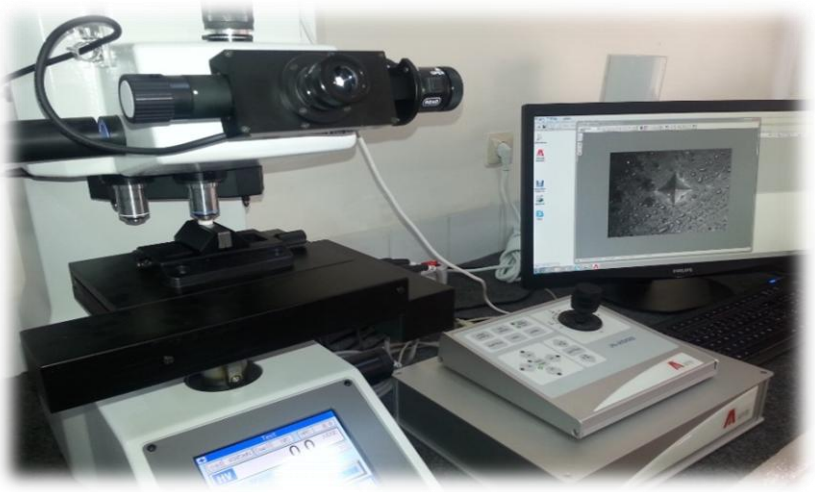

Figure 5. 12 Experimental set-up for measurement of mechanical proprieties

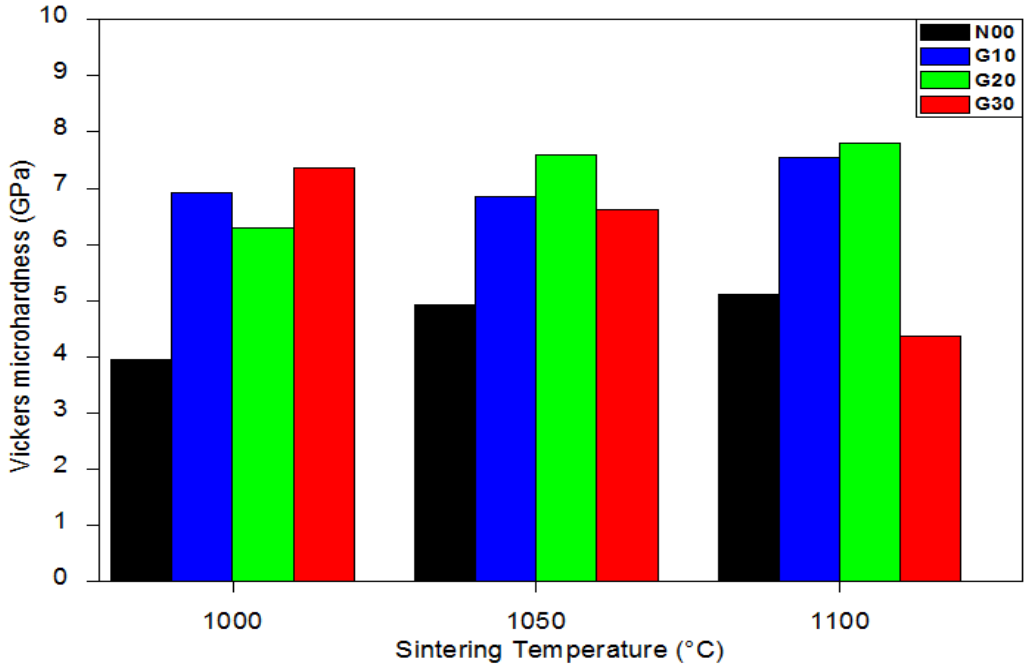

Figure 5. 13 Vickers micro-hardness versus the sintering temperatures for samples containing N00, G10, G20 and G30

Figure.5.13 shows the Vickers micro-hardness (Hv) as function of sintering temperatures. The Vickers hardness values increased from 4 to 8 GPa as the sintering temperatures between (1000 and 1100°C) and it is influenced by glass additions. The existence of mullite increases the micro hardness of porcelain (mullite hardness ≈ 15 GPa) [5.20, 5.21].

It is observed that the addition of glass in porcelain composition leads to an increase in micro hardness values. For G10 and G20 samples, the micro-hardness increase by 33 % and 38 % respectively, in relation to the reference porcelain sample N00 sintered at 1100°C. The increase in both mullite content and bulk density resulting from glass addition porcelain contribute to this improvement. Mullite is considered a key phase during the formation of the porcelain [5.22]. According to XRD patterns, the concentration of mullite increases by adding glass. The concentration of any phase is related to the intensity of their peaks [5.23]. It can be observed also that G30 sample (containing glass instead of Feldspar) sintered at 1000°C shows a high micro-hardness value, which decreases in sample prepared at 1100°C. This is due to a higher densification at 1000°C, which is followed of an increase in residual porosity as temperature increases. However, the micro-hardness values of G10 and G20 samples are approximately constant at the limit of 8 GPa. This is due to presence of feldspar and glass (K_2O, Na_2O) in the original raw material mixture since these fluxing elements facilitate the sintering process and eliminate the residual porosity.

The addition of glass has a positive effect on mechanical properties. The optimal Vickers micro-hardness (8 GPa) is observed in G20 sample thermal treated at 1100°C. This value is relatively raised when compared to that (6.5 GPa) obtained by [5.23, 5.24] but near to that (8.5 GPa) reported by [5.25]. The variation of mechanical properties is mainly related to the vitrification degree and residual porosity [5.26].

Developing an insulator having excellent mechanical strength was realized. The composition has 20 wt % sintered at 1100 °C found to be most suitable for mechanical applications

5.3.2.3. Dielectric properties

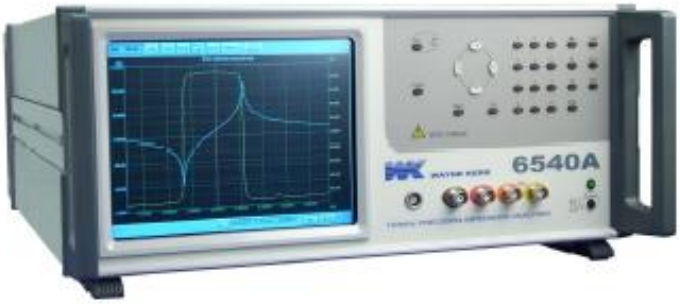

Figure 5. 14 Precision impedance analyzers

The dielectric constant (ε'), dielectric loss factor (ε'') and dielectric loss tangent (tan δ) were measured using a Precision Impedance Analyzer model wayne kerr N°6420. Figure 5.14. In this test, samples of 1.5mm thickness and 13mm diameter were used. Samples were inserted between two planar copper electrodes. This capacitor is subjected to an alternating electric field for different frequencies (200 KHz – 1 MHz).

The dielectric values were improved by adding a glass content of 20 wt % in the base composition. A change of dielectric properties as function of both; conditions of the manufacture of the porcelain body and conditions of measuring was observed, the dependence of dielectric constant (ε'), dielectric loss factor (ε'') and dielectric loss tangent (tan δ) on the frequency (f) is shown in Figure. 5.15(a, b) and Figure 5.16, respectively. It is noted that N00 and G20 samples sintered at 1100 ˚C show a slight decrease and relative stability of the dielectric constant (ε') with the increase in the frequencies as shown in (Fig. 5.15a). This is due to the decrease in the polarization of the space charges. The stability of the dielectric constant (ε') at high frequencies means that the effect of space charge was suppressed [6.25]. On further addition of glass, the dielectric constant value decreases for G20 sample compared with N00 values when measured within the frequency range of 200 KHz–1MHz.

Figure.5.15b shows the dielectric loss factor (ε'') as function of frequency (Hz). It is clearly shown that N00 and G20 samples sintered at 1100 ˚C show a reduction of dielectric loss factor (ε'') values when measured within the frequency range of 200

KHz–1MHz. After that a stability of loss factor values is noted. The results concerning the loss factor values are approximately similar to those reported by several authors [5.16, 5.26].

(a)

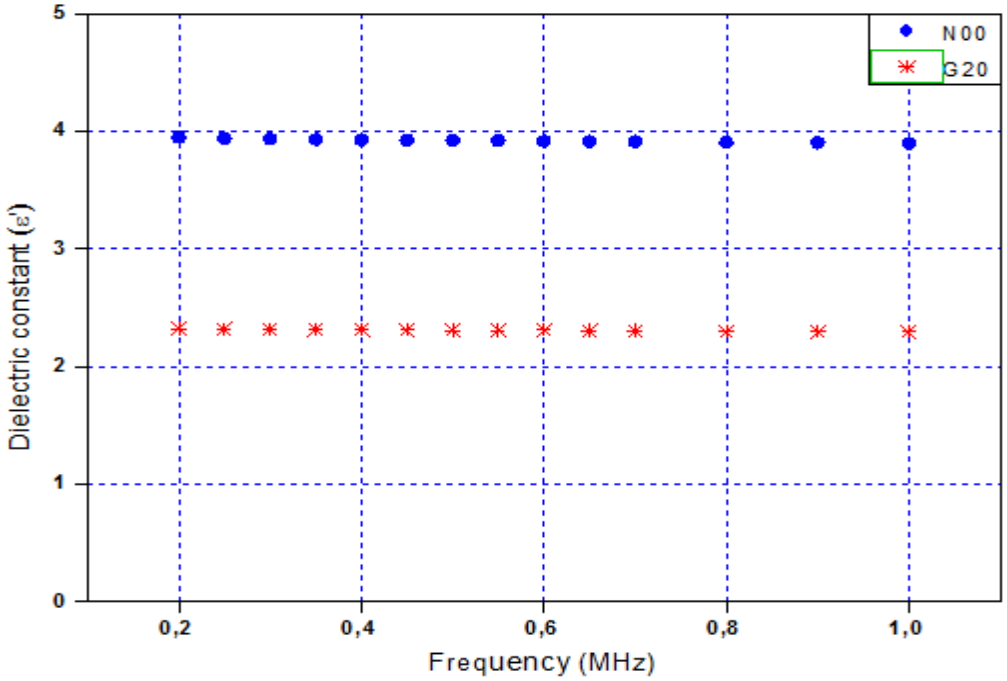

(b)

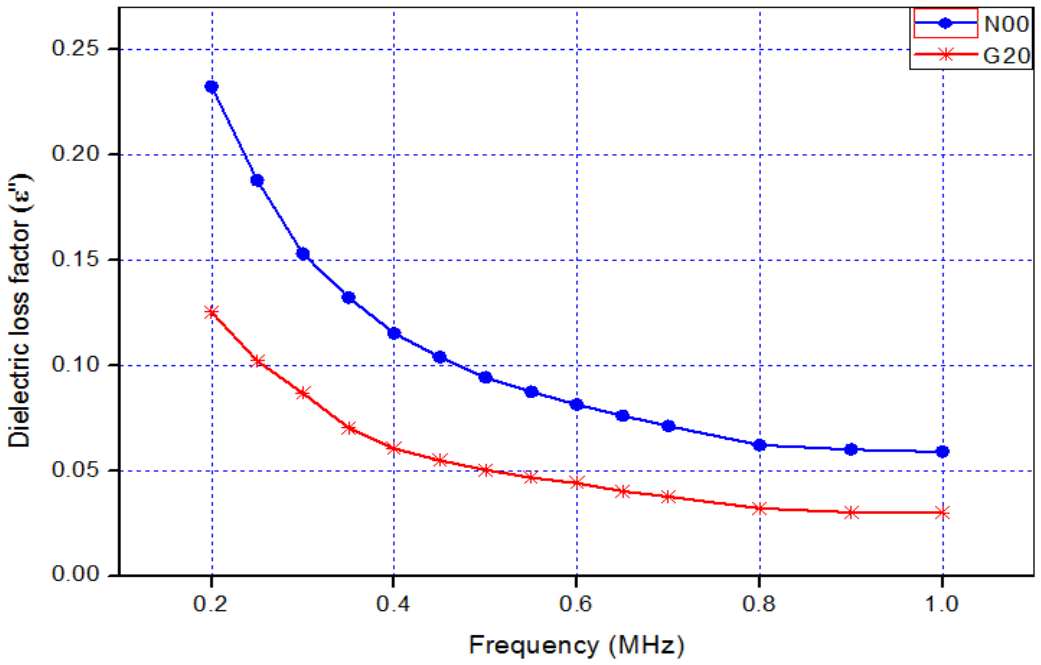

Figure 5. 15 Dielectric constant (ε'), (b): Dielectric loss factor (ε'') versus frequency (MHz)

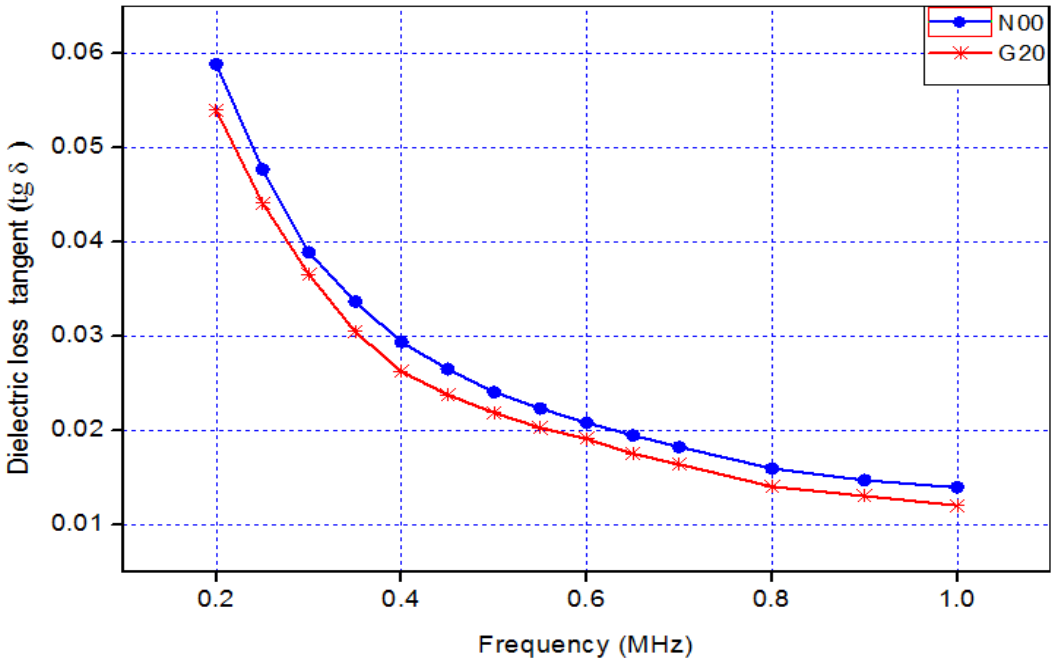

Figure 5. 16 Dielectric loss tangent (tan δ) versus frequency (MHz).

Fig. 5.16 shows the dielectric loss tangent (tan δ) as function of frequency (Hz). A decrease of (tan δ) is found within the range of 200 KHz–1MHz. These values are also approximately similar to values archived by [5.20]. A minor improvement of (tan δ) by adding glass (G20) is reported.

It is known that the dielectric constant of porcelain increases in presence K^+ and Na^+ cations [5.27] and decreases when they are replaced by Ca^{2+}, Mg^{2+}, and Ba^{2+} cations [5.28]. These dielectric properties decrease with the glass addition. Thus, G20 sample showed a 31.02 % of improvement in relation of the reference porcelain sample (N00) at high frequency. Glass phase has a dominant influence on electrical and dielectric properties of fired ceramics. These properties are determined by the concentration and mobility of K^+ and or Na^+ ions in this phase [5.29]. On the other hand, mullite has a vital role on dielectric properties. XRD analyses indicated that samples with added glass showed higher percentage of crystalline phases than classic porcelain without glass addition, which can explains the improvement of dielectric strength.

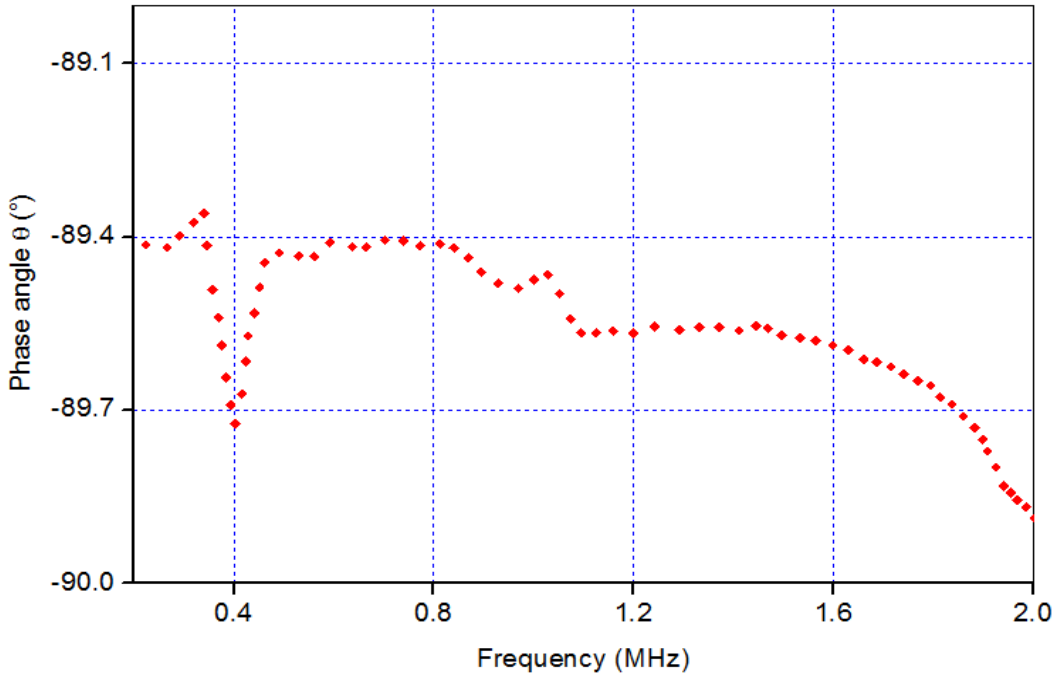

Figure 5. 17 Phase angle θ (°) versus frequency (MHz).

Fig. 5.17 shows phase angle (θ) as function of frequency (Hz). A significant decrease of phase angle values was observed with increasing frequencies. It brings near to (-89.2°). It is important to notify that this result proves that our prepared insulator is a capacitor circuit. This porcelain sample is suitable for application as electrical insulators in the present form because of its higher dielectric.

5.4. Electrical performance of porcelain coated with TiO_2 thin film

5.4.1. Introduction

In order to improve porcelain insulator performance, coatings were used to mitigate surface leakage current, surface discharges and reduce flashover occurrence on existing and installed porcelain insulators. In this section, TiO_2 was added to the surface of our prepared porcelain to study its effect on the electrical properties.

5.4.2. Importance of high voltage insulator's coating

Flashover of insulators due to the accumulation of contaminants poses a threat to the reliability of power systems. Insulator flashover results in undesirable power outages

which are expensive. A combination of contaminants and moisture due to fog or rain on the surface of the insulator will give rise to a leakage current, and uncontrolled leakage currents in this manner leads eventually to complete insulator flashover. The washing of insulators is a common method used to remove the accumulations of surface contaminants in polluted areas. This practice is labour intensive, and therefore expensive. The application of a suitable protective coating to these insulators eliminates the requirement for frequent washing, thus reducing maintenance costs. The coating systems are able to suppress leakage currents. This enables an insulation system to attain increases in flashover voltage of up to 30% when compared with uncoated insulators. Additionally, due to the reduced leakage current magnitudes on the surface of the coated insulators, power dissipation and hence energy losses are reduced, and the resulting reduction of surface heating lessens material degradation. This serves to increase the working life of the coating system. Increasing the insulation level allows power systems engineers to utilise more compact transmission tower designs, which leads to reduced cost to the utilities [5.30].

Several type of coating, such the application of silicones or grease on the insulator surface; have been developed to increase the anti flashover ability, but this alternative is relatively expensive. Also, TiO_2 films are coated on the suspension porcelain insulator surface to improve the anti contamination performance. Based on the testing results of photo-induced self-cleaning performance. In this part of the present work, TiO_2 was added to the surface of porcelain samples, and its effect on the electrical properties was studied.

5.4.3. Experimental procedure

5.4.3.1. Preparation of TiO_2 thin film

Many methods have been used to prepare TiO_2 thin films; electric beam evaporation, sputtering, sol-gel method and vapor deposition. The latter, which is a gas deposition process, provides homogeneous deposits, requiring less equipment. Titanium dioxide is known to crystallize in one of three phases, rutile (tetragonal), anatase (tetragonal) and brookite (orthorhombic). In nature, rutile is the most common crystalline phase,

while brookite is rare. The rutile phase is the most stable at high temperatures. On the other hand, anatase and brookite are metastable phases; and are transformed into rutile by increasing the temperature [5.31]. The aim of the work is to study the effect of a thin layer of TiO_2 on the porcelain properties. In this study, the TiO_2 thin films were obtained by the chemical phase deposition process vapor at atmospheric pressure. The precursor used is titanium tetrachloride ($TiCl_4$) and the reactor gas is Oxygen. The tests evaluated the performance of porcelain, coated and un-coated samples.

5.4.4. Coating evaluation

5.4.4.1. Atomic Force Microscopy (AFM)

Atomic force microscopy (AFM) is one of most important imaging techniques in nanotechnology. Within two and half decades, AFM has been quickly developed as a multi-functional tool to probe rich information related to mechanical, electrical, magnetic, chemical and capacitive properties of surfaces at nanometer scale.

In this thesis, AFM analysis provides very detailed information about the structural details of the porcelain surface, coated with TiO_2 thin film.

Samples surface was scanned in a liquid medium using a microscope with commercial atomic force (PSIA Xe-100) equipped with a scanner and a liquid quartz cell. The topographic images (512 X 512 pixels) are acquired in semi- contact mode comparable with the tapping mode at ambient temperature using points “silicon nitride V” Si3N4. In each case, the excitation frequency of the tip is fixed around 300 KHz and the scanning rate on the surface of the sample is 0.5 HZ.

The measurement of thickness and roughness parameters are prime importance in thin film technologies. First In this work the AFM images have been studied to obtain the roughness and thickness using gwyiddion software (Figure 5.18)**.** The statistical parameters obtained through the software provide the depth in the understanding the texture and morphology in AFM data measurements. In this regards gwyddion helps in providing the user friendly software for measuring thickness and roughness from the scanned profiler data.

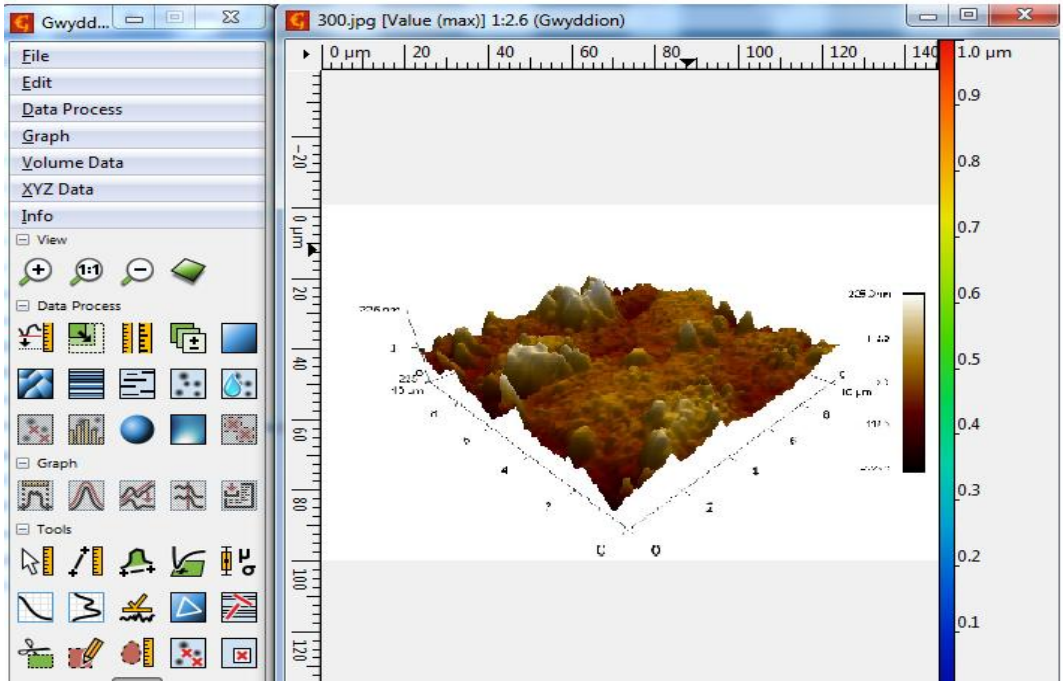

Figure 5. 18 Gwyddion GUI (Graphical User Interface) with AFM Data

The surface morphology and thickness of the TiO_2 film were evaluated (Figure 5.19) The result showed that the film was homogeneously distributed on the surface, so it can be said that the coated surface is highly improved the surface- finish of the substrate. On the other hand, the adhesion to the substrate is one of property that evaluates the durability of coating [5.32]. The obtained results such as smooth and homogeneous surface, enhance the adhesion between the substrate and nano TiO_2 coatings [5.33]. Coatings which do not adhere well to porcelain are not useful as maintenance tool. From the AFM measurements, the roughness and thickness were calculated for a surface of 10 µm x 10 µm. The measured thickness was 133.11 nm. Surface roughness parameters were obtained also from AFM analysis (Figure.5.19). The sample showed a decreasing roughness value 192.766 nm compared with un-coated sample 223.768 nm. A low roughness is a condition to obtain a surface with hydrophilic characteristics [5.34]. The measured value in this study is obeyed to this requirement. It is difficult to compare these results with the data in the literature because roughness parameters depend strongly on the scanning length and the thickness of the film.

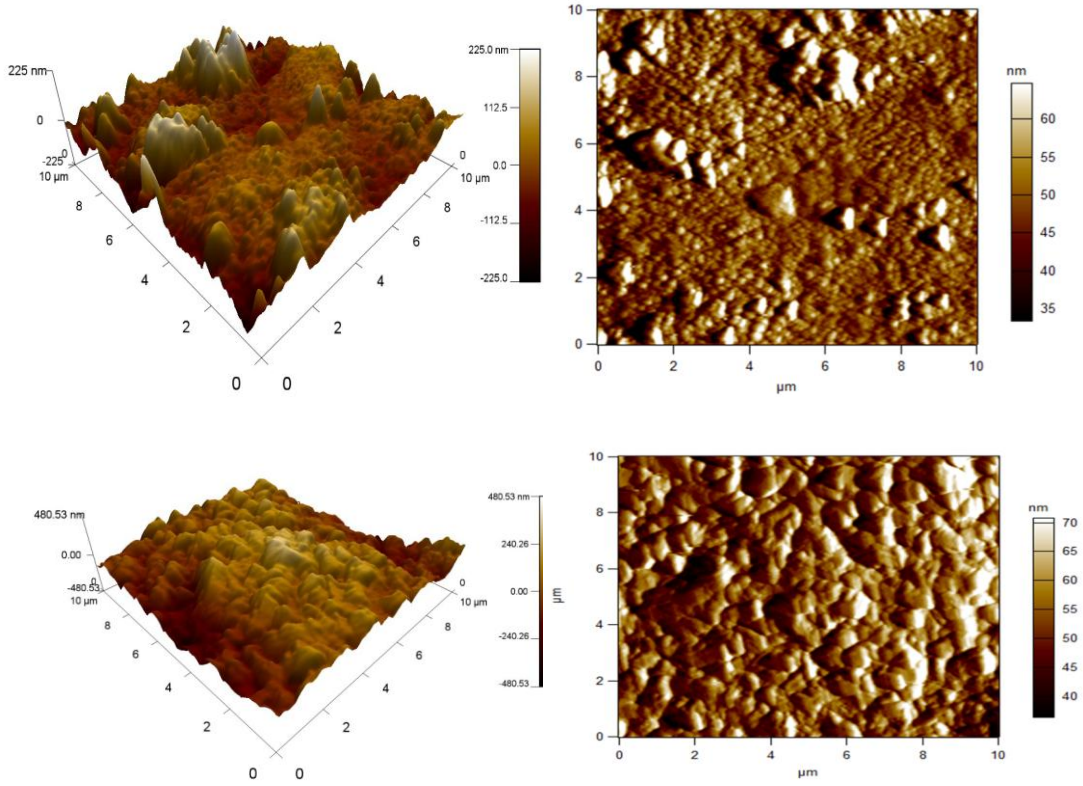

Figure 5. 19 3D and 2 D image profiles of (a) uncoated sample and (b) coated sample with TiO_2 film.

The analysis by Raman technique was carried out in a closed microscope chamber of the spectroscope, with samples being placed on the microscope plate. This technique is used to evaluate the coating and confirm the presence of TiO_2.

To assess the presence of TiO_2, The analysis by Raman technique was carried out in a closed microscope chamber of the spectroscope, with samples being placed on the microscope plate. This technique is used to evaluate the coating and confirm the presence of TiO_2 on the surface. Figure.5.20. shows Micro-Raman spectra obtained from the surface of the coated insulator. TiO_2 was found and identified on the basis of the main titanium band at 144 cm^{-1} as a characteristic band. This Raman map made it possible to assess the presence of TiO_2 on a micro-scale on the surface. The characteristic bands at 144, 399, 519 and 638 cm^{-1} correspond to the anatase TiO_2.

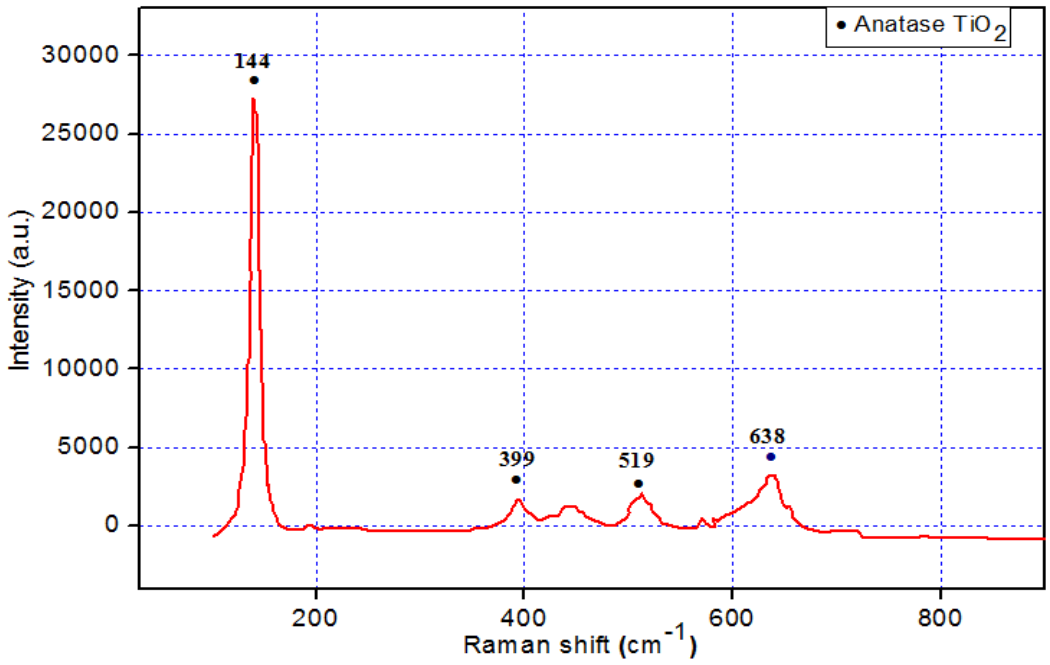

Figure 5. 20 Micro-Raman spectra of TiO_2 of the surface of coated insulator.

The examination of TiO_2 coating by Raman, in consistent with AFM results, confirms the presence of TiO_2 and the films are homogeneous and crack free on the entire surface which shows a proper homogenization of the coating used in this study.

5.4.5. Electrical tests and results

The study of the development of leakage current was made using DC voltage source. The experimental setup is shown in Figure 5.21.The measuring circuit of the flashover voltage is composed of a high-voltage transformer Tr, which delivers a maximum voltage of (120 kV). This circuit is rectified by a diode D and is smoothed by a condenser C. A sample is connected at the boundaries of the protection resistance Ra and at the resistive voltage divider (R0, Ru). The voltage of each test is read directly on a digital crest voltmeter (V).The maximum speed of the slope of the voltage is fixed at (4 kV/s). The selection of this value was made to prevent the partial draining of the pollution's layer deposited on the material surface during the variation of the test's applied voltage. The visualization of the parallel electric discharges is performed by a fast camera (Cam).

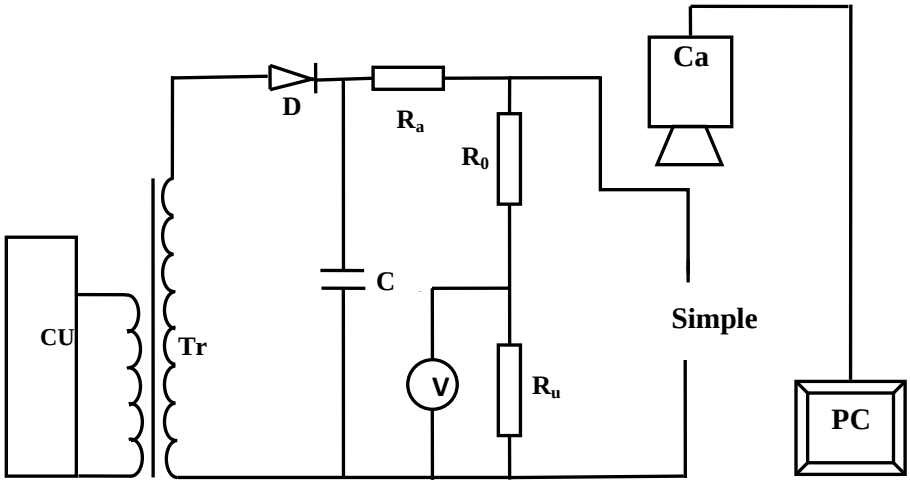

Figure 5. 21 Overall view of Experimental setup.

CU: transformer control unit; Tr: HV transformer; D: Diode; R0, Ru and Ra: resistances; V:digital peak voltmeter; PC :personal computer; Ca: Camera

In this work, pollution was prepared in the laboratory using NaCl and distilled water to achieve a conductivity of 30 **µ**S.

Disc specimens of 13 mm diameter and 5 mm thickness were tested. Samples of each, coated and uncoated were polluted at the ambient temperature. After that, the samples were energized at different values Figure. 5.22 The leakage current was continuously monitored by the equipment display.

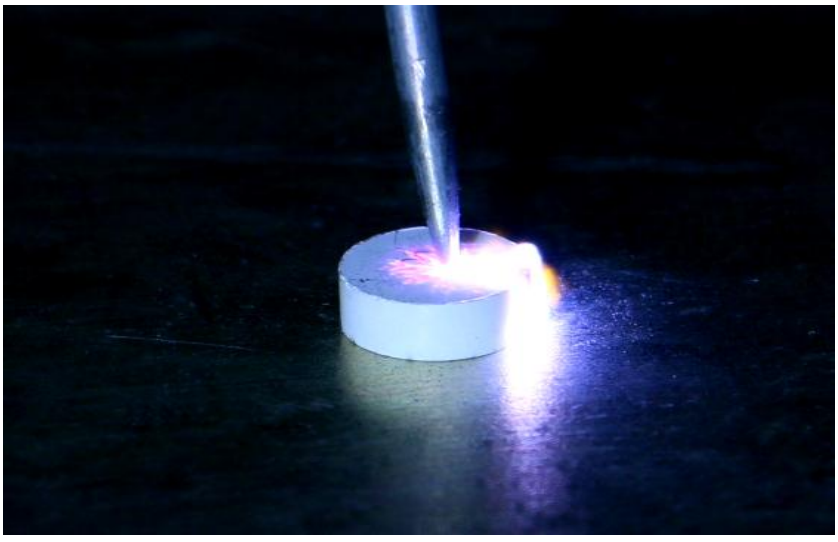

Figure 5. 22 Studied insulator model.

This part deals with the analysis of the performance of coating by monitoring the leakage current on the polluted insulator surface. The applied voltage and the leakage current for both coated and uncoated porcelain were investigated. It was observed that the coating reduces the leakage current under positive and negative polarity Figure.5.23. It is clearly seen that the leakage currents recorded for the coated insulators are lower than those of the uncoated insulators, for all the applied voltage values. In porcelain with-out coating, for a voltage of 6Kv, the obtained value for leakage currents was 148.2.mA, under positive polarity. For the same applied voltage, the leakage current becomes 130.1mA with coating which had ability to suppress leakage current by about 13%. On the other hand, in coated porcelain under negative polarity, the leakage current becomes lower than porcelain with coating under positive polarity. The leakage current depends on the bias polarity. As a result, the conduction mechanism should be electrode limited for at least one of the metal–insulator junctions. From the same tests conducted, the voltage breakdown values for both types of insulator (coated and non- coated) tested under positive and negative polarity, it can be summarized that the value of the breakdown voltage is higher when tested under a positive polarity compared to a negative polarity. It was observed also that the presence of TiO_2 thin film presented the lower leakage current with higher breakdown voltage compared to uncoated sample.

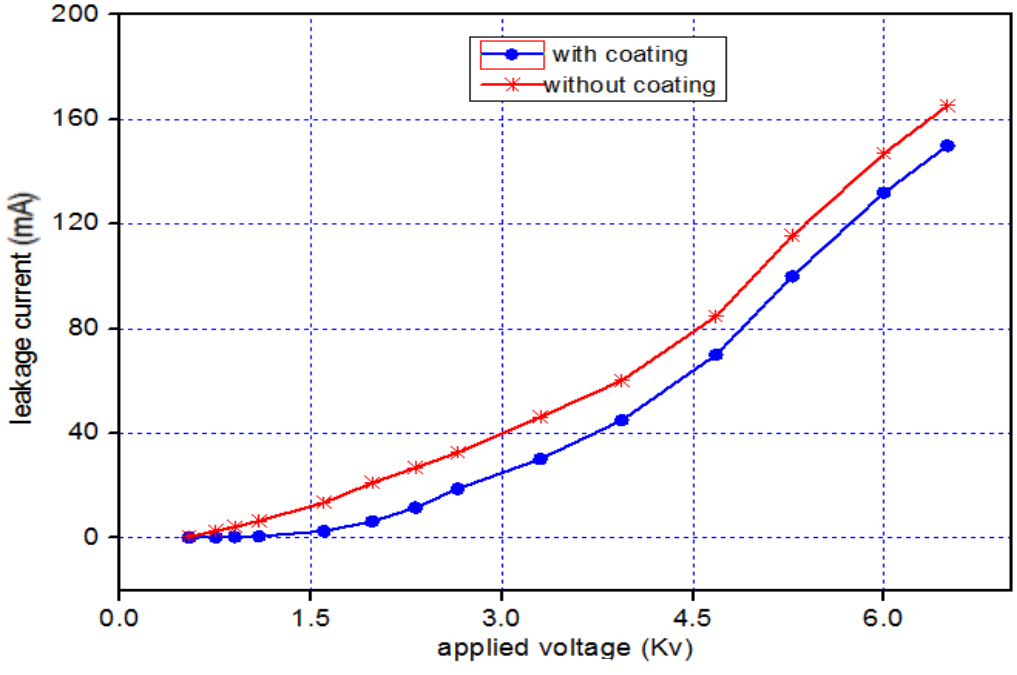

(a)

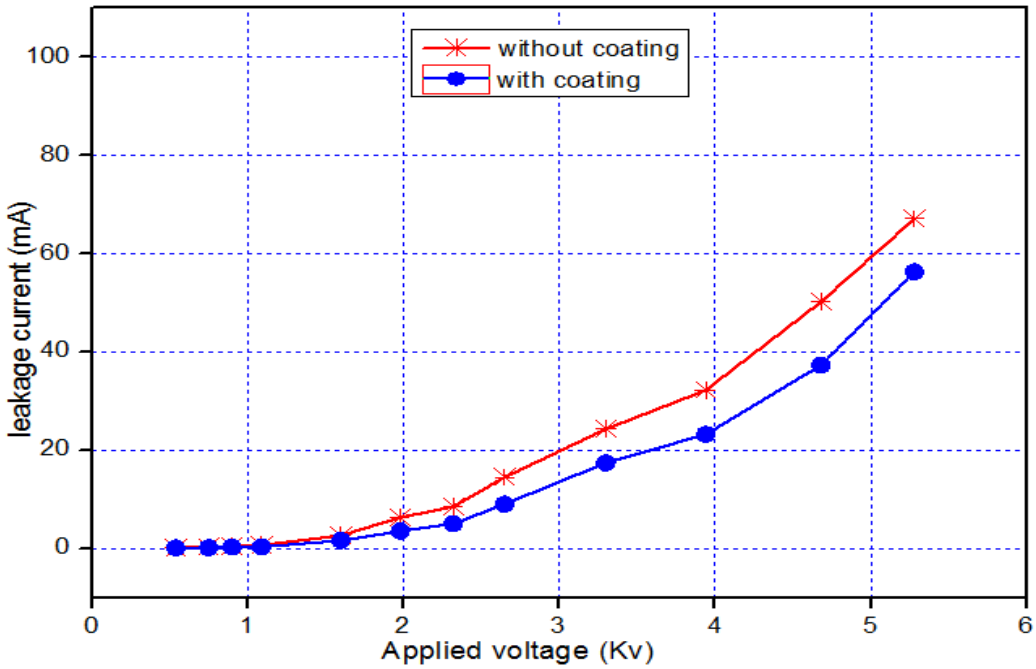

(b)

Figure 5. 23 Leakage current as function of applied voltage for coating and un-coated samples at (a) positive polarity (b) negative polarity.

According to the obtained results;

- The presence of the coating showed superior performance over the non-coated porcelain in suppressing leakage current.
- The low leakage current corresponds with high surface resistance which indicates high quality of insulator [5.35].
- The presence of coating affects the current voltage characteristic of the positive polarity, in Fig. (5.23.a) and negative polarity in Fig. (5.23.b)
- The leakage current and breakdown depends on the polarity.
- Coating of insulator surface using TiO_2 film improving the breakdown strength of the porcelain.

5.4.6. E-field distribution and current density analysis

The finite element method (FEM) aims at modeling insulators to determine the electric potential and the distribution of the electric field. The regions with high stress on the surface of the insulator are determined by the simulation of the field on the surface of

the insulator [5.36]. The present insulator model is developed for coated and uncoated insulator. The porcelain structure can be simplified into a 2-D model. The simulation was performed using COMSOL multiphysics® 4.3b software and the results were given in figures 5.24 and 5.25. The simulation was carried out under identical conditions, whether for the coated or uncoated insulator.

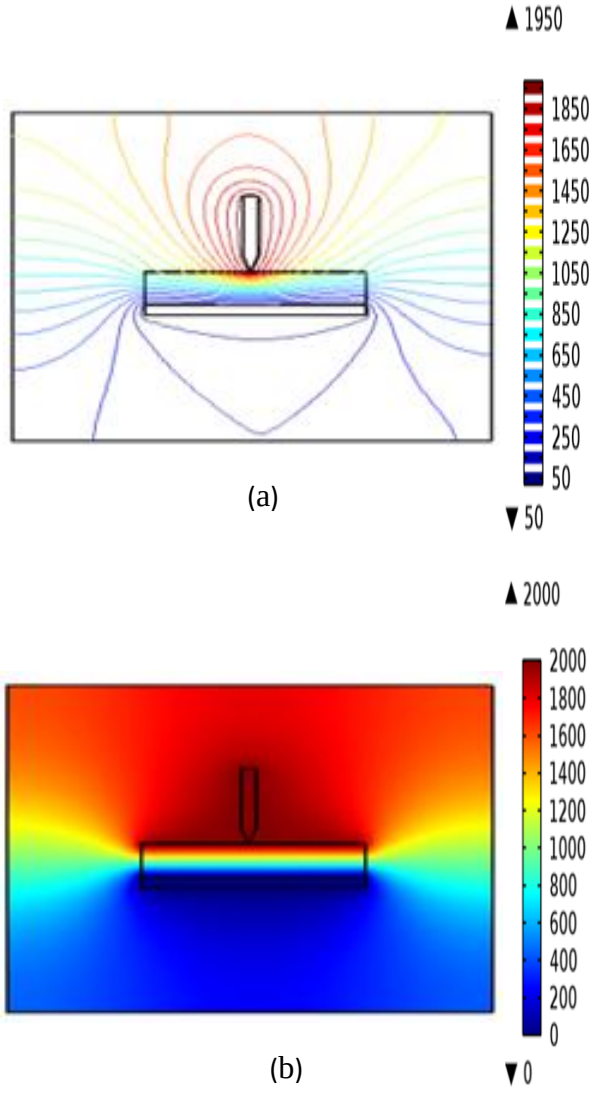

Figure 5. 24. Results of COMSOL simulations of coated sample (a) E-field distribution and (b) electric potential

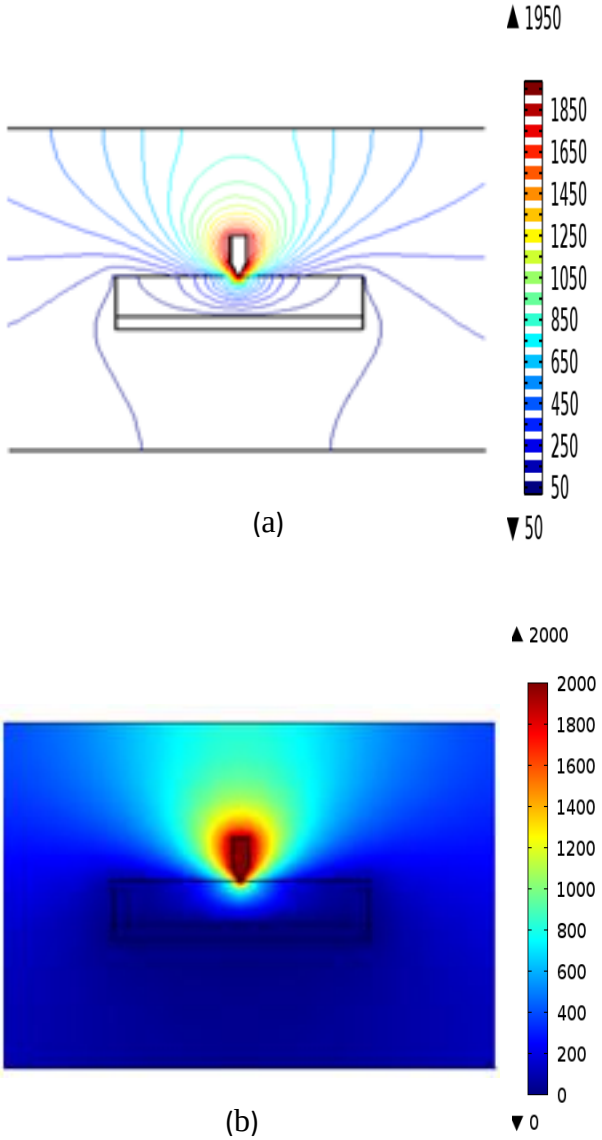

Figure 5. 25 Results of COMSOL simulations of un-coated sample (a) E-field distribution and (b) electric potential

The Figure 5.24(a) shows a fairly regular distribution for the coated insulator by comparing with sample without coating Figure 5.25(a). This distribution is the consequence of the improvement of the surface by the deposited coating. When the distribution is not regular, it will cause an increase of the temperature of the surface and consequently the degradation of this one because of the thermal stress [5.37]. Figures 5.25(b) and 5.24(b) show the equi-potential contours along the surface distance of coated and uncoated insulators respectively.

It is noticed that the potential contours in the case of the coated sample, are concentrated near the metal fittings, indicating high field regions with less field intensity along the insulator surface compared with uncoated sample. From the simulation results obtained, it can be seen that the field stress is very much improved in the case of an insulator coated with TiO2. The measured electric field and current density profiles are shown in Figures 5.26(a) and 5.26(b) respectively.

The values of current density and the electrical field in coated sample with TiO_2 are less than the uncoated one for the same applied voltage. This indicates that the film has good insulating property. A difference in the electric field distribution has been observed along the coating sample, compared with un-coating one. This is due to the amelioration of the surface. Good agreement was obtained between the results, which were obtained by electrical tests and those obtained by simulation.

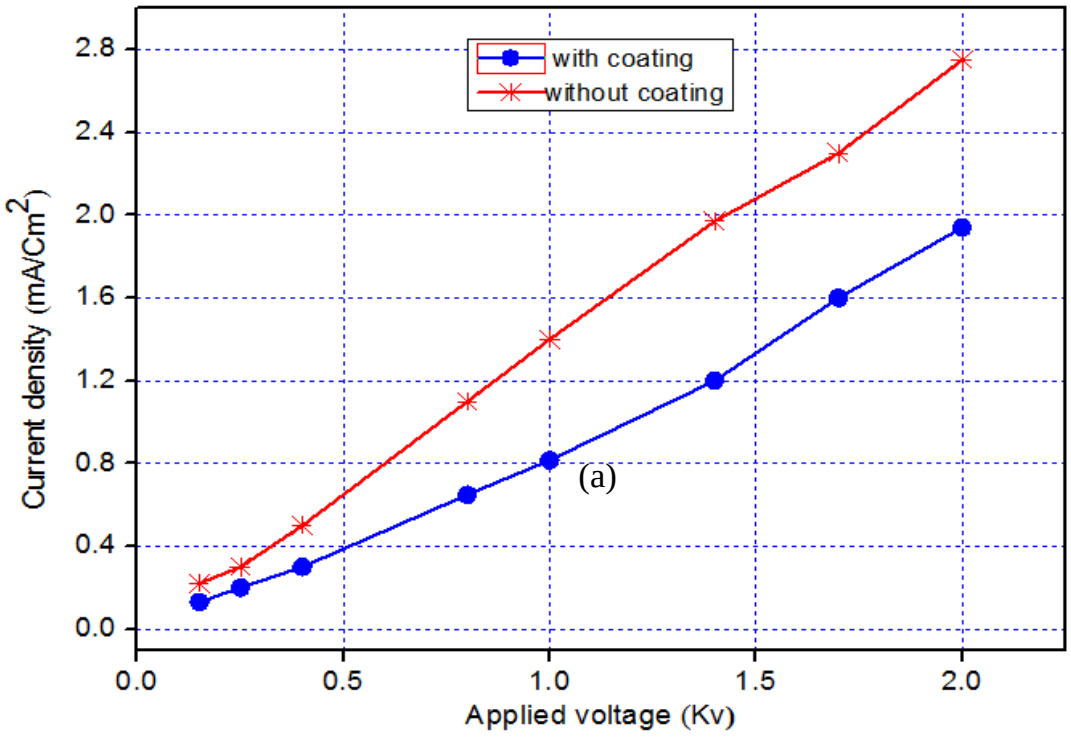

(a)

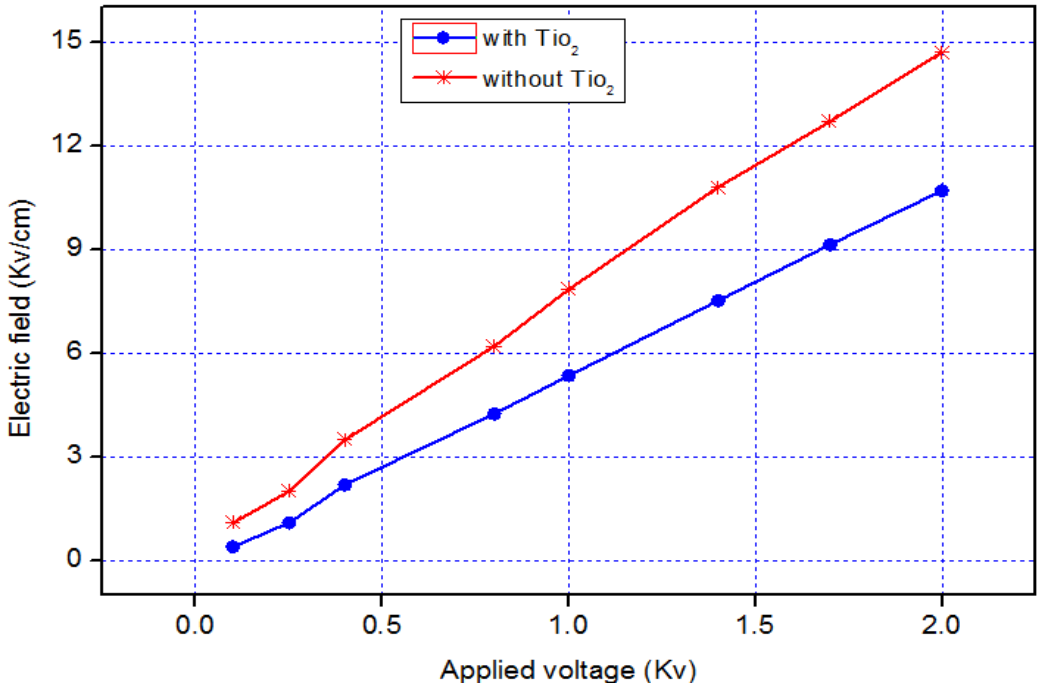

(b)

Figure 5. 26 E-field (a) and current density (b) as function of applied voltage.

5.5. Conclusion

In this chapter, the development of porcelain from locally raw materials was lighted. The effects of recycled waste glass in partial replacement of feldspar for porcelain are discussed. Measurements have been performed by different characterization methods. Experimental results showed significant effects of recycled waste glass substitution on physico-mechanical properties. TiO_2 thin film was added to the surface of porcelain samples and its effect on the electrical properties was studied and discussed. AFM analysis provides very detailed information about the structural details of the porcelain surface. Electrical tests showed that Coating of insulator surface improves the breakdown strength of the porcelain and the presence of the coating showed superior performance over the non-coated porcelain in suppressing leakage current.

Chapter 06

General Conclusions

Chapter 06

General Conclusions

6.1. Conclusions

Outdoor insulators are widely used in overhead transmission lines. Surface degradation which is caused by electrical stress on the high voltage terminal of the insulators is the major cause its failure. That is why reliability of the insulator is the most important property that must take into consideration whether it is a polymeric insulator or ceramic insulator. The good insulator should offer optimum electrical and mechanical strengths.

The work presented in this thesis concerns the study of performances of composite and porcelain insulators. The first part of this study deals with the use of corona ring at the HV end fitting for improving the electric field and potential distributions and then for minimizing the corona discharges on composite insulator. To achieve this, optimization technique based Bat algorithm is developed for obtaining the optimized corona ring parameters. The reduced intensify of electric field can help the insulator to improve its performance and furthermore will improve its reliability. The potentials and electric fields distribution along developed polymeric insulator has been evaluated by using Finite Element Method (FEM) computational simulation. Maximum electric field strengths on the live end side were importantly decreased. Reported results show also that the potential distribution has become more uniform in this case. Compared to other methods, Bat Algorithm was found faster, more efficient and sustainable compared with other methods of optimization in the literature. The second part of the thesis concerns the other type of insulator: Porcelain. In this part we study the possibility of development porcelain from locally raw materials using recycled waste glass. This last, is responsible for the improvement in the Vickers micro-hardness as well as the dielectric constant value. The low dielectric constant provides the

advantage of using the insulator in high voltage. Moreover, The TiO_2 thin film was added to the surface of porcelain samples and its effect on the electrical properties was studied and discussed. Simulations for coated and uncoated insulators surfaces were also performed. The obtained results showed that Coating of insulator surface using TiO_2 film enhances the breakdown strength of the porcelain and the presence of the coating showed superior performance over the non-coated porcelain in suppressing leakage current. A good agreement was achieved between the results of the experiments, those obtained using the electrical tests and those obtained using the simulation program. This correlation provides useful information about the influence of TiO_2 thin film and its role in i0mproving the electric properties of porcelain.
The proposed techniques in this thesis give an efficient fast working tool to examine and optimize the performance of the two studied insulators without extra high effort.

6.2. Recommandations

The work can be extended to further studies as mentioned below:

- Study of degradation and ageing of composite insulator under various contingenesis conditions like, contamination and other degrading effects to assess short and long-term grading performance.

- Development of 3D FEM modeling to take into account the effect of practical configurations for a better and more realistic electric field computation and analysis.

- Measurements of surface conductance of polluted insulator require repetitions. In order to establish a reliable non-linear pollution model for computational modeling and simulation.

Bibliographic References

Bibliographic References

Chapter 1

[1.1] E. Cherney, A. Baker, J. Ku_el, Z. Lodi, and D. S. G. Phillips, A.and Powell."Evaluation of and replacement strategies for aged high voltage porcelain suspension-type insulators," IEEE Transactions on Power Delivery, 2014.

[1.2] R. Znaidi."Research and Assessment of Insulator Performance in Marine and Desert Environment", Insulator News Marketing Report, pp. 12-22, 2000.

[1.3] R. Hackam. "Outdoor HV composite polymeric insulators," IEEE Transactions on Dielectrics and Electrical Insulation, vol. 6, pp. 557-585, 1999.

[1.4] E. Da Silva, S. M. Rowland. "In Service Surface Degradation of MV Composite Insulators Under Severe Environmental Conditions and Low Electric Stress", Annual Report Conference On Electrical Insulation Dielectric Phenomena, pp. 224-227, 2008.

Chapter 2

[2.1] R. S. Gorur, E. A. Cherney, R. Hackam and T. Orbeck. "The Electrical Performance of Polymeric Insulating Materials under Accelerated Aging in Fog Chamber", IEEE Trans. PD, Vol. 3, pp. 1157-1164, 1988.

[2.2] F. J. Liptrot. "An examination of the service performance of ceramic insulators", in IEE Colloquium on Review of Outdoor Insulation Materials, , pp. 4/1-4/7,1996

[2.3] C. Bayliss, B. Hardy. "Transmission and Distribution Electrical Engineering", 4th edition: Elsevier, ISBN 0080969135, 2011.

[2.4] P. S. Ghosh and N. Chatterjee. "Polluted Insulator Flashover Model for AC Voltage", IEEE Transactions on Dielectrics and Electrical Insulation, vol. 2, no. 1, pp. 128-136, 1995.

[2.5] A. Rawat and R. Gorur. "Microstructure based evaluation of field aged and new porcelain suspension insulators," IEEE Transactions on Dielectrics and Electrial Insulation, vol. 16, no. 1, pp. 107-115, 2009.

[2.6] E.Cherney and R.Hooton."Cement growth failure mechanism in porcelain suspension insulators," IEEE Transaction on Power Delivery, vol.2, no.1, pp.249-255, 1987.

[2.7] J. Looms. " Insulators for high voltages. Peter Peregrinus Ltd", vol. 7. 8, 15, 29, 1987.

[2.8] J.Looms. T. Insulators for High Voltages, London: The Institution of Electrical Engineers, 1988.

[2.9] A. Mishra, R. Gorur, and S. Venkataraman. "Evaluation of porcelain and toughened glass suspension insulators removed from service," Dielectrics and Electrical Insulation, IEEE Transactions on, vol. 15, no. 2, pp. 467-475, April 2008.

[2.10] J. Li, C. Sun, and S. Sebo. "Humidity and contamination severity impact on the leakage currents of porcelain insulators," IET Generation, Transmission & Distribution, vol. 5, no. 1, pp. 19.

[2.11] L. Grigsby. "The electric power engineering handbook". Chemical Rubber Company Pr I Llc, 2001.

[2.12] K. Naito, Y. Mizuno, and W. Naganawa. "A study on probabilistic assessment of contamination ashover of high voltage insulator," Power Delivery, IEEE Transactions on, vol. 10, no. 3, pp. 1378-1384, Jul 1995.

[2.13] Selection and dimensioning of high-voltage insulators for polluted conditions, Std. IEC 2002.

[2.14] D. Williams, A. Haddad, A. Rowlands, H. Young, and R. Waters. "Formation and characterization of dry bands in clean fog on polluted insulators," IEEE Transactions on Dielectrics and Electrical Insulation, vol. 6, no. 5, pp. 724-731, 1999.

[2.15] K. Naito, Y. Mizuno, and W. Naganawa. "A study on probabilistic assessment of contamination flashover of high voltage insulator," Power Delivery, IEEE Transactions on, vol. 10, no. 3, pp. 1378-1384, Jul 1995.

[2.16] E.Kuffel, W. S. Zaengl, and J. Kuffel. "High Voltage Engineering: Fundamentals". 2nd edit., Newness Publications, UK, 2003.

[2.17] B. Hampton. "Flashover mechanism of polluted insulation," Electronics and Power, vol. 10, no. 4, p. 113, 1964.

[2.18] R. S. Gorur, E. A.Cherney, J. T. "Burnham, Outdoor Insulators", Phoenix, Arizona, USA, 1999.

[2.19] A. Celine Mahieux. "Environmental Degradation in Industrial Composites". Elsevier, 2005.

[2.20] B. R.Varlow, J. Robertson and K.P. Donnelly. "Nonlinear fillers in electrical insulating materials", IET Sci. Meas. Technol., vol 1 (2), pp. 96-102, 2007.

[2.21] M.A.Laughton , D.F Warne."Electrical Engineer's Reference Book".Oxford, Newnes., 2002.

[2.22] J.Crespo-Sandoval. "Condition Monitoring of Outdoor Insulation using Artificial Intelligence Techniques," PhD Thesis, University of Wales Cardiff, 2005.

[2.23] C. A.Spellman, H. M.Young, A.Haddad, A. R.Rowlands, and R. T.Waters. “Survey of polymeric insulator ageing factors,” in Proceedings of the Eleventh International Symposium on High Voltage Engineering, Conf. Publ. No. 467, Vol. 164. pp. 160-163, 1999.

[2.24] A.L Souza, I.J.S. Lopes. “Electrical field distribution along the surface of high voltage polymer insulators and its changes under service conditions”, IEEE International Symposium on ELINSL, pp. 56-59. 2006.

[2.25] R.Hartings. “Electrical Fields Along a Post Insulator: AC Measurements and Calculations”, IEEE Transaction on Power Delivery, Vol. 9, pp. 912-918, 1994.

[2.26] B.Venkatesulu and M. J.Thomas. “Corona agind studies on silicone rubber nanocomposites, “IEEE Transactions on Dielectrics and Electrical Insulation, vol. 17, pp. 625-634, 2010.

[2.27] G. G. Karady, and R. L.Brown. “Flashover Mechanism of Silicone Rubber Insulators Used For Outdoor Insulation”, IEEE Trans. On Power Delivery,Vol. 10 (No. 4): pp. 1965-1971, 1995.

[2.28] C.Muniraj, K. Krishnamorthi, and S.Chandrasekar. “Investigation on Flashover Development Mechanism of Polymeric Insulators by Time Frequency Analysis”, J Electrical Eng. Tech., Vol. 8, No. 6, pp. 1503-1511, 2011.

[2.29] M. Bouhaouche, A. Mekhaldi, M. Teguar. “Composite Insulators in a 400 kV AC Line in Algeria for Improving Electric Field Distribution”, 3rd CISTEM’18 - Algiers, Algeria, October 29-31, 2018.

[2.30] Q. Yang, W. Sima, Y. Deng Jiazhuo uan Tao, L. Chen. “New Optimization Method on Electric Field Distribution of Composite Insulator”,Electrical Insulation and Dielectric Phenomena (CEIDP) Annual Report Conference, pp. 1-4, Oct 2010.

[2.31] W. Sima, F.P. Espino-Cortes, E.A. Cherney, S.H. Jayaram.“Optimization of Corona Ring Design for Long-Rod Insulators Using FEM Based Computational Analysis”, Conference Record of the 2004 IEEE International Symposiumon Electrical Insulation, pp. 480-483, Sept 2000.

[2.32] D.C.Dominguez, F.P. Espino-Cortes, P.Gomez. “Optimization of Electric Field Grading Systems in Non-Ceramic Insulators”, Electrical Insulation Conference (EIC), pp. 231-234, June 2011.

[2.33] E.Niedospial. “Design and Application of Corona and Grading Rings forComposite Insulators”, Transmission and Distribution Conference and Exposition (T&D), IEEE PES, pp. 1-3. 2012.

[2.34] E. Akbari et al. “Effects of Disc Insulator Type and Corona Ring on Electric Field and Voltage Distribution over 230-kV Insulator String by Numerical Method”, Iranian Journal of Electrical & Electronic Engineering, Vol. 9, No. 1, March 2013.

[2.35] S. Ilhan; Aydogan Özdemir. "Effect of Corona Ring Design on Electric Field Intensity and Potential Distribution Along an Insulator String," IEEE ELECO, 2007.

[2.36] T. Zhao, M. G. Comber. "Calculation of Electric Field and Potential Distribution Along Non-Ceramic Insulators Considering the Effects of Conductors and Transmission Towers," IEEE Transactions on Power Delivery, Vol. 15, No. 1, pp. 313-318, January 2000.

[2.37] B. Shuaib Mohamed, "Coatings for outdoor high voltage insulators". School of Engineering. Cardiff University, Cardiff. 2013.

Chapter 3

[3.1] Jasem A.O. AlQallaf "Corona Discharge" Bachelor thesis Academic year: 2009/2010.

[3.2] C. Bayliss, B. Hardy, "Transmission and Distribution Electrical Engineering", 4th Edition, Elsevier, ISBN 0080969135, 2011.

[3.3] R. A. Bernstorf, R. K. Niedermier and D. S. Winkler. "Polymer Compounds Used In High Voltage Insulators," Hubbell Power Systems, The Ohio Brass Company.

[3.4] Laughton, M. A., Warne, D. F., "Electrical Engineer's Reference Book," Sixteenth Edition, Newnes Publication, 2002.

[3.5] W. Sima, F.P, Espino-Cortes, A.C Edward. and H.S., Jayaram. "Optimization of Corona Ring Design fo Long-Rod Insulators Using FEM Based Computational analysis" .IEEE International Symposium on Electrical Insulation, Indianapolis, in USA, 19-22 September, pp. 480-483. 2004

[3.6] W. Sima, K. Wu, Q. Yang, C.Sun. "Corona Ring Design of +/-800 kV DC Composite Insulator Based on Computer Analysis", IEEE International Conference on electrical Insulation and Dielectric Phenomena, pp. 457-460, 2006.

[3.7] B. M'hamdi, M. Teguar, A. Mekhaldi. "Optimal Design of Corona Ring on HV Composite Insulator Using PSO Approach with Dynamic Population Size", IEEE Trans on DEI. Vol. 23 pp.1048-1057,2016.

[3.8] S. Zhang, Z. Peng, L. Peng, H. Wang. " Optimization of corona ring structure for UHV composite insulator using finite element method and PSO algorithm", in:2013 IEEE International Conference on Solid Dielectrics (ICSD), Bologna, pp. 210-213,2013.

[3.9] H. Terrab, A.Kara. "Parameters design optimization of 230 kV corona ring based on electric field analysis and response surface methodology", Electr. Power Syst. Res. Vol.163, pp782-788, 2017.

[3.10] D. Cruz Domínguez, F. P. Espino-Cortés, and P. Gómez , Optimized design of electric field grading systems in 115 kV non-ceramic insulators, Electrical Insulation Conference, Annapolis, Maryland, 5 to 8 June 2011 .

[3.11] A. Diako , A.Gholami , A.Siadatan. "Corona ring optimization for different cases of polymer insulators based on its size and distance, J.Artificial Intellin Elect Engineering". Vol, PP. 1-7, 2012.

[3.12] X.S.Yang, A.H. Gandomi, Bat algorithm. "A novel approach for global engineering optimization". Eng. Comput.Vol.29 pp.464-483, 2012.

[3.13] X.-S. Yang. "A new metaheuristic bat-inspired algorithm". In Nature in-spired cooperative strategies for optimization (NICSO 2010). Springer, pp. 65-74, 2010.

[3.14] A.Colorni, , M.Dorigo, V.Maniezzo, et al. "Distributed opti-mization by ant colonies". In Proceedings of the first European conference on artificial life, vol. 142, Paris, France, pp. 134-142, 1991.

[3.15] Y. Del Valle, G. K. Venayagamoorthy, S. Mohagheghi, J.-C.Hernandez and R. G. Harley. "Particle swarm optimization: basic concepts, variants and applications in power systems". IEEE Transactions on evolutionary computation. Vol. 12, n° 2, pp.171-195, 2008.

[3.16] M. Dhivya, M. Sundarambal, , J. O. and Vincent. " Energy efficient cluster formation in wireless sensor networks using cuckoo search". In International Conference on Swarm, Evolutionary, and Memetic Computing, Springer, pp. 140-147. 2011

[3.17] O. B.Haddad, M. Solgi, H. A. "Loáiciga, Bat algorithm, meta-heuristic and evolutionary algorithms for Engineering Optimization", John Wiley & Sons, Inc.pp. 213-222, 2017.

[3.18] Jr. I.Fister, D. Fister, and X.-S. Yang. "A hybrid bat algorithm. arXiv preprint arXiv". pp.1303-6310, 2013.

[3.19] G. Wang, and L. Guo. "A novel hybrid bat algorithm with harmony search for global numerical optimization". Journal of Applied Mathematics, 2013.

[3.20] J. Xie, , Y. Zhou, , and H. Chen. "A novel bat algorithm based on differential operator and levy lights trajectory". Computational intelligence and neuroscience, 2013.

[3.21] A. H. Gandomi, X.-S.Yang, A. H. Alavi, and S. Talatahari. "Bat algorithm for constrained optimization tasks". Neural Computing and Applications. Vol. 22, n°6, pp.1239-1255, 2013

[3.22] S. Goel, N. Goel, and D. Gupta. " Unconstrained optimisation through bat algorithm". International Journal of Intelligent Engineering Informatics Vol. 2, n°4, pp. 259-270, 2014.

[3.23] X.-S. Yang. "Bat algorithm for multi-objective optimization". International Journal of Bio-Inspired Computation". Vol. 3, n° 5, 267-274, 2011.

[3.24] L. M. Amine, and K. A Nadjet. “multi-objective binary bat algorithm”. In Proceedings of the International Conference on Intelligent Information Processing, Security and Advanced Communication, ACM, p. 75, 2015.

[3.25] S. Mishra, K.Shaw, and D.Mishra. “A new meta-heuristic bat inspired classification approach for microarray data”. Procedia Technology Vol.4, pp.802-806, 2012.

[3.26] Khan, K., and Sahai, A. “A comparison of BA, GA, PSO, BP and LM for training feed forward neural networks in e-learning context”. International Journal of Intelligent Systems and Applications Vol.4, pp 7- 23, 2012.

[3.27] K.Khan, A.Nikov, and A. Sahai. “A fuzzy bat clustering method for ergonomic screening of once workplaces”. In Third International Conference on Software, Services and Semantic Technologies S3T, Springer, 2011.

[3.28] K. Khan, A.Sahai and A. A. Campus. “fuzzy c-means bi-sonar-based metaheuristic optomization algorithm”. IJIMAI Vol. 1, n° 7, 26-32. 2012.

[3.29] G. Komarasamy, and A. Wahi. “An optimized k-means clustering technique using bat algorithm”. European Journal of Scientific Research. Vol.84,n° 2, 26-273, 2012.

[3.30] Y. Aboubi, H. Drias, and N. Kamel. “ Bat-clara: Bat-inspired algorithm for clustering large applications”. IFAC-Papers OnLine. Vol. 49, n°12, pp. 243-248, 2016.

[3.31] M. A. Laamari, , and N. Kamel. “A hybrid bat based feature selection approach for intrusion detection”. In Bio-Inspired Computing-Theories and Applications. Springer, pp. 230-238, 2014.

[3.32] J. Senthilnath, S. Kulkarni, , J. Benediktsson, and X.-S. Yang. “A novel approach for multispectral satellite image classification based on the bat algorithm”. IEEE Geoscience and Remote Sensing Letters. Vol. 13, n° 4, pp. 599-603, 2016.

[3.33] J. W.Zhang, , and G. G. Wang. “Image matching using a bat algorithm with mutation. In Applied Mechanics and Materials”, Trans Tech Publ, vol. 203, pp. 88-93, 2012.

[3.34] S. Akhtar, A. Ahmad, and E.Abdel-Rahman. “A metaheuristic bat- inspired algorithm for full body human pose estimation”. In Computer and Robot Vision (CRV), 2012 Ninth Conference on 2012, IEEE, pp. 369-375, 2012.

[3.35] P.Musikapun, and P. Pongcharoen. “Solving multi-stage multi- machine multi-product scheduling problem using bat algorithm”. In 2nd international conference on management and artificial intelligence, IACSIT Press Singapore, vol. 35, pp. 98-102 2012.

[3.36] S. Raghavan, P. Sarwesh, C.Marimuthu, and K. Chandrasekaran. “Bat algorithm for scheduling work applications in cloud”. In Electronic Design, Computer Networks & Automated Veri_cation (EDCAV), 2015 International Conference on (2015), IEEE, pp. 139-144, 2015.

[3.37] E. Ali. “Optimization of power system stabilizers using bat search algorithm. International Journal of Electrical Power & Energy Systems”. Vol. 61, pp.683- 690, 2014.

[3.38] S. Biswal, A. Barisal, A.Behera, , and T. Prakash. "Optimal power dispatch using bat algorithm. In Energy Efficient Technologies for Sustainability", (ICEETS), International Conference on (2013), IEEE, pp. 1018-1023, 2013.

Chapter 4

[4.1] A.J. Phillips, et al. "Electric fields on AC composite transmission line insulators", IEEE Trans. Power Delivery. pp. 823-830, 23 (April (2)), 2008.

[4.2] A. Phillips. "Electric field distribution and their impact on transmission line composite insulators", in: PES T&D 2012, Orlando, FL, pp. 1-3, 2012.

[4.3] M. K.Karagöz, H.Demirel. "Novel MPPT Method for PV Arrays Based on Modified Bat Algorithm with Partial Shading Capability", J. Int. Comput. Sci. New. Secur. pp. 1761-66, 2017.

Chapter 5

[5.1] F. Chouia, H. Belhouchet, F. Sahnoune, F. Bouzrara."Reaction sintering of kaolin-natural phosphate mixtures", J. Ceramics international. Vol. 41, pp. 8064-8069, 2015.

[5.2] ASTM standard C326. "Standard Test Method for Drying and Firing Shrinkages of Ceramic Whiteware Clays", 2018.

[5.3] SQ. Yang, P. Yuan , HP. He, ZH. Qin, Q. Zhou, JX. Zhu, D. Liu. "Effect of reaction temperature on grafting of γ–aminopropyl triethoxysilane (APTES) onto kaolinite", J. Applied Clay Science. Vol. 62, pp. 8-14, 2012.

[5.4] HA. Seung-Ryong, K. Sung-Hun, L. Jai-Bong, H. Jung-Suk, Y. In-Sung. "Improving shear bond strength of temporary crown and fixed dental prosthesis resins by surface treatments", J. Materials Science. Vol. 51 pp. 1463-1475, 2016.

[5.5] E. Bernardo, Y. Pontikes, GN. Angelopoulos. "Optimization of low temperature Sinter crystallization of waste derived glass", J. Advances Applied Ceramics. 111pp. 472-479. 2012.

[5.6] HR. Fernandes, JMF. Ferreira. "Recycling of chromium–rich leather ashes in porcelain tiles production", J. European Ceramic Society. 27 pp. 657-4663, 2007.

[5.7] VS. Nandi, F. Raupp-Pereira, ORK. Montedo, APN. Oliveira. "The use of ceramic sludge and recycled glass to obtain engobes for manufacturing ceramic tiles", J. Clean production. 86 pp. 461-470, 2015.

[5.8] E. Khalil, FH. El Batal, Y. Hamdy, H. Zidan, M. Aziz, A. Abdelghany. "Infrared absorption spectra of transition metals–doped soda lime silica glasses", J. Physica B. 405, pp. 1294-1300, 2010.

[5.9] A. Tucci, L. Esposito, E. Rastelli, C. Palmonari, E. Rambaldi, "Use of soda–lime scrap–glass as a fluxing agent in a porcelain stoneware mix", J. European Ceramic Society. Vol. 24, pp. 83-92, 2004.

[5.10] A.A. Wereszczak, K. Breder, M.K. Ferber, T.P. Kirkland, E.A. Payzant, C.J. Rawn,E. Krug, C.L. Larocco, R.A. Pietras, M. Karakus. " Dimensional changes and creep of silica core ceramics used in investment casting of superalloys", J. Materials Science. Vol. 37, pp. 4235-4245, 2002.

[5.11] ISO 10545-3, Ceramic Tiles—Part 3: "Determination of Water Absorption, Apparent Porosity, Apparent and Relative Density and Bulk Density", 1997.

[5.12] SR. Braganca, CP. Bergmann. "Waste glass in porcelain", J. Materials Research". Vol. 8 pp. 39-44, 2005.

[5.13] M. Heraiz, F. Sahnoune, H. Belhouchet, N. Saheb. "Synthesis of Al_2O_3 containing mullite from Algerian Kaolin and Boehmite", J. Optoelectronics and Advanced Materials. Vol. 15, pp. 1263 - 1267, 2013.

[5.14] AJ. Souza, BCA. Pinheiro, JNF. Holanda. "Recycling of gneiss rock waste in the manufacture of vitrified floor tiles", J. Environmental Management.Vol. 91 pp 685-689. 2010.

[5.15] IM. Bakr, "Effect of waste glass and zircon on ceramic properties and Microstructure of porcelain tiles", J. Advances Applied Ceramics. Vol. 104, pp. 243-248, 2005.

[5.16] S. Maity, BK. Sarkar. "Development of high-strength whiteware bodies", J. European Ceramic Society". Vol. 16 pp.1083-1088. 1996.

[5.17] N. Montoya, F. Serrano, M. Reventós, JM. Amigo, J. Alarcón," Effect of TiO2 on the mullite formation and mechanical properties of alumina porcelain", J. European Ceramics Society. Vol. 30, pp. 839-846, (2010).

[5.18] L. Sidjanin, D. Rajnovica, J. Ranogajec, E. Molnar. "Measurement of Vickers hardness on ceramic floor tiles", J. European Ceramics Society. Vol.27, pp. 1767-17773, 2007.

[5.19] R. Santos, FS. Silva, RM. Nascimento, FV. Motta, JC. Souza, B. Henriques. "The mechanical properties and microstructure of zirconia-reinforced feldspar-based porcelain", J. Ceramics international. Vol. 42, pp.14214-14221, 2016.

[5.20] F. Muthafar, B. AL-Hillin, T. Kalid, C. AL-RASOUL. "Characterization of alumino-silicate glass/kaolinite composite", J. Ceramics international. Vol. (2)39, pp. 5855-5862 .2013

[5.21] F. Muthafar, B. AL-Hilli, T. Kalid, C. AL-Rasoul. "Influence of glass addition and sintering temperature on the structure, mechanical properties and dielectric strength of high-voltage insulators", J. Materials and Design. Vol. 31 pp3885-3890, 2010.

[5.22] A. Yunlong, X. Xianghua, H. Wen, L. Bingliang, F. Yaqi, "Microstructure and properties of Al_2O_3 (n)/ ZrO_2 dental ceramics prepared by two-step microwave sintering", J. Materials and Design. Vol. 65 pp. 1021-1027, 2015.

[5.23] K. Alexander, K. Emilia , M F. Anna , F. Fabiola , P. Mario. "The effect of fired scrap addition on the sintering behavior of hard porcelain", J. Ceramics international. Vol. 32, pp. 727-732, 2006.

[5.24] W. Shunhua, W. Xuesong, W. Xiaoyong, Y. Hongxing, G. Shunqi. "Effect of Bi2O3 Additive on the Microstructure and Dielectric Properties of BaTiO3-Based Ceramics Sintered at Lower Temperature", J. Materials Science and Technology. Vol. 26 pp.472-476, 2010.

[5.25] Y. Ling, L. Richard, B. Nicholas, P. Zhongxiao, S. Richard. "Damage morphology produced in low-cycle high-load indentations of feldspar porcelain and leucite glass ceramics", J. Materials Science. Vol. 4 pp 101-107, 2013.

[5.26] SP. Chaudhuri, P. Sarkar. "Dielectric behaviour of porcelain in relation to constitution", J .ceramics international. Vol. 26, pp 865-875, 2000.

[5.27] VP. Ll'ina. "Feldspar material from Karelia for electrical engineering", J. Glass and Ceram. Vol. 6, pp. 195-197, 2004.

[5.28] V. Tmovcova, I. Fura, F. Hanic. "Influence of technological texture on electrical properties of industrial ceramics", J. Physics and Chemistry of Solution. vol.*68*, no.5-6, pp.1135-1139, 2007.

[5.29] A. Tucci, L. Esposito, E. Rastelli, C. Palmonari, E. Rambaldi. "Use of soda–lime scrap–glass as a fluxing agent in a porcelain stoneware mix", J. Eur. Ceram. Soc. Vol. 24, pp. 83-92, 2004.

[5.30] B. Arafa, et al. "Experience of using polymer insulators in Egyptian environment", in: CIGRE Regional meeting for the African continent, Cairo, Egypt, 27-30 September,1997.

[5.31] V.G. Besserguenev. "TiO_2 thin film synthesis from complex precursors by CVD, its physical and photocatalytic properties", Int. J. Photoenergy, pp.99-105, 2003.

[5.32] A.A. Wereszczak, K. Breder, M.K. Ferber, T.P. Kirkland, E.A. Payzant, C.J. Rawn, E. Krug, C.L. Larocco, R.A. Pietras, M. Karakus. "Dimensional changes and creep of silica core ceramics used in investment casting of superalloys", J. Mater. Sci. Vol. 37 pp. 4235-4245, 2002.

[5.33] IM. Bakr, Effect of waste glass and zircon on ceramic properties and Microstructure of porcelain tiles, J. Adv Appl Ceram. Vol. 104 pp.243-248, 2005.

[5.34] A. Tucci, L. Esposito, E. Rastelli, C. Palmonari, E. Rambaldi. "Use of soda lime scrap glass as a fluxing agent in a porcelain stoneware mix", J. Eur. Ceram. Soc. Vol. 24 pp 83-92. 2004.

[5.35] SA. Whitehead, A.C. Shearer, DC. Watts, NH. Wilson. "Comparison of methods for measuring surface roughness of ceramic", J. Oral Rehabil. Vol. 22(6), pp 421-427, 1995.

ملخص الرسالة

تعتبر العوازل من بين الأجزاء الأكثر أهمية في نظام الطاقة. لهذا الصدد تمت دراسة العوازل السيراميكية وغير السيراميكية المستخدمة في خطوط نقل الطاقة الكهربائية في هذا البحث بهدف الحد من تدهور أسطحها وبالتالي تقديم ها أفضل أداء. تم تنفيذ هذه الأطروحة من أجل تحليل أداء العوازل عن طريق دراسة توزيع الحقل الكهربائي. سيساعد تحسين توزيع المجال الكهربائي على تحسين أداء العوازل على المدى الطويل. الجزء الأول من هذا البحث يهدف إلى دراسة استخدام الحلقة الاكليلية في نهايات أطراف العوازل المركبة (غير السيراميكية) و تأثيرها على توزيع الحقل الكهربائي وتخفيض قيمه القصوى. للقيام بذلك ، تم تطوير خوارزمية الخفافيش (BAT Algorithm) المستندة إلى تقنية التحسين للحصول على معايير التصميم الأمثل للحلقة الاكليلية. لقد تم تصميم نموذج للعازل المركب للمح اكاة وتم استخدام طريقة *الحدود المتناهية* (FEM) لدراسة توزيع الحقل الكهربائي على طول سطح هذا العازل. الجزء الثاني من الأطروحة يتعلق بالبورسلان. حيث يدرس هذا الجزء إمكانية تطوير البورسلان من مواد خام محلية وباستعمال الزجاج المعاد تدويره. كما أجريت محاكاة لسطح هذا العازل في الحالتين: مغلف و غيرمغلف. وقد أظهرت النتائج أن الغلاف المستخدم يحسن من مقاومة العازل وأن توزيع الحقل الكهربائي على طول هذا سطح يظهر تحسنا كبيرا.

إن النتائج التي تم الحصول عليها تعطي معلومات أكثر دقة للعثور على أفضل الحلول لمشاكل عوازل الجهد العالي.

الكلمات المفتاحية: *عازل مركب ، حلقة كورونا ، الحقل الكهربائي ، خوارزمية الخفافيش ، طريقة الحدود المتناهية (FEM)، بورسلان ، إنشاء.*

Résumé

Les isolateurs sont parmi les parties les plus importantes du système d'alimentation électrique. Les isolateurs céramiques et non céramiques utilisés dans les lignes de transport d'énergie ont été étudiés dans le but de réduire la dégradation de la surface et d'offrir les meilleures performances. Cette thèse a été réalisée dans le but d'analyser les performances des isolateurs via leur distribution de champ électrique. En améliorant la distribution du champ électrique, cela contribuera à améliorer les performances à long terme des isolateurs. La première partie de ce travail vise à étudier l'utilisation de l'anneau corona au niveau du raccord d'extrémité HT pour améliorer le champ électrique et les distributions de potentiel, puis pour minimiser les décharges par effet corona sur un isolateur polymérique. Pour ce faire, un algorithme BAT basé sur une technique d'optimisation est développé pour obtenir les paramètres optimisés de l'anneau corona. L'isolateur polymérique est modélisé pour la simulation et une méthode FEM a été utilisée pour étudier la contrainte de champ électrique le long de la surface de cet isolateur. La deuxième partie de la thèse concerne l'isolateur en porcelaine. Cette partie étudie la possibilité de développer une porcelaine à partir de matières premières locales et de verre recyclé. Des simulations de surfaces isolantes revêtues et non revêtues de porcelaine ont également été effectuées. Les résultats obtenus montrent que le revêtement améliore la résistance à la rupture de la porcelaine et que la distribution de la tension le long de la surface montre une amélioration significative. Les résultats obtenus présentent une conclusion plus précise dans la recherche des meilleures solutions aux problèmes des isolateurs haute tension.

Mots-clés *: Isolateur composite, anneau corona, champ eléctrique, algorithme chauve-souris, MEF, porcelaine, élaboration.*

Abstract

Insulators are the important part of the power system. Ceramic and non ceramic insulators used in power transmission lines were studied with the aim of reducing degradation over its surface and presenting the best performance. This thesis has been made to analyze insulator performance via their electric field distribution. By improving the electric field distribution, it will help in enhancing their long term performance of insulator. The first part of this work is aimed to investigate the use of corona ring at the HV end fitting for improving the electric field and potential distributions and then for minimizing the corona discharges on composite insulator. To achieve this, optimization technique based Bat algorithm is developed for obtaining the optimized corona ring parameters. Composite insulator is modeled for simulation and FEM method has been employed to investigate the electric field stress along the insulator surface. The second part of the thesis concerns the porcelain insulator. In this part the possibility of development porcelain from locally raw materials using recycled waste glass is studied. Simulations for coated and uncoated insulator surfaces of porcelain were also performed.

The obtained results showed that Coating enhances the breakdown strength of the porcelain and the voltage distribution along the leakage surface of coated ceramic insulators show a significantly improvement. The obtained results present more accurate result in finding best solutions for high voltage insulators problems.

Keywords*: Composite insulator, corona ring, electric field, bat algorithm, FEM, porcelain, elaboration.*